NORTHWESTERN UNIVERSITY

Holocene Climate Change in Greenland:
Investigations Using Oxygen Isotopes of Lacustrine Organic Materials

A DISSERTATION

SUBMITTED TO THE GRADUATE SCHOOL
IN PARTIAL FULFILLMENT OF THE REQUIREMENTS

for the degree

DOCTOR OF PHILOSOPHY

Field of Earth and Planetary Sciences

By
Gregory Everett Lasher

EVANSTON, ILLINOIS

June 2019

ABSTRACT

This dissertation explores Holocene climate change along the west coast of Greenland and late Holocene climate variability in the subpolar North Atlantic region using paleolimnology. Lake sediment archives and the climate proxies contained within them provide a valuable window into past temperature change on Greenland, home to one of Earth's two remaining ice sheets. The studies presented here primarily use oxygen isotopes ($\delta^{18}O$) measured in sub fossil midges (Diptera: Chironomidae) to infer climate change over the last 10,000 years. Holocene temperature records from three lakes on the west coast of Greenland, and a late Holocene record from a south Greenland lake are presented and discussed.

Chapter 2 provides a review of chironomid $\delta^{18}O$ proxy advances over the last two decades and presents new data demonstrating the fidelity of these subfossils as indicators of past variations in lake water $\delta^{18}O$. An investigation of chironomid taphonomy using a novel Fourier Transform Infrared Spectroscopy (FT-IR) approach indicates that these subfossils are molecularly stable in Holocene age sediments, and possibly stable in Eemian sediments over 100,000 years old. Chironomids have the potential to provide reliable and rare records of paleo lake water where last interglacial sediments are preserved.

Chapters 3 and 4 investigate millennial scale climate change from lake sediment cores in northwest and southwest Greenland. In Chapter 3, I present chironomid $\delta^{18}O$ from Secret Lake in northwest Greenland near the Thule Air Base and find that temperatures were warmer than present for much of the last 8000 years due to high Northern Hemisphere summer insolation in the early Holocene. Temperatures were between 2.5 and 4 °C warmer than present between 7.7 (start of the record) and 6 ka (ka = thousands of years ago) and cooled by ~ 6 °C over the next 5000 years.

Chapter 4 focuses on sub-Arctic Holocene climate change in southwest Greenland coast near Nuuk. Chironomid $\delta^{18}O$ values from two lakes show that peak warmth occurred in the early Holocene, between at least 9 and 7 ka (though possibly earlier) and was followed by gradual cooling over the next 7000 years. The magnitude of likely temperature change at this southwest Greenland site is less than in northwest Greenland, demonstrating different regional responses to insolation trends, and regional modulation of climate via other mechanisms (e.g. ocean circulation).

Chapters 5 and 6 focus on late Holocene climate change at a higher temporal resolution, investigating centennial scale variability in south Greenland, Baffin Bay and the subpolar North Atlantic area. Chapter 5 presents a 3000-year temperature record from Scoop Lake in south Greenland lake near Narsaq. This study provided the first quantitative temperature estimates showing Medieval warmth within an area of Norse settlement on Greenland. Evidence for coeval cold conditions elsewhere on Greenland and Baffin Island cited a hypothesized positive North Atlantic Oscillation (NAO) anomaly to explain glacier advance, however the new isotope record from Scoop Lake argues against such an anomaly. Instead there is growing evidence that enhanced delivery of warm sea surface waters to south Greenland via a strong subpolar gyre (SPG) caused the warmth between 900 and 1400 CE. These conclusions are further explored in Chapter 6, which employs principal component analysis (PCA) of 29 temperature sensitive proxy records from the high latitude North Atlantic region, Baffin Bay and Greenland to explore spatial – temporal climate heterogeneity over the last 3000 years.

Acknowledgements

I wish to thank several individuals for their support over the last six years. First and foremost, I would like to thank my advisor, Yarrow Axford, who welcomed me to Evanston, the Earth and Planetary Sciences Program and Northwestern University. I am incredibly fortunate to have received encouragement and guidance from such an amazing, caring and understanding human. I can only hope to emulate her mentorship skills in the future. I will always be grateful for the opportunities provided to live, learn and ponder the sedimentary records of paleoclimate.

I would also like to thank my fellow committee members, Neal Blair and Matt Hurtgen, for their time and guidance during my graduate school journey. Also, thanks to Matt for letting me take over class once a year to perform an interpretive Milankovitch dance in front of a few hundred Northwestern students. I thank the rest of the Earth and Planetary Sciences faculty and staff for making my six years in Evanston an enjoyable and rewarding experience. Special thanks to Maggie Osburn for helping with water isotope analysis, and to Trish Beddows for allowing me to travel to Mexico; coring lakes with water temperatures above four °C was a much-appreciated assignment.

Also, I would not have been able to successfully complete my many field seasons to Greenland without the assistance of Ben, Lisa and Robin. To our department lab managers, past and present, particularly Grace and Andy, thank you for helping me navigate Hogan Hall, and helping me analyze all those chironomid head capsules. To my fellow graduate students, it has been a pleasure to study alongside you all. A special shout out to my fellow lab and office mates, Laura, Matt, Melissa and Pete. You made many long weeks in Greenland, the lab and the office truly enjoyable.

Importantly, I would not be writing this Earth Science dissertation if it were not for my amazing parents. Mom and Dad, thank you for introducing rock collections to me at a young age, for providing endless gateways to nature, and for being patient during my rebellious years.

Finally, thank you Margaret, for your endless encouragement, support, and patience over the last few years, particularly during my multiple trips to Greenland. You've made my time in Chicago truly wonderful. I wouldn't have finished this without you, and I can't wait for our next adventure.

List of Common Abbreviations

GrIS – Greenland Ice Sheet

HTM – Holocene Thermal Maximum

RWP – Roman Warm Period

MCA – Medieval Climate Anomaly

LIA – Little Ice Age

SGL – South Greenland

TAB – Thule Air Base

EGC – East Greenland Current

WGC – West Greenland Current

IC – Irminger Current

NAC – North Atlantic Current

NH – Northern Hemisphere

SPG – Sub polar gyre

CHC – Chironomid head capsule

PCA – Principal component anlysis

ka – thousands of years ago

CE – Common Era

FT-IR – Fourier transform infrared spectroscopy

$\delta^{18}O$ – Stable isotope ratio of ^{18}O to ^{16}O normalized to a standard

List of Figures

List of Tables

TABLE OF CONTENTS

CHAPTER 1:

Introduction

Over the last 20 years, our understanding of Northern Hemisphere Holocene climate change has advanced considerably. The knowledge gained is largely due to three related factors: the hard work of paleoclimate scientists gathering seminal data before the new millennium, the regular re-evaluation of published records, and the continued efforts of the next generation of climate explorers filling in the gaps – both spatial and temporal. Since 2000, broad geographic climate synthesis studies have gathered, sifted, sorted, interpreted (and occasionally narrowed) a steadily growing library of climate and climate proxy records around the world (PAGES 2k Consortium, 2013; 2017; Sundqvist et al., 2014). These syntheses, as well as new datasets from specific locations, are being published at an increasing rate, and each adds new insights into what is clearly a complex past. While this dissertation narrowly focuses on Greenland and surrounding Arctic and high latitude North Atlantic regions, scientists continue to explore the world over, gathering new data to better understand climate change over centuries, millennia and longer, in recognition that such changes through time are not uniform on Earth.

The Holocene, encompassing the last 11,700 years, represents a period of relative warmth and climate stability in the broader context of the last 3 million years. Global temperatures likely varied by less than 1°C since the Holocene began at the end of the last ice age (Marcott et al., 2013). However, changes in temperatures of this magnitude did result in global environmental change and responses of the cryosphere in the Arctic. In the next 200 years, Earth will continue to warm well beyond the limits of Holocene temperatures due to the burning of fossil fuels (IPCC, 2014). The rise in temperature will be greatest in the Arctic, home to the Greenland Ice Sheet

(GrIS) and many small mountain glaciers and ice caps (Rastner et al., 2012; Serreze and Francis, 2006). Future warming will result in enhanced melting of the ice sheet, contributing to sea level rise which will ultimately affect many millions of people living on the coasts. However, uncertainties remain about how Greenland and its ice sheet will respond to this rise in temperature. To better understand what lies ahead for the GrIS in a warmer world, we can look at how the ice sheet, and nearby ice masses, responded to past temperature change.

This dissertation investigates Greenland and broader Arctic climate change within the Holocene at varying temporal resolutions and explores the mechanisms responsible for those changes. When I started my Ph.D., quantitative estimates of temperature change from Greenland were sparse; they were largely limited to isotope inferred records from ice cores over the central ice sheet (e.g. Johnsen et al., 2001) but also included a handful of non-ice core proxy records (Axford et al., 2013; Frechette and de Vernal, 2009; Gajewski, 2015; Wooller et al., 2004). My research has been dedicated to improving and utilizing non-traditional lake sediment proxies to infer climate change in under- or un-studied areas of Greenland.

Lakes are ubiquitous features of the post-glacial Arctic, and the sediment deposited in them year after year forms an archive of regional climate and local environmental history. Preserved among these sedimentary layers are organic materials, for example: plant fragments, diatom remains, pollen grains, and chironomids (Insecta: Diptera: Chironomidae). The larval stage exoskeletons of these aquatic non-biting midges are as widespread in sediments as lakes are on Earth's surface, and their ubiquity makes them worthy of special attention as tracers of past environments. The sub-fossil remains of these insects have been commonly used to infer temperature change based on variations in the species preserved in the sediments (e.g. Brooks and

Birks, 2001), but the molecules that make up their exoskeletons provides an additional window into their past world, which has been little used up to this point.

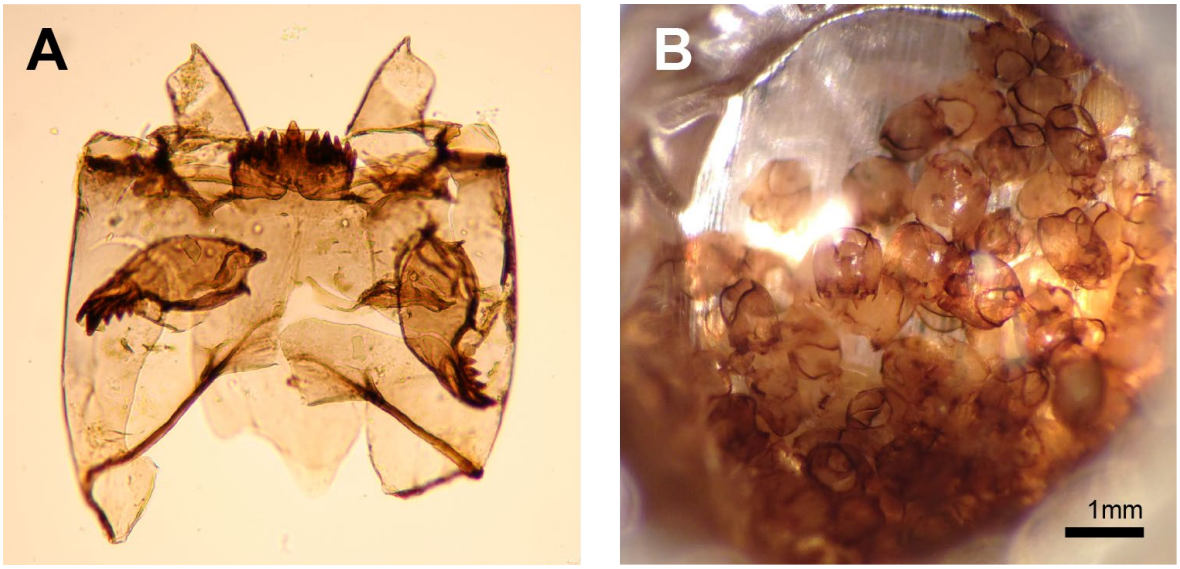

Figure 1.1. A: Head capsule of a chironomid (Tanytarsini: *Micropsectra*). Photograph courtesy of Y. Axford, Northwestern University. B: Chironomid head capsules collected in a silver capsule, ready for isotope analysis.

Chironomid larval head capsules are composed of chitin and protein and preserve well through geologic time (Schimmelmann et al., 1986). The atoms that make up these exoskeleton parts are 30 to 40 % oxygen, and there is strong evidence that this oxygen is derived from the lake water in which the insects grow (Verbruggen et al., 2010; Wang et al., 2009). Oxygen has three naturally occurring stable isotopes (^{16}O, ^{17}O and ^{18}O), and the ratio of $^{18}O/^{16}O$ in organic and inorganic materials and natural waters is an exceptionally useful fingerprint of climate change. Fluctuations in climatic variables such as temperature, humidity, and precipitation amounts will all result in characteristic changes in oxygen isotope ratios. Differences in isotopic ratios are

commonly reported as relative differences between the $^{18}O/^{16}O$ ratio in a given sample, and that of a known standard in parts per thousand (or per mil, ‰) using delta notation (δ) outlined in Equation 1.1. (Criss, 1999).

$$\delta^{18}O = \left(\frac{{}^{18}O/{}^{16}O_{sample}}{{}^{18}O/{}^{16}O_{standard}} - 1 \right) \times 1000$$

Equation 1.1.

Observation based temperature - $\delta^{18}O$ relationships in precipitation are well constrained over much of the world (Bowen et al., 2019; Dansgaard, 1964) and allow paleoclimatologists to infer quantitative changes in temperature for a given change in $\delta^{18}O$ of precipitation, or to qualitatively infer hydroclimatic variability where those relationships are not well understood. In promising early chironomid $\delta^{18}O$ pilot studies, variations in lake water oxygen isotopes inferred from conventional $\delta^{18}O$ methods (e.g. $\delta^{18}O$ of carbonate) showed remarkable agreement to new values measured from the insect remains (Verbruggen et al., 2010). Improvements in isotope ratio mass spectrometers (IRMS) and peripheral instruments such as the Thermal Conversion Elemental Analyzer (TC-EA) over the last decade now allow us to reliably measure variations in $\delta^{18}O$ from small (< 100 μg) masses of organic matter and has greatly expanded our ability to decipher past climate change at the wide range of sites where chironomids are preserved. In Chapter 2, I review and add to our understanding of chironomid $\delta^{18}O$ as a viable proxy for past climate change. Some of the data and analysis presented in Chapter 2 was contributed to a *Quaternary Science Reviews* paper on stable isotopes in organic and inorganic lake sediment matter (van Hardenbroek et al., 2018).

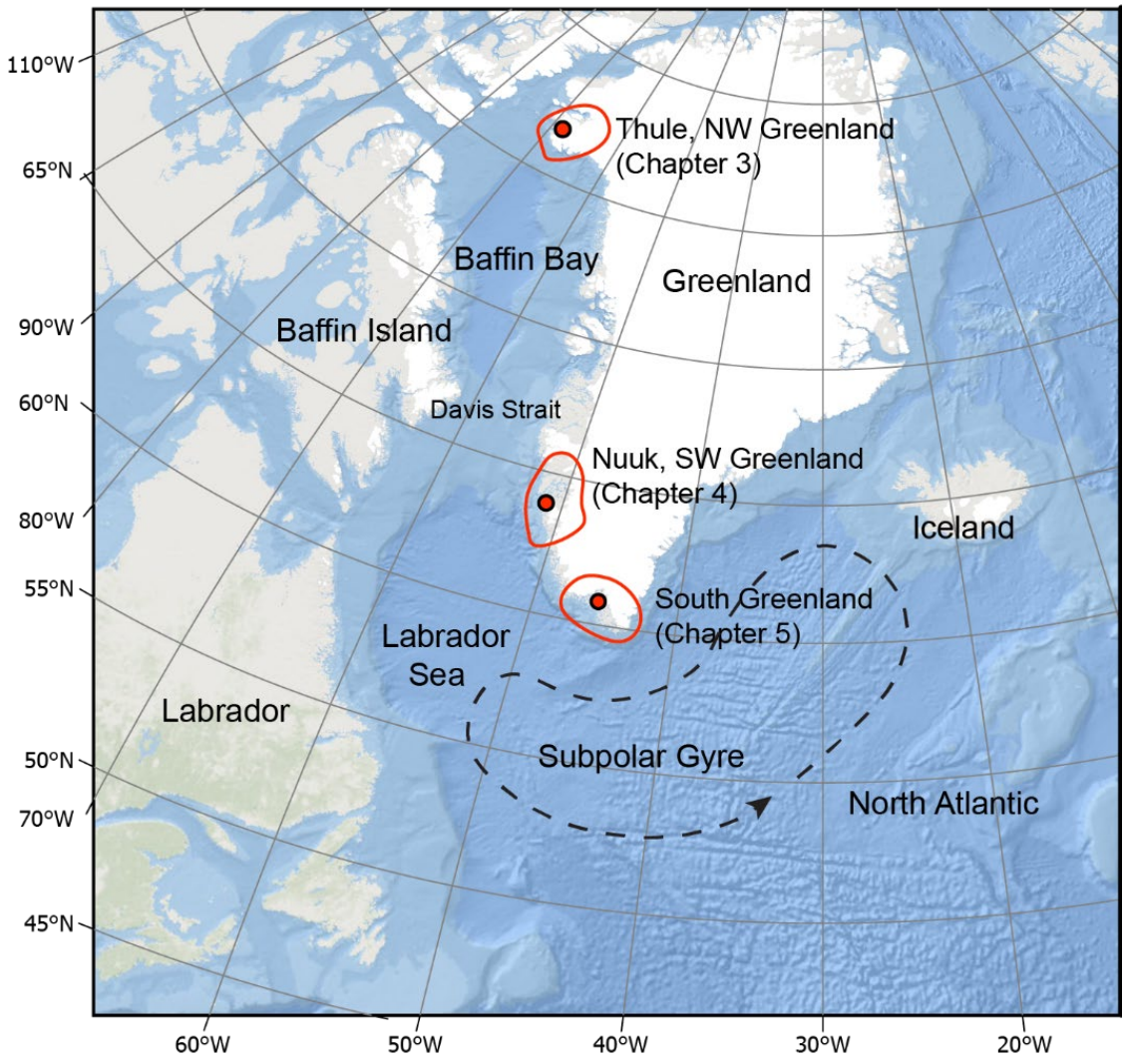

Figure 1.2. Geographic locations discussed in this chapter and locations of new lake records presented in this dissertation marked as red points.

In Chapters 3 and 4, I explore millennial scale Holocene climate change on the west coast of Greenland using a suite of geochemical approaches. Millennial scale Holocene climate change in the Arctic is mostly defined by insolation forced cooling, the result of the changing position of the Northern Hemisphere in relationship to the sun (Kaufman, 2004; Miller et al., 2010). However, it is increasingly clear that other factors such as residual ice sheets, ocean currents and sea ice

feedbacks have important roles in modulating regional differences on 1000 year time scales (Briner et al., 2016). These two chapters primarily utilize chironomid $\delta^{18}O$, but also make use of more traditional sedimentary geochemical methods to infer climate and environmental change including: biogenic silica ($bioSiO_2$), carbon and nitrogen isotopes ($\delta^{13}C$ and $\delta^{15}N$ respectively), X-Ray Florescence Spectroscopy (XRF) and $\delta^{18}O$ of aquatic plant material.

The objective of Chapter 3 was to develop a quantitative temperature record using chironomid $\delta^{18}O$, and better constrain Holocene temperature change in northwest Greenland. More intense Northern Hemisphere insolation in the early Holocene led to warmer than present temperatures over much of the Arctic, a time known as the Holocene Thermal Maximum (HTM). The timing and magnitude of the HTM was not uniform across the NH (Kaufman, 2004), but peak warmth in many locations is now associated with retreat of the Greenland Ice Sheet (Larsen et al., 2015b; Lecavalier et al., 2014). In northwest Greenland, the timing and more so the magnitude of the HTM remained elusive until recently. Early Holocene temperature estimates from the Camp Century ice core (Dansgaard et al., 1969) are difficult to constrain due to rapid ice sheet thinning and elevation change effects on $\delta^{18}O$ values between 11.7 and 6 ka (Vinther et al., 2009). I argue that chironomid $\delta^{18}O$ in northwest Greenland is a strong proxy for summer and autumn biased temperatures during the Holocene, and find that temperatures were between 2.5 to 4°C warmer than present from 7.7 ka (the beginning of my record) to ~6 ka. Temperatures gradually decreased over much of the 7,700-year record, suggesting a strong influence of declining NH insolation on summer climate in northwest Greenland. A late Holocene cold anomaly (which includes the Little Ice Age) was between 1.5 to 3 °C colder than present. While the data presented do not extend back to the early Holocene and therefore likely did not capture peak temperatures, this study placed

some of the first local constraints on possible HTM temperature ranges. Other northwest Greenland temperature records do indeed show higher temperatures in the earliest part of the Holocene before our record begins, but corroborate the likely anomaly range described between 7.7 and 6 ka (Lecavalier et al., 2017; McFarlin et al., 2018). These insights, paired with glacial investigations of nearby glaciers, ice caps and the GrIS (Farnsworth et al., 2018; Goldthwait, 1960; Reusche et al., 2018) can help constrain the sensitivity of the cryosphere to future temperature change. This chapter was originally published as Lasher et al. (2017) in *Quaternary Science Reviews*.

Chapter 4 investigates climate change over a similar timeframe to Chapter 3, but at a site ~1,500 km south on the sub-Arctic southwest Greenland coast. Climatically distinct from the high Arctic environment in northwest Greenland, this study site provides the opportunity to explore how regionally heterogeneous phenomena can modulate climate on millennial timescales; e.g. ocean circulation, sea ice feedbacks, or the effects of ice sheets in the early Holocene. The GrIS in southwest Greenland experienced rapid retreat in the early Holocene, and left much of the present-day ice-free landscape inundated by the sea temporarily due to residual isostatic depression (Larsen et al., 2014; Winsor et al., 2015; Woodroffe et al., 2014). Within a thousand years, relative sea level fell as the landscape rebounded, and lakes formed in the residual depressions. I document the marine to lacustrine transition in two such lakes near Nuuk between 9.4 and 8.6 ka. Chironomid $\delta^{18}O$ values, as well as other chemostratigraphic data, are used to infer millennial scale climate change at this coastal site. Chironomid $\delta^{18}O$ values suggest that peak warmth occurred early in southwest Greenland, between 9 and 7 ka, and was followed by gradual cooling into the neoglacial.

This temperature history agrees well with reconstructions of glacier behavior around the west coast that show gradual advances over thousands of years in response to the cooling trend.

In Chapter 5 and 6, I focus on the last 3000 years and explore climatic changes that happen on centennial to sub-centennial time scales around the high latitudes of the North Atlantic region, including south Greenland. This time period and place are of interest for multiple reasons. First, the last 3000 years includes well known climate events, such as the Medieval Climate Anomaly (MCA) and the Little Ice Age (LIA), that have long garnered the attention of paleoclimatologists (Lamb, 1965). Second, there is considerable interest in the Norse settlement history of the region. The Norse arrived in Iceland around 870 CE and later settled in Greenland at 985 CE (Jones, 1986). It has long been hypothesized that favorable climate conditions around Iceland and southern Greenland enabled Medieval Norse exploration, with subsequent climate deterioration responsible for the ultimate demise of the Greenland settlements (Barlow et al., 1997; Dugmore et al., 2012). Actual evidence for mild climate during this time was largely Euro-centric, and existing records within the settlement areas were ambiguous regarding temperature (Lassen et al., 2004; Millet et al., 2014; Moller et al., 2006; Nørgaard-Pedersen and Mikkelsen, 2009). More recently, studies of glacier advance around the coasts of Baffin Bay showed that some glaciers advanced as the Norse settled Greenland (Jomelli et al., 2016; Young et al., 2015). These glacier studies, as well as a handful of marine records in Baffin Bay, invoked the North Atlantic Oscillation (NAO; an atmospheric pressure system that dictates temperature patterns and moisture availability around much of the North Atlantic (Hurrell et al., 2003) to explain localized cold conditions favorable for glacier growth during this time. Chapter 5 investigates whether NAO-attributed cold conditions affected south Greenland during the time of Norse settlement. Chironomid $\delta^{18}O$ values measured

at sub-centennial resolution in a south Greenland lake within the Norse settlement area shows generally warmer temperatures superimposed on the insolation forced Holocene cooling trend during the MCA. Furthermore, the results of this study suggest that the NAO mechanism used to explain Medieval cooling at some sites in the high-latitude western North Atlantic requires re-evaluation. This chapter, including Appendix A, was originally published as Lasher and Axford (2019) in *Geology*.

Chapter 6 expands on the work and conclusions of Chapter 5 by investigating, in greater detail, centennial-scale late Holocene climate change around Greenland, Baffin Bay and much of the high latitude North Atlantic. Centennially resolved temperature-sensitive proxy records between 50° to 80° N latitude and 80° W to 20° E longitude show gradual cooling over the last 3000 years, in agreement with other high latitude proxy reconstructions (Briner et al., 2016; Kaufman et al., 2009; Sejrup et al., 2016). Through the use of principal component analysis, major sub-millennial climate trends become apparent in the region, including localized warmth over south Greenland and Iceland, coincident with cooling in the western Labrador Sea, between 1000 and 1400 CE. I find a strong relationship between centennially resolved indicators of subpolar gyre strength and temperature over the last 3000 years. Together, Chapter 5 and 6 affirm that ocean currents in the subpolar North Atlantic play an important role in modulating regional climate on centennial time scales.

Finally, in Chapter 7, I provide a brief concluding review of Chapters 3 through 6. comparing and contrasting Holocene climate trends from the high Arctic northwest Greenland coast, to the low Arctic? maritime south Greenland coast. Additionally, I highlight the different forcings and mechanisms responsible for Holocene climate change there. This chapter also

includes a summary of the most important implications of all the research presented in this dissertation, as well as recommendations regarding the future use of chironomid head capsules in reconstructing past climate change.

CHAPTER 2:

Chironomid head capsules as a proxy for paleo lake water $\delta^{18}O$: investigations of isotopes and taphonomy in modern, Holocene and Late Pleistocene subfossils

Abstract

Chironomid head capsules hold great promise for providing new insights into changing climate conditions via interpretation of the paleo lake water $\delta^{18}O$ archived in their subfossil remains. This chapter explores the relationship between $\delta^{18}O$ values measured in head capsules and $\delta^{18}O$ of lake water in which the insects grow, highlights the range of possible effects that different chemical treatments can have on head capsule molecular composition as well as $\delta^{18}O$ values, and investigates diagenetic alteration of head capsule remains in sediments spanning the last 130,000 years. A global compilation of paired surface sediment chironomid $\delta^{18}O$ and lake water $\delta^{18}O$ values indicates that head capsules are enriched relative to growth water by 22.5 ± 2.3 ‰. While strong relationships have previously been reported between chironomid $\delta^{18}O$ values and mean annual air temperatures, studies that wish to use chironomid $\delta^{18}O$ values as a proxy for temperature change through time should conduct a thorough assessment of lake water hydrology to determine local connections between measured $\delta^{18}O$ values and potential climate variables.

Previous work has shown that intense chemical pretreatments can alter the molecular composition of head capsules. Strong acid treatments preferentially remove chitin moieties from chironomid subfossils, and results in an artificial shift towards more negative $\delta^{18}O$ values, possibly due to oxygen exchange with laboratory water. Conversely, strong base treatments remove protein from head capsules artificially increasing $\delta^{18}O$ values.

Fourier Transform Infrared Spectroscopy (FT-IR) analysis of chironomids from two Greenland sediment cores indicates that the subfossil remains are molecularly stable over tens of thousands of years. Absorbance spectra from Holocene age remains show no indication that either chitin or protein are being lost over time, though variable Amide I and II peaks between 1400 and 1700 cm^{-1} may show incipient alteration of these components. Spectra from some head capsule remains older than 100,000 years show evidence of decreased protein content and possible loss of catechol moieties responsible for linking chitin and protein molecules. Considering the potential of chemical pretreatments to preferentially remove chitin or protein from head capsules, and alter $\delta^{18}O$ values, studies using chironomid head capsules to reconstruct climate change beyond the Holocene should carefully consider pretreatment approaches.

2.1. Introduction

Chironomid larvae (Insecta: Diptera: Chironomidae) in lake sediments have long been used as indicators of environmental change. This single lake sediment component offers multiple advantages over other organic archives in reconstructing past environmental and climate change; the cuticle (mainly composed of chitin-protein complexes) seems to preserve well over geologic time (Schimmelmann et al., 1986), the remains are easily isolated from bulk sediment (Walker et al., 2001), and are common and generally abundant in lakes around the world. To date, the use of chironomids as indicators of environmental change has largely been accomplished by inferring changes in the taxonomy of sub fossil remains (e.g. Axford et al., 2009a; Brooks and Birks, 2001; Samartin et al., 2017; Walker, 1987). Recent and ongoing research now shows that the stable oxygen isotopic composition ($\delta^{18}O$) of these aquatic insects is a good proxy for lake water $\delta^{18}O$ (Lasher et al., 2017; Lombino, 2014; Mayr et al., 2014; van Hardenbroek et al., 2018; Verbruggen et al., 2011; Wooller et al., 2004). Armed with this new knowledge, studies are increasingly utilizing chironomid $\delta^{18}O$ to reconstruct paleoclimate conditions in parts of the world previously off limits to oxygen isotope based lacustrine research. Paleo lake water $\delta^{18}O$ has now been reconstructed from chironomid $\delta^{18}O$ in the United Kingdom (Lombino, 2014), Switzerland (Verbruggen et al., 2010), Alaska (Graham et al., 2016), Svalbard (Arppe et al., 2017), Iceland (Wooller et al., 2007), and Greenland (Lasher and Axford, 2019; Lasher et al., 2017; Wooller et al., 2004).

In addition to being relatively easy to isolate for paleoclimate analysis, isotopic analysis of chironomid head capsules has additional advantages. For example, many areas of the world are precluded from conventional and well-validated lacustrine isotope-based proxy approaches; catchments lacking carbonate bedrock are unlikely to precipitate authigenic carbonate for $\delta^{18}O$

analysis in the sediments, or in the case of cellulose $\delta^{18}O$ analysis, terrestrial plant material contamination can make interpretation difficult (Leng and Marshall, 2004). There is a definite need for the continued development of an isotope proxy that is not restricted by bedrock geology or rendered impractical by preparation techniques.

While studies to date show increasingly promising results for the use of chironomid $\delta^{18}O$ as a paleo lake water proxy, a number of outstanding questions remain that invite further investigation. First, while there is growing consensus that $\delta^{18}O$ measured from chironomid head capsules is a strong proxy for lake water, some studies comparing modern lake water and chironomid $\delta^{18}O$ show weak or non-existent relationships. Section 2.3 explores this isotopic relationship, possible reasons for the apparent failure of chironomids to record lake water $\delta^{18}O$ in certain studies and assesses potential limitations of this proxy. Second, among the early applications of this proxy (n = 9), no single agreed upon method exists for the preparation of samples (n = 5), varying with respect to chemicals used, concentrations, temperature, exposure time, or pre analysis preparation (Lombino et al., 2014; Mayr et al., 2014; Verbruggen et al., 2010; Verbruggen et al., 2011; Verbruggen et al., 2009; Wang et al., 2008; Wang et al., 2009; Wooller et al., 2007; Wooller et al., 2004). Many of these early studies explored the impact of these different treatments on the isotopic and molecular composition of modern head capsules. Results indicate that certain treatments and preparations can remove chitin or protein from the subfossils and alter $\delta^{18}O$ values in head capsule samples. Section 2.4 summarizes the effects of these pretreatment studies and makes recommendations about future methodology. Finally, diagenetic effects on chironomid head capsules are assumed to be minimal over long time scales (e.g. thousands of years – ka), though to date no one has studied these insects directly. Section 2.5 reviews literature on

taphonomy of comparable aquatic invertebrates and presents new data on molecular change in chironomid head capsules over thousands of years using Fourier Transform Infrared Spectroscopy (FT-IR).

2.2. Molecular composition of chironomid head capsules

Insect cuticles are molecularly complex, thought to be mainly composed of chitin and protein, cross-linked through histidine and catecholamine moieties (Fig. 2.1) (Schaefer et al., 1987). The major component of interest, chitin (*N*-acetyl-D-glucosamine) is described as the second most abundant and important biopolymer on earth after cellulose and is advantageously resistant to degradation under appropriate sedimentary conditions (Gupta, 2010). Morphological studies of insect cuticles by scanning electron microscope (SEM) show repeating and overlapping layers of chitin fibrils embedded within a protein matrix (Verbruggen et al., 2009). In modern larvae, this chitin-protein matrix is further surrounded by an outer epicuticle composed of lipids, pigments, and additional protein (Allison and Bottjer, 2011; Gupta and Briggs, 2011; Nation, 2011). As a whole, the absolute amount of chitin and protein in insect cuticles remains poorly constrained; estimates of chitin as a percent of total biomass in insects vary from 10 to 50% (Majtan et al., 2007; Zhang et al., 2000). Another estimate of composition, specifically for chironomids, is based on Curie point pyrolosis products: 1,6-Anhydro-2-acetamido-2-deoxyglucose and its isomer for chitin, and the C1-phenol and 3-(2-Methylpropenyl)-5-(2-methylbutyl)-3,4-dihydro-2H-pyrrole-2,4-dione for protein (Verbruggen et al., 2009). Comparison of the area ratio of these product peaks produced from head capsule analysis suggests that modern head capsules have a chitin to protein ratio (by mass) of 0.77.

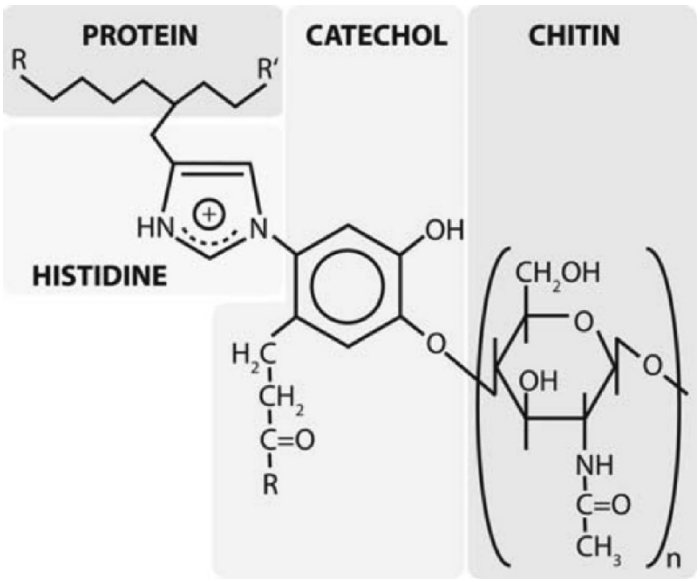

Figure 2.1 Proposed molecular structure of insect cuticles. Chitin (N-acetyl-D-glucosamine) is cross linked to proteins through catecholamines and histidine moieties. After Verbruggen et al. (2009), modified from Schaefer et al. (1987).

2.3. Controls on chironomid head capsule isotope values

Laboratory culturing and field-based studies of aquatic invertebrates have helped constrain the environmental factors responsible for the different elements that make up exoskeletons. Carbon and nitrogen of aquatic invertebrates is controlled by the diet of the organism, and the isotopic composition is known to vary depending on the organisms and their feeding habits (DeNiro and Epstein, 1978). For an extensive review of studies quantifying $\delta^{13}C$ and $\delta^{15}N$ differences in aquatic organisms, see van Hardenbroek et al. (2018) and references therein. While less is known about oxygen and hydrogen in aquatic organisms, there is strong evidence that between 56 and 84% of oxygen in a variety of invertebrates derives from the lake water in which they grow, with minor contributions attributed to dietary oxygen (Table 2.1) (van Hardenbroek et al., 2018). Like carbon and nitrogen, diet exerts a strong influence on hydrogen composition (van Hardenbroek et al.,

2018; Wang et al., 2009), however up to 47% has also been linked to growth water since in most environments, hydrogen in chironomid food sources will also be derived from lake water.

Table 2.1. Estimates of growth water-derived oxygen in aquatic invertebrates.

Organism	Compound	% O - growth Water	Ref.
Chironomid	Whole	69%	(Wang et al., 2009)
Chironomid	Isolated protein	84%	(Soto et al., 2013)
Brine shrimp	Isolated chitin	69%	(Nielson and Bowen, 2010)
Daphnia	Whole	56 - 69%	(Schilder et al., 2015)

A recent compilation of published field-based paired surface sediment chironomid and lake water $\delta^{18}O$ values indicates a strong relationship exists between these two variables (Fig. 2.2) (van Hardenbroek et al., 2018). Data compiled from Greenland (Lasher et al., 2017), Europe (Lombino, 2014; Verbruggen et al., 2011), South America (Mayr et al., 2014), and Australia (Chang et al., 2017; Chang et al., 2016) suggest that chironomid $\delta^{18}O$ is enriched relative to lake water by 22.5 ± 2.3 ‰. This enrichment factor (in units of ‰) is defined as:

$$\varepsilon = \left(\left(\frac{1000 + \delta^{18}O_{chironomid}}{1000 + \delta^{18}O_{lake\ water}} \right) - 1 \right) \times 1000$$

Equation 2.1.

This value, compiled from multiple sites around the world, is close to enrichment factors reported in pilot studies between freshwater arthropods and lake water (21.3 ± 2.3 ‰) (Schimmelmann and DeNiro, 1986) demonstrating consistent results in comparable organisms over multiple decades. However, some significant variability is apparent in the enrichment factor between chironomid head capsules and lake water at certain lakes documented in recent studies.

Most reported enrichment factors are between + 22 and + 25 ‰ (Table 2.2), but values reported from some Australian lakes differ greatly from the mean ε of + 22.5 ‰ (Chang et al., 2017; Chang et al., 2016). Chang et al., (2016) explored a number of possible explanations for the poor relationship observed between chironomid $\delta^{18}O$ values and lake water $\delta^{18}O$ values in their study including seasonality of precipitation, lake water residence time, nutrient availability, salinity, local estimated aridity, and local potential evapotranspiration.

Table 2.2. Summary of published chironomid – lake water enrichment factors.

Region	n	Mean ε	1σ	Ref.
Greenland	8	+ 22.5 ‰	1.31	(Lasher et al., 2017)
Europe	29	+ 22.9 ‰	1.36	(Verbruggen et al., 2011)
Europe	54	+ 22.2 ‰	0.08	(Lombino, 2014)
South America	7	+ 23.4 ‰	1.48	(Mayr et al., 2014)
Australia	11	+ 23.9 ‰	4.54	(Chang et al., 2017)
Australia	16	+ 12.9 ‰	6.05	(Chang et al., 2016)

Exact lake water residence times were not reported for these Australian lakes, but paired chironomid – lake water enrichment values that deviate most from the best fit line of all data in Fig. 2.2 were all sampled from lakes described as closed basins with residence times greater than 5 years. One possibility for the anomalous enrichment factors at these sites is that in lakes with long residence times, lake water $\delta^{18}O$ values used to estimate fractionation factors from a single sample likely do not reflect the $\delta^{18}O$ values of the water in which the chironomids grew. Alternatively, Chang et al., (2016) proposed that many of these lakes, also subject to enhanced evaporation in the arid environments of southern Victoria, Australia, were becoming nutrient and

salt concentrated, resulting in stressful ecological conditions that affected the enrichment factor in chironomids there.

Comparing calculated enrichment factors from all sites compiled in van Hardenbroek et al. (2018) with modeled site aridity and potential evapotranspiration (PET) reveals interesting patterns. Enrichment factors plotted against Aridity Index values (a quantification of average annual precipitation minus potential evapotranspiration, (Antonio and Robert, 2019)) at each lake site shows that sites with ε values that deviate most from the best fit line located generally located in arid, semi-arid or dry sub humid environments (Fig. 2.3). Many of the Australian lake sites sampled by Chang et al., 2016 are in such environments. ε values from other studies located in arid to dry sub-humid show better agreement with the mean enrichment value of 22.5 ‰. Additionally, several sites that also deviate from the best fit are located in particularly humid environments, suggesting other factors are responsible other than a measure of aridity. A comparison of enrichment factors with modeled PET (Antonio and Robert, 2019) may provide an answer for this conundrum. Lake sites that deviate most from the mean ε value are consistently located in regions with elevated PET (Fig 2.4). In the case of the Australian lakes, the combined effect of high PET, long lake water residence time, and singular lake water $\delta^{18}O$ samples likely explains anomalous ε values reported there. Furthermore, if local modeled mean annual precipitation $\delta^{18}O$ is substituted for lake water $\delta^{18}O$ values at the anomalous Australian sites, chironomids appear to have a ‰ offset closer to the expected mean value (Fig. 2.5). While AI does not appear to be a strong predictor for anomalous enrichment values, higher PET values at a lake site may result in apparent enrichment factors that differ greatly from the expected value. At lake

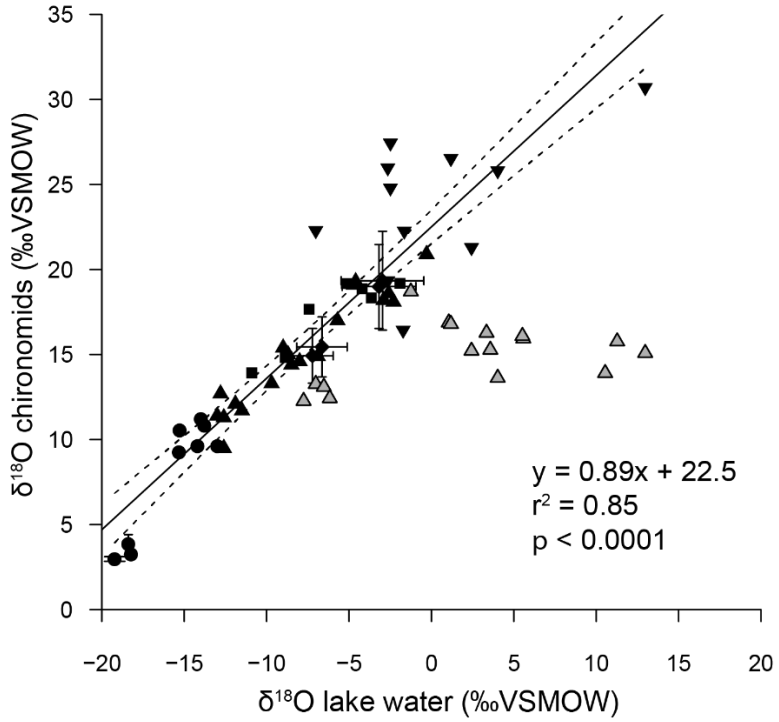

Figure 2.2. Relationship between $\delta^{18}O$ values of lake water and $\delta^{18}O$ values of chironomid head capsules from surface sediment samples. Plotted data points are from Verbruggen et al. (2011) (closed triangles), Lombino 2014 (closed diamonds), Mayr et al., 2015 (closed squares), Chang et al., 2016 (shaded triangles), Chang et al., 2018 (closed inverted triangles), and Lasher et al., 2017 (closed circles). Error bars indicate 1σ variability in replicate data from individual sites, where available. Sites from Chang et al., 2016 (shaded triangles) were not included in the regression. After van Hardenbroek et al., 2018.

sites subject to high PET, long term monitoring of lake water $\delta^{18}O$ should be employed to better characterize the relationship between chironomid and lake water $\delta^{18}O$ values.

Several studies have explored whether taxonomy plays an important role in determining chironomid enrichment factors. Unlike $\delta^{15}N$ and $\delta^{13}C$, there is currently no firm evidence that $\delta^{18}O$ enrichment factors vary among organisms at the sub-family level, though differences are documented between distinct aquatic invertebrates, e.g. Cladoceran ephippia vs. chironomids (Verbruggen et al., 2011). Differences in both $\delta^{18}O$ values and enrichment factors were reported

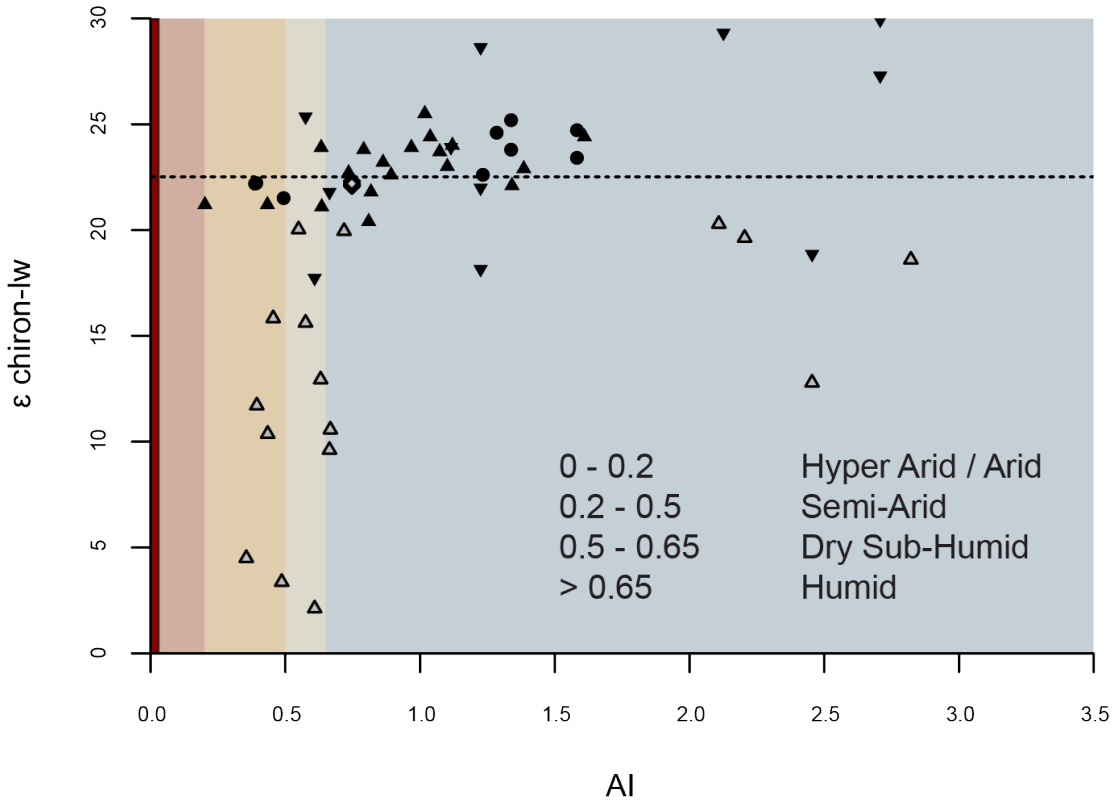

Figure 2.3. Demonstrated chironomid – lakewater enrichment factor (ε, ‰) versus the modeled aridity index (AI) (Antonio and Robert, 2019) at lake sites included in van Hardenbroek et al. (2018). Plotted data points are from Verbruggen et al. (2011) (closed triangles), Lombino 2014 (diamonds), Mayr et al., 2015 (closed squares), Chang et al., 2016 (shaded gray triangles), Chang et al., 2018 (closed inverted triangles), and Lasher et al., 2017 (closed circles).

on head capsules of two classifications of chironomids: the subfamily Tanypodinae, as well as the genus level *Chironomus*, in a suite of lakes from Australia (Chang et al., 2017; Chang et al., 2016). While values differ between the two groups, reported $\delta^{18}O$ values of Tanypodinae are not uniformly more positive or more negative than those of *Chironomus*, nor is there a systematic difference in enrichment factors. Additional research exploring whether differences in enrichment factors between growth water and chironomid $\delta^{18}O$ exist at the genus level are currently underway at Northwestern University.

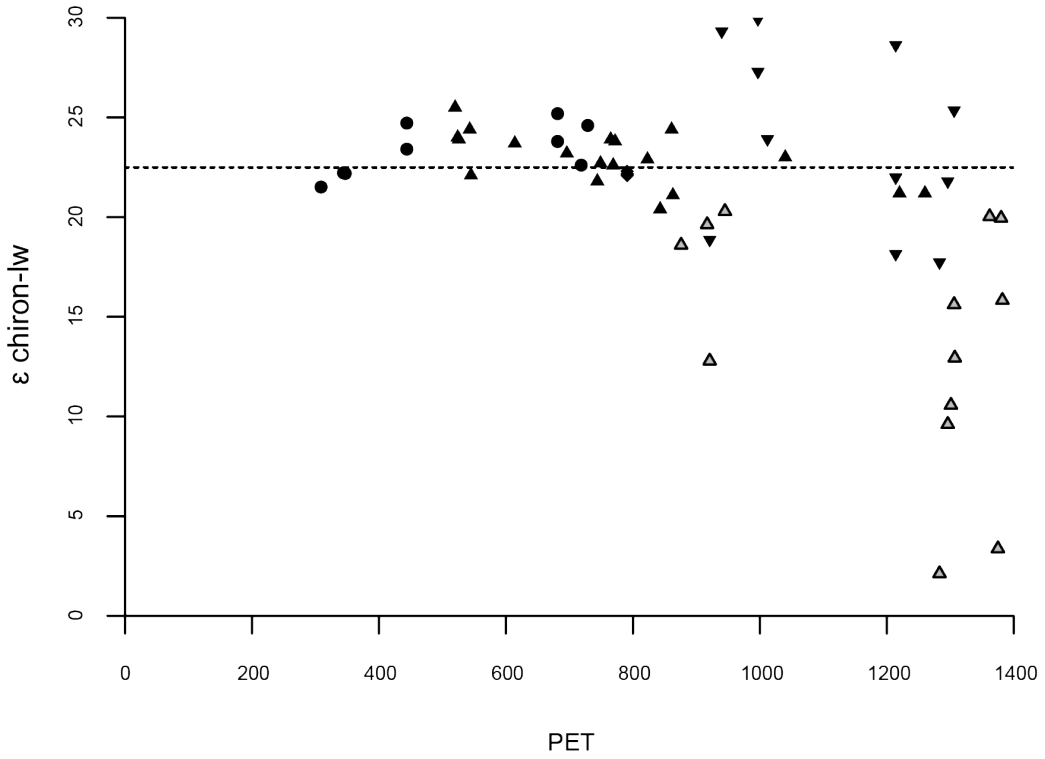

Figure 2.4. Demonstrated chironomid – lakewater enrichment factor (ε, ‰) versus potential evapotranspiration (PET, mm yr-1) (Antonio and Robert, 2019) at lake sites included in van Hardenbroek et al. (2018). Plotted data points are from Verbruggen et al. (2011) (closed triangles), Lombino 2014 (diamonds), Mayr et al., 2015 (closed squares), Chang et al., 2016 (shaded gray triangles), Chang et al., 2018 (closed inverted triangles), and Lasher et al., 2017 (closed circles).

2.4. Chemical pretreatment of chironomid head capsules for isotopic analysis

Chemical pretreatments of varying intensity are often used in chironomid based paleoecology studies. Gentle acid and base solutions have been used to clean and remove adhering clastic material from head capsules and generally assist in the deflocculation of sub samples prior to manual sorting. Commonly used treatments involve soaking sediment in a heated 5 to 10% potassium hydroxide (KOH) solution for up to an hour (Walker, 2001). Acid treatments involving hydrochloric acid (HCl) or sequential exposure to HCl and hydrofluoric acid (HF) have also been

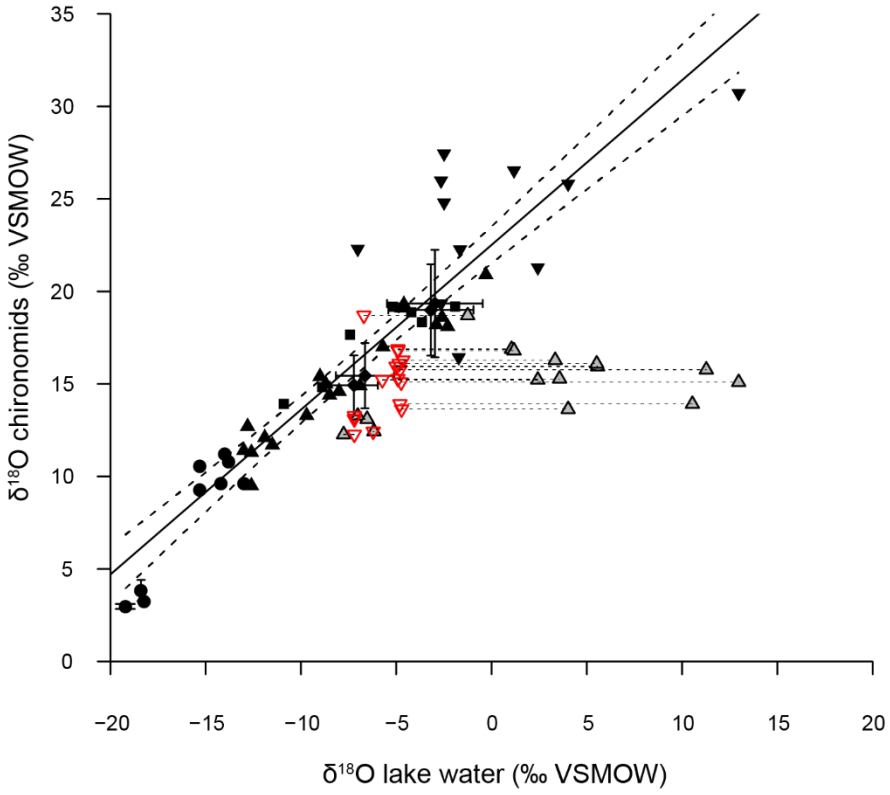

Figure 2.5. Data from Figure 2.2, replotted from van Hardenbroek et al. (2018). Red triangles correspond to modeled mean annual precipitation $\delta^{18}O$ values at lake sites plotted in gray (linked by the dashed lines) reported by Chang et al., (2016).

used when significant carbonate build up prevents easy identification (Walker, 2001). Though not used in paleoecology studies, the isolation of chitin from head capsules has been suggested for $\delta^{18}O$ analysis (Schimmelmann and DeNiro, 1986). A cellulose extraction technique, adapted for chitin, involving accelerated solvent extraction (ASE) with dichloromethane and methanol (DCl:MeOH) (9:1), followed by boiling in deionized water, and subsequent exposure to sodium chlorite ($NaClO_2$) and glacial acetic acid has also been tested on chironomid larvae (Leavitt and Danzer, 1993). While these methods do not alter head capsule morphology enough to prohibit taxa

identification, they can alter the isotopic composition and often produce a yield too low for isotopic analysis (Verbruggen et al., 2009).

These different pretreatment methods can result in up to 5 ‰ shifts in $\delta^{18}O$ values measured from chironomid head capsules (Verbruggen et al., 2009). Experiments comparing these various chemical methods on modern head capsules suggest two possible reasons for the apparent changes in $\delta^{18}O$. Pyrolysis gas chromatography mass spectrometry (py-GC/MS) and SEM evaluation of head capsules subjected to the different pretreatments showed changes in the ratio of chitin to protein products for acid and base treatments (Verbruggen et al., 2009). Strong acid treatments (e.g. prolonged exposure to HCl or HF) preferentially removed chitin from the head capsules and resulted in more negative $\delta^{18}O$ values compared to untreated head capsules. Conversely, strong base treatments (e.g. concentrated KOH) effectively removed the protein matrix, resulting in more positive $\delta^{18}O$ values than untreated head capsules (Verbruggen et al., 2009). The change in $\delta^{18}O$ due to the selective removal of the major molecular compounds suggests that chitin $\delta^{18}O$ in head capsules is more positive relative to protein, likely due to different fractionation effects during synthesis (Lombino, 2014; Nation, 2011). Alternatively, Verbruggen et al., (2009) proposed that strong acid treatments may have induced isotope exchange between isotopically light laboratory water and the head capsules. However, because the preferential removal of chitin also results in more negative $\delta^{18}O$ values in head capsules, it is difficult to assess the magnitude of this effect. One implication of the work by Verbruggen et al., (2009) is that if there is a natural loss of protein or chitin as the subfossils decay, then there may be a natural drift in $\delta^{18}O$ values over long time scales. Limiting the use of harsh chemical pretreatments (e.g. hot acid baths, or concentrated base

solution) when preparing chironomids, or other aquatic invertebrates, for $\delta^{18}O$ analysis may help preserve the original $\delta^{18}O$ values archived in the subfossils.

2.5. Diagenetic effects on chironomid head capsules

2.5.1. Diagenesis and taphonomy of marine and aquatic invertebrates

Preservation of chitinous organisms is largely dependent on the depositional environment. Though most studies classify chitinous invertebrates as relatively resistant to chemical and physical degradation (Baas et al., 1995; Tegelaar et al., 1989), remains do undergo degradation and diagenesis on short time scales (i.e. days to months). A handful of experiments have explored the decay (and conversely, preservation) of chitinous organisms in the geosphere, though most of these are limited to marine environments. The degree to which insect cuticles are sclerotized (intensity of bonding between chitin and protein complexes) appears to be vital for preservation as easily isolated and soluble proteins become recalcitrant, and add an additional matrix effect around the already resistant chitin molecules (Flannery et al., 2001; Schimmelmann, 2011). In chironomids, increased sclerotization is evident as a darkening or tanning in parts of the head capsule, e.g. the mentum (mouth parts) (Fig. 1.1).

Chitinous remains of insects are preserved in sediments spanning the Holocene to the Oligocene (Gupta et al., 2007). Though molecularly intact insect fossils are not known to exist beyond this, isolated chitin molecules from sponge remains have now been found in Cambrian strata (Ehrlich et al., 2013) supporting the idea that under ideal conditions this molecule can be incredibly resistant to decay. Environmental factors known to influence the rate of degradation include, temperature, pH, sediment deposition rate, oxygen content and organic productivity. An assessment of environments conducive to preservation indicates that high sedimentation rates, high

productivity and reducing conditions results in slower mineralization of chitinous organisms (Lehmann et al., 2002; Stankiewicz et al., 1998a).

Most studies exploring the degradation of insect cuticle under various conditions have only done so from a molecular composition or morphological perspective (e.g. Gupta et al., 2007; Stankiewicz et al., 1997), and to date, only a few studies have attempted to quantify diagenetic alteration effects on invertebrate isotopes. Laboratory based experiments of chitinous crustacean cuticle decay suggest that rapid biodegradation of proteins occurs in the first two weeks, exposing chitin fibrils to the environment (Poulicek and Jeuniaux, 1991). Experiments mimicking marine burial conditions showed that at ~8 weeks, partial alteration of the chitin molecule was detected using FT-IR, possibly reflecting a transition from chitin to chitosan through de-acetylation (Stankiewicz et al., 1998b). Schimmelmann et al. (1986) also explored diagenetic effects on isotopes of marine arthropods in simulated depositional environments. In a separate study, partial degradation of the arthropod carapaces under increasing thermal conditions was inferred from SEM imaging, however regular measurements of $\delta^{13}C$, $\delta^{15}N$ and $\delta^{18}O$ isotopes on samples throughout the 10 week study showed no substantial change (Schimmelmann et al., 1986). These conclusions are supported by the results of more recent studies of aquatic invertebrate isotopes. Perga (2011) found that $\delta^{13}C$ and $\delta^{15}N$ values of Cladoceran exoskeletons changed little over a three-month period if the remains were buried in sediments. Larger changes in isotope values were observed over a matter of weeks in exoskeletons that remained entrained in both oxic and anoxic water, but values stabilized after one to two months (Perga, 2011). In summary, changes in stable isotopic values (if any occur) likely happen in the first weeks of deposition. Over time scales of

months or longer, isotope values appear to remain stable, though this question clearly requires further examination, particularly regarding $\delta^{18}O$ values.

2.5.1. Fourier Transform Infrared Spectroscopy (FT-IR) examination of chironomid head capsules

To assess how the molecular structure of chironomid changes over longer time scales (e.g. thousands of years), subfossil head capsules from two northwest Greenland sediment cores were analyzed using Fourier Transform Infrared Spectroscopy (FT-IR). Head capsules from core 14-SEC-N1 (Secret Lake) were collected from modern (0-1 cm, 2014 CE) surface sediments, and at six depth intervals (10, 35, 55, 96, 118 and 143 cm) throughout the core. Head capsules were also collected from surface sediments (0-1 cm, 2014 CE) at Wax Lips Lake and from core 14WLL-2A at 15 depth intervals (18, 34, 43, 71, 81, 91, 141, 161, 176, 181, 187, 196, 201, 206, and 211 cm).

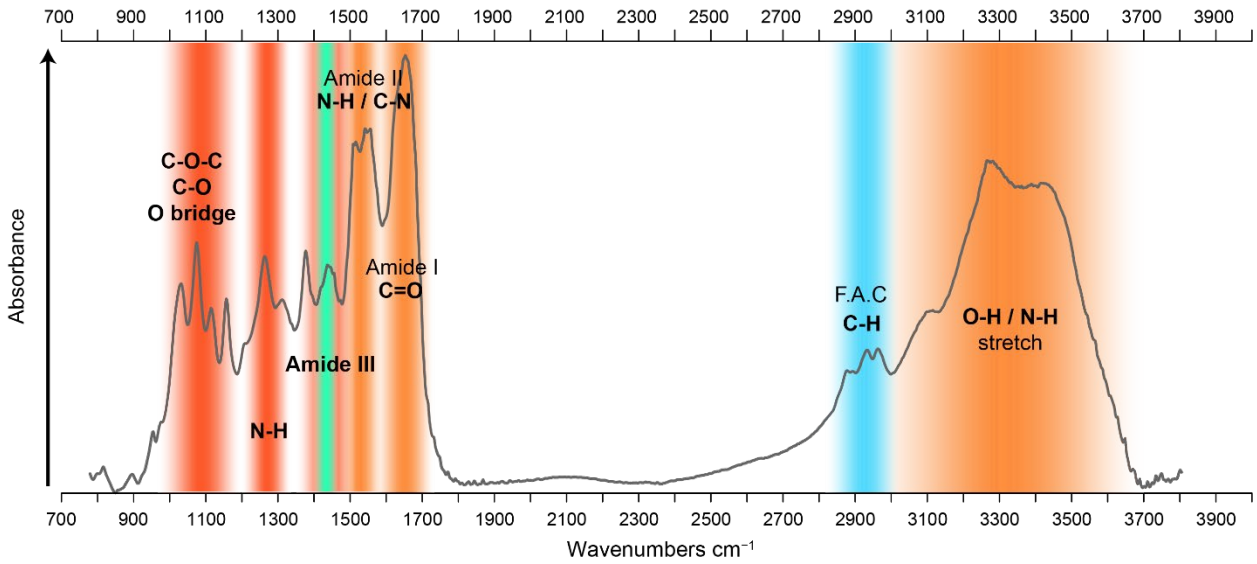

Figure 2.6. Characteristic Fourier Transform Infrared Spectroscopy (FTIR) spectra of a chironomid head capsule from a northwest Greenland lake (14-SEC-N1). Important band assignments are highlighted and attributed to the major molecular components in head capsules: orange – chitin and protein, red – chitin, green – protein, blue – aliphatic chains (FAC = fatty acid chains).

The core descriptions and chronologies for 14-SEC-N1 and 14WLL-2A are discussed in Chapter 3; Lasher et al., (2017) and McFarlin et al., (2018), respectively. Head capsules were cleaned with dilute (5%) KOH and DI water and then freeze dried to remove any adhering water, following standard procedure for stable isotope analysis. Then, two to five whole subfossils from each depth subsample were individually scanned using a Bruker Hyperion 2000 series FT-IR Microscope system between 700 and 4000 cm^{-1} at 32 times per 4 cm^{-1} resolution. The base line of raw spectra between 780 and 3800 cm^{-1} was then subtracted using the software package, Peak Fit.

FT-IR spectra from both Secret Lake and Wax Lips Lake show absorbance peaks characteristic of material composed of chitin and proteins (Fig. 2.6, 2.7, 2.8A). Broad peaks between 3000 and 3600 cm^{-1} correspond to the O-H and N-H stretching region in both compounds (Barth, 2007; Kaya et al., 2014). The shoulder on the O-H and N-H stretch peak at ~3100 cm^{-1} may also correspond to C-H stretching of aromatic structures present in proteins (Laity et al., 2015; Siddiqui et al., 2010). C-H stretching vibrations between 2800 and 3000 indicate the presence of aliphatic chains, likely fatty acids (Coelho et al., 2006; Lu et al., 2005). The region between 800 and 2000 cm^{-1} consists of many peaks attributable to both chitin and protein. Common peaks include the Amide I (C=O) and II (N-H / C-N) between 1550 and 1680 cm^{-1} (Barth, 2007; Kaya et al., 2014; Kaya et al., 2015; Kumirska et al., 2010). Some research has attempted to assign specific wavenumbers in the Amide I and II range to specific chitin and protein bonds. For example, peak deconvolution results on purified compounds indicate a strong C=O stretch at 1640 and 1630 cm^{-1} in isolated chitin (Kumirska et al., 2010). In isolated protein samples, similarly strong Amide I C=O stretch absorbances exist at 1650 and also at 1630 cm^{-1}; the latter peak overlaps directly with the previously mentioned chitin assignment (Barth, 2007). Unfortunately,

because both chitin and protein have common molecular bonds and associated absorbances in this region, it is difficult to assign specific peaks to one compound or the other in head capsules even with advanced peak deconvolution tools (e.g. Peak Fit). However, a decrease in the overall intensity of the Amide I or Amide II peak may indicate a loss of chitin or protein.

A comparison of the intensity of the Amide I peak at ~1660 cm^{-1} with the glucosamine associated C-O-C asymmetric stretching (a strong indicator of chitin) absorbance at ~1070 cm^{-1} (Kaya et al., 2014) shows some variability in the Holocene age sediments at Wax Lips Lake (Fig. 2.8B). Four of the Eemian age chironomid head capsules approach a ratio closer to one. This same ratio in a sample of purified Sigma Aldrich chitin is presented a red line in Fig. 2.8B for comparison. The intensity of the C-O-C peak exhibits high variability through time, but no long-term trend from the Holocene to the Eemian. This implies that the shift towards a 1:1 ratio between the peaks at ~1070 and ~1660 cm^{-1} is driven by a decrease in the intensity of the Amide I peak, likely due to progressive protein loss and is particularly evident in Eemian age samples. A separate comparison between peaks at ~1660 cm^{-1} (Amide I) and ~3260 cm^{-1} (N-H stretch) shows a similar trend towards the ratio present in purified chitin in Eemian age head capsules (Fig. 2.8C). Finally, there is also a rapid decrease in the intensity of a peak at 1508 cm^{-1} in the Eemian age samples through time (Fig. 2.7D). This peak could not be confidently assigned to likely molecular candidates present in head capsules but could be attributed to the disappearance of catechol moieties thought to enable bonding of the chitin and protein molecules as this peak has assigned to other aromatic compounds (Zhang et al., 2014). These same ratios were explored in the Secret Lake chironomid samples, but no clear trends are evident.

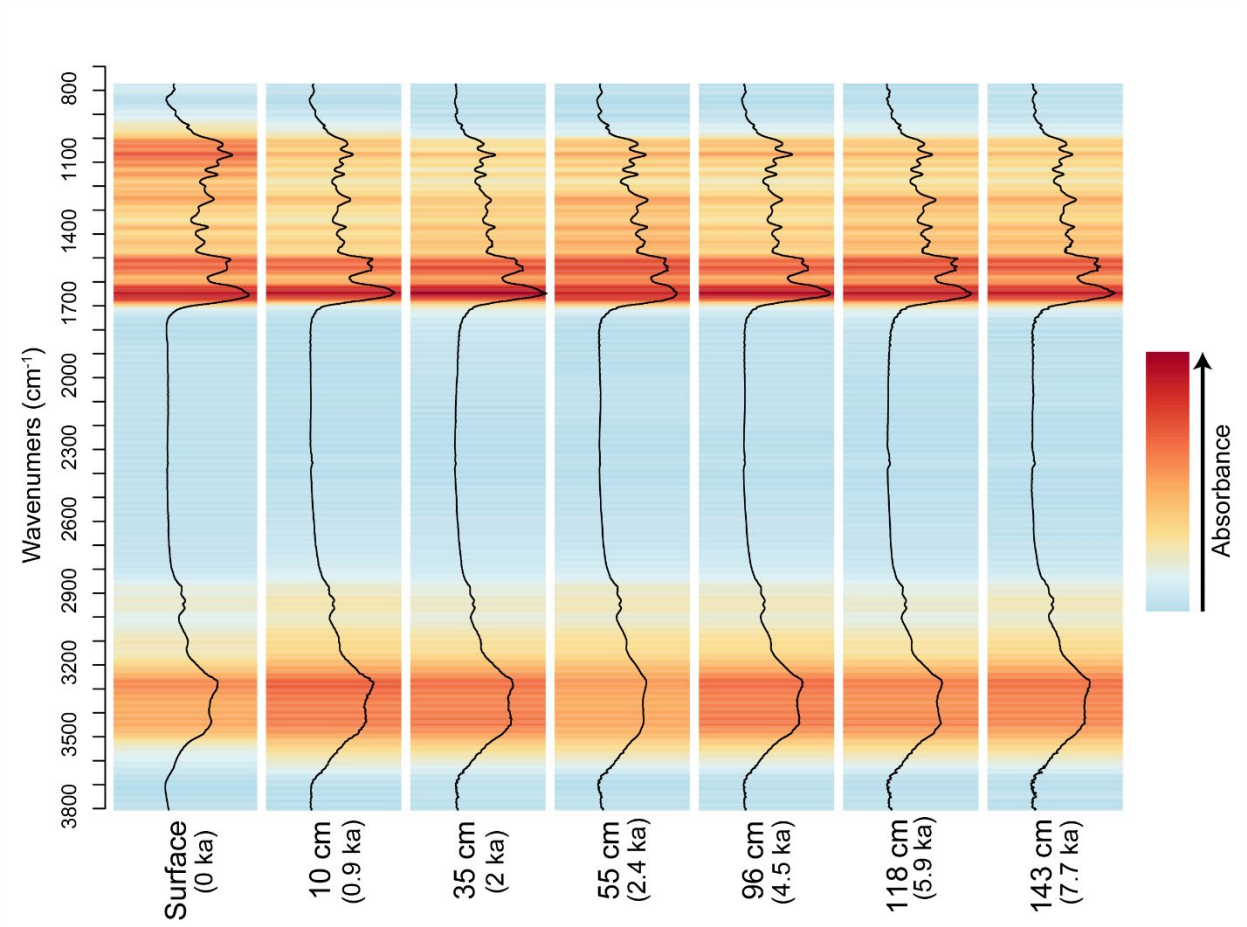

Figure 2.7. FT-IR spectra from chironomid head capsules in Secret Lake, northwest Greenland (core 14-SEC-N1, chronology and core description discussed in Chapter 3, Lasher et al. (2017)), spanning the Holocene.

Figure 2.8. (next page) A: FT-IR spectra from chironomid head capsules in Wax Lips Lake, northwest Greenland (core 14WLL-2A, chronology and core description discussed in McFarlin et al. (2018)), spanning the Holocene and the Eemian (the last interglacial period). Ages in the Eemian samples are estimated to be between 129 and 116 ka. B: Ratio of peaks at ~ 1070 cm^{-1} (corresponding to the C-O-C bonds between chitin monomers) and ~1660 cm^{-1} (amide I, C=O bond present in both chitin and many protein molecules). C: Ratio of peaks at ~1660 cm^{-1} and ~ 3270 cm^{-1} (N-H stretch in chitin and protein). The black and red band in B and C represents the same ratios in a purified Sigma – Aldrich chitin product. D: Ratio of peaks at ~1070 cm^{-1} and ~1508cm^{-1} (possible catechol aromatic structure). Blue line represents the base line of this ratio is Holocene age samples.

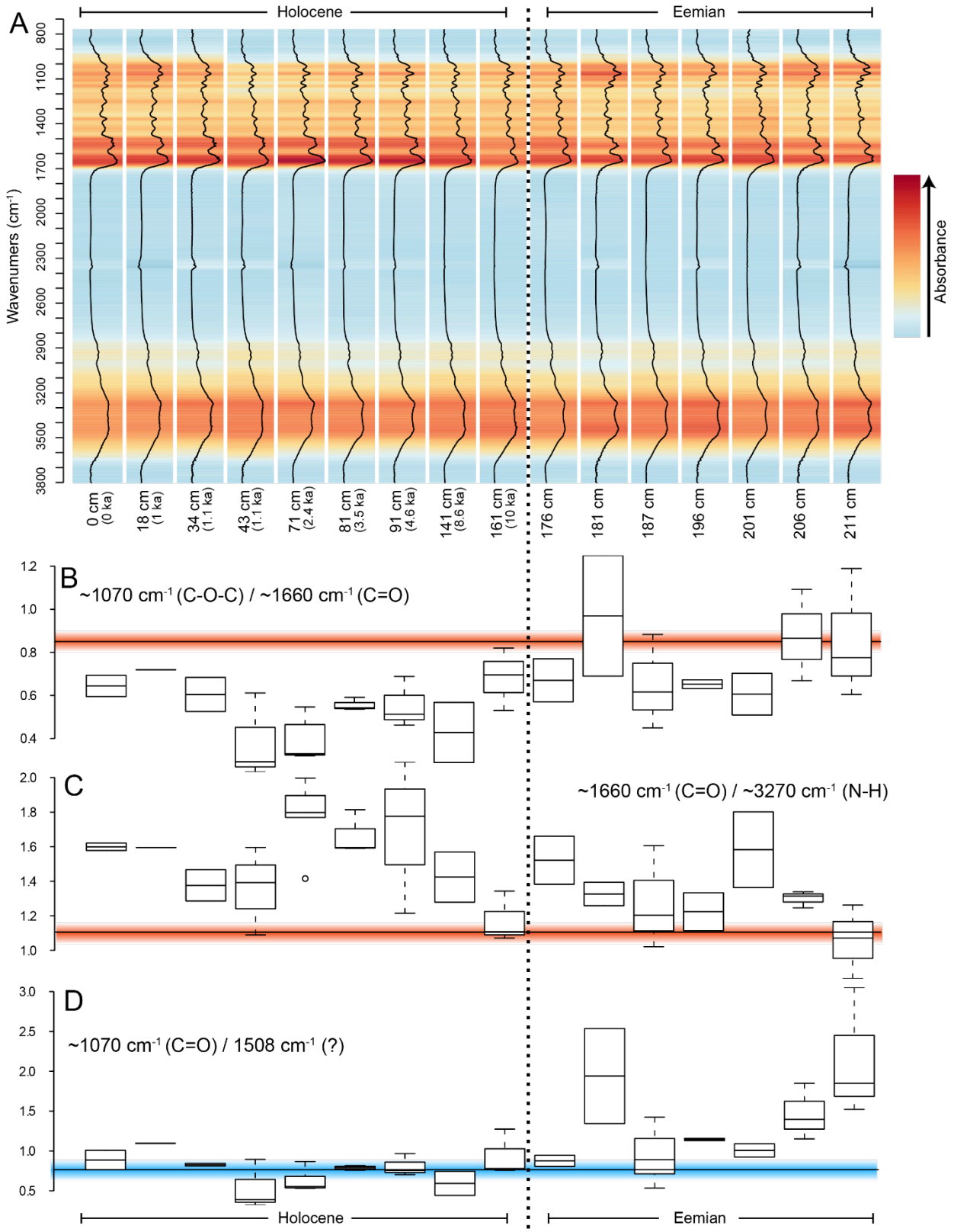
A
Holocene
Eemian
Wavenumers (cm-1)
800
1100
1400
1700
2000
2300
2600
2900
3200
3500
3800
Absorbance
0 cm (0 ka)
18 cm (1 ka)
34 cm (1.1 ka)
43 cm (1.1 ka)
71 cm (2.4 ka)
81 cm (3.5 ka)
91 cm (4.6 ka)
141 cm (8.6 ka)
161 cm (10 ka)
176 cm
181 cm
187 cm
196 cm
201 cm
206 cm
211 cm
B
~1070 cm-1 (C-O-C) / ~1660 cm-1 (C=O)
C
~1660 cm-1 (C=O) / ~3270 cm-1 (N-H)
D
~1070 cm-1 (C=O) / 1508 cm-1 (?)
Holocene
Eemian

2.6. Implications and conclusions

Chironomid head capsules, and other common aquatic invertebrates, are particularly well suited for stable isotope analysis due to their chemical composition (van Hardenbroek et al., 2018). While the focus of this Chapter, and this dissertation as a whole, is on the applicability of $\delta^{18}O$ in aquatic insect remains as a proxy for paleo lake water, some conclusions presented here may be widely applicable to other isotope systems, e.g. $\delta^{15}N$ or $\delta^{13}C$.

$\delta^{18}O$ values in chironomid head capsules reliably record the $\delta^{18}O$ values of the water in which they grow in many lakes around the world (van Hardenbroek et al., 2018). Interpreting climatic change from chironomid $\delta^{18}O$ values requires a thorough understanding of lake water hydrology and controls on lake water $\delta^{18}O$ values (Leng and Marshall, 2004). Chironomids collected in lakes with high precipitation/evaporation influences, or long residence times may be poorly suited for inferring temperature change, but are likely excellent candidates for reconstructions of effective moisture through time (e.g. Anderson and Leng, 2004; Leng and Anderson, 2003).

Taphonomic and diagenetic changes in the molecular composition of head capsules appear to be minimal over thousands of years. The results here confirm a Curie point pyrolysis investigation of chironomid head capsules from late glacial sediments in Europe (~16 ka) that showed chitin and protein composition comparable to modern head capsules (Verbruggen et al., 2009). Results from FT-IR analysis of chironomids show that absorbance peaks, characteristic of major chironomid head capsules biomolecules are present well into the Eemian interglacial (129 to 116 ka). In the most ancient samples analyzed, head capsules may have experienced some degree of selective loss of protein. Additionally, head capsules may experience a possible break

down in the cross-linking bonds joining chitin and protein moieties via loss of catechol moieties. However, better classification of catechols via FT-IR is needed to improve the confidence of this conclusion.

As described in section 2.4, the selective removal of protein over chitin in modern head capsules samples can lead to artificially more positive $\delta^{18}O$ values. A consequence of this protein loss is that in ancient samples, more positive $\delta^{18}O$ values may be due in part to diagentic effects. However, because the FT-IR approach used in this chapter is qualitative, placing constraints on an absolute amount of protein lost or a $\delta^{18}O$ (‰) shift associated with progressive protein loss is currently impossible. Furthermore, in the Secret Lake and Wax Lips Lake samples presented in this chapter, disentangling diagentic from climatic effects on $\delta^{18}O$ values is difficult. More positive $\delta^{18}O$ values in the oldest sediments in Secret Lake are expected due to warm climatic influences on $\delta^{18}O$ values in lake water during the early Holocene (Lasher et al., 2017). Similarly, high temperatures during the Eemian also likely resulted in more positive $\delta^{18}O$ values in chironomids. Considering these limitations, while it is possible that $\delta^{18}O$ values in ancient chironomid samples are slightly more positive than they would be if molecular composition remained truly unchanged over time, further research is needed to constrain the $\delta^{18}O$ changes associated with diagenesis (e.g. protein loss).

Significant, progressive loss of protein from head capsules through time is, however, problematic for interpreting $\delta^{18}O$ values in down core studies. FT-IR could be a useful pre-analysis tool to assess if molecular composition of head capsules is significantly different through time, thus preventing interpretation of altered $\delta^{18}O$ values. Also, FT-IR can provide a relatively easy way to check for contamination of samples compared to SEM analysis. Carbonate or diatom

contamination is problematic when attempting to use chironomids to reconstruct paleo lake water $\delta^{18}O$ values (Leng et al., 2006), and characteristic FT-IR wavenumbers can show the presence or absence of unwanted materials adhering to chironomid head capsules.

FT-IR is a fast, inexpensive and nondestructive method that can help assess potential diagenetic alteration of head capsules in ancient sediments, or contamination of samples. Though the approach used in this study is largely qualitative, quantitative results could be achieved variations on using attenuated total reflectance (ATR) FT-IR. Future paired FT-IR and $\delta^{18}O$ analysis comparing untreated and treated head capsules will be vital to better understanding the effects that pretreatments (and possibly diagenesis) have on head capsule molecular and isotope composition.

Acknowledgements

I thank N. Blair for providing lab access and training on the use of FT-IR and Peak Fit. I also thank P. Puleo, C. Lee and P. Kotecki who assisted with preparation of head capsules prior to FT-IR analysis.

CHAPTER 3:

Holocene temperatures and isotopes of precipitation in Northwest Greenland recorded in lacustrine organic materials

This chapter of research originally appeared in: Lasher, G.E., Axford, Y., McFarlin, J.M., Kelly, M.A., Osterberg, E.C., Berkelhammer, M.B., 2017. Holocene temperatures and isotopes of precipitation in Northwest Greenland recorded in lacustrine organic materials. Quaternary Science Reviews 170, 45-55. https://doi.org/10.1016/j.quascirev.2017.06.016

Abstract

Reconstructions of Holocene lake water isotopic composition based upon subfossil aquatic organic material offer new insights into Arctic climate. We present quantitative estimates of warmth during the Holocene Thermal Maximum in northwest Greenland, inferred from oxygen isotopes of chironomid head capsules and aquatic moss preserved in lake sediments. $\delta^{18}O$ values of chironomids from surface sediments of multiple Greenland lakes indicate that these subfossil remains record the $\delta^{18}O$ values of the lake water in which they grow. Our lake water $\delta^{18}O$ reconstruction is supported by downcore agreement with $\delta^{18}O$ values in aquatic moss and chironomid remains. $\delta^{18}O$ of both organic materials from Secret Lake decrease after 4 ka (ka = thousands of years ago) by 3 ‰ into the Neoglacial. We argue that lake water at Secret Lake primarily reflects precipitation $\delta^{18}O$ values, which is strongly related to air temperature in northwest Greenland, and that this signal is biased towards summer and early autumn conditions. Other factors may have influenced Secret Lake $\delta^{18}O$ values through the Holocene, including evaporation of lake water and changing seasonality and source of precipitation. The maximum early Holocene summer and early autumn-biased temperature anomaly at Secret Lake is 2.5 to 4°C

warmer than present from 7.7 (the beginning of our record) to ~6 ka. The maximum late Holocene cold anomaly (which includes the Little Ice Age) is 1.5 to 3°C colder than present. These ranges of possible temperature anomalies reflect uncertainty in the $\delta^{18}O$ – temperature relationship for precipitation at the study site through the Holocene.

3.1. Introduction

By the end of this century, temperatures are predicted to increase in the Arctic between 2 and 9 °C (IPCC, 2013). Reducing the uncertainty around these estimates has important societal implications, and studies of past climate conditions can help clarify how climate change may occur in the Arctic. During an early to middle Holocene Thermal Maximum (HTM), summers were warmer than present across most of the Arctic between 9 and 5 ka, driving the most extensive retreat of the Greenland ice sheet (GrIS) since the end of the last glacial maximum at ~11 ka (Lecavalier et al., 2013). This time period provides an opportunity to test the sensitivity of the GrIS to the most recent sustained warm period in the Arctic, however the magnitude and spatiotemporal expression of the HTM in Greenland (and the Arctic as a whole) was heterogeneous and is not yet fully characterized (Briner et al., 2016; Kaufman et al., 2016). Climate records in northwest Greenland are sparse, leaving the timing and magnitude of the HTM in this sector of the Arctic largely unresolved. Estimates of sea surface temperatures in nearby Baffin Bay (Levac et al., 2001) and air temperature estimates based upon oxygen isotopes ($\delta^{18}O$) in the Agassiz ice core (Lecavalier et al., 2017; Lecavalier et al., 2013) and pollen in lake sediments (Gajewski, 2015) provide evidence for temperature shifts at nearby sites during the Holocene, but differ in the timing and magnitude of past warmth. Additional proxy records from beyond the Greenland Ice Sheet will aid in clarifying the region's climate response to insolation trends.

To reconstruct a Holocene climate history for the Thule region of northwest Greenland, we employ $\delta^{18}O$ values from analyses of subfossil aquatic organic material in lake sediments. We measured $\delta^{18}O$ of chironomid larval head capsules and aquatic moss stems preserved in the sediments of a precipitation-fed lake to infer past lake water isotopic composition and, by

extension, interpret possible climatic controls on precipitation $\delta^{18}O$. Previous work has demonstrated that $\delta^{18}O$ values of chironomid head capsules reflects the isotopic composition of the water in which they grow in both laboratory culturing experiments and modern lakes (Mayr et al., 2014; Verbruggen et al., 2011; Wang et al., 2009; Wooller et al., 2004), and we report chironomid $\delta^{18}O$ values from surface sediments of four Greenland lakes that further support this observation. Additionally, parallel downcore measurements of bulk carbonate and chironomid head capsule $\delta^{18}O$ values yielded very similar reconstructions of lake water isotopes through the late glacial at Rotsee (Switzerland) (Verbruggen et al., 2010). Given the fidelity of chironomid oxygen isotopes as a proxy for lake water, and the relationship between oxygen isotopes of precipitation and air temperature, we employ our down core record of oxygen isotopes measured from chironomids in Secret Lake to constrain the amplitude and timing of Holocene temperature trends and HTM warmth in northwest Greenland. This record also provides estimates of shifts in the stable isotopes of precipitation over northwest Greenland through the Holocene, providing an independent comparison with $\delta^{18}O$ records from nearby ice cores obtained from northern Greenland and the eastern Canadian Arctic.

3.2. Methods, Study Sites and Materials

3.2.1. Study sites and field work

Modern lake water and surface (top 1 cm) sediment samples containing aquatic organic material from four Greenland lakes were collected in the summers of 2014 and 2015. Two lakes are in northwest Greenland, near Thule, and two are in southwest Greenland, near Nuuk (Table 3.1). Results from these new lakes add to existing datasets describing modern chironomid $\delta^{18}O$ –

lake water relationships (Mayr et al., 2014; Verbruggen et al., 2011). Surface sediments were recovered using a 6" x 6" Ekman dredge. Water samples from lakes, their inflows and, when available, precipitation were collected at surface sediment sites. Lake water and inflow samples were collected in 10 mL zero headspace glass vials or 30 mL HDPE Nalgene bottles, and taped to prevent evaporation. Samples from lakes and inflows were collected by hand up to 30 cm below the water surface. Snow from a single storm in 2014 was gathered from the ground (< 12 hours after snowfall in late August) into a 1000 mL Nalgene bottle and taped.

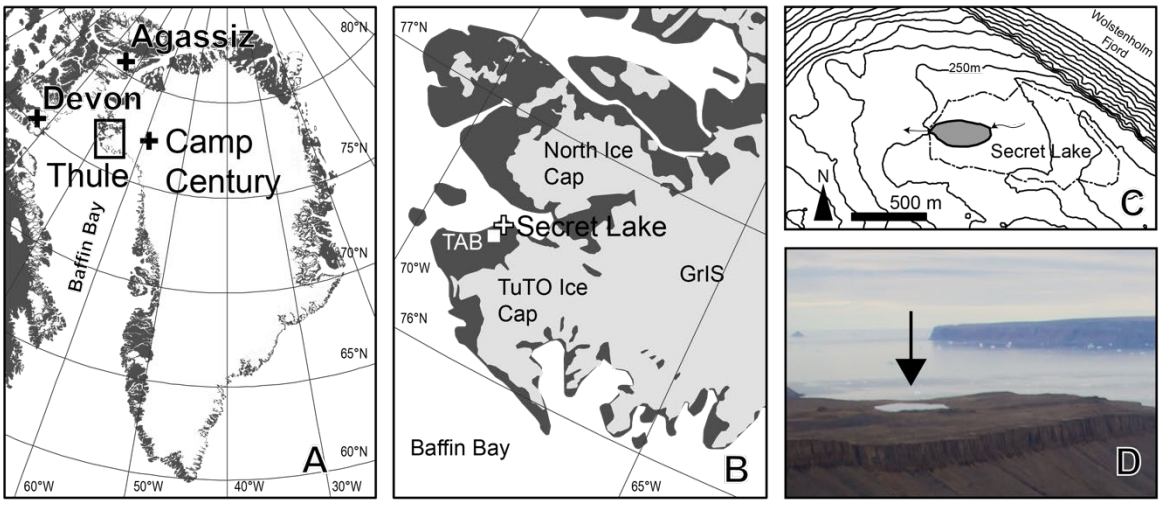

Figure 3.1. A: Location of Thule, Greenland and the Agassiz, Devon and Camp Century ice core sites. B: Regional map of the Thule region with major glacial features and Secret Lake. GrIS is the Greenland Ice Sheet, TAB is Thule Air Base. Shaded light gray areas represent modern glaciers / ice sheets, and dark gray represents ice-free land. C: Local topography around Secret Lake. Contours are at 20 m intervals (asl). The dashed line represents Secret Lake's watershed. D: Oblique aerial view of Secret Lake indicated by the arrow looking west towards Baffin Bay in the distance.

Secret Lake (informal name; 76.5798°N, 68.6619°W, Fig. 3.1) is a shallow (3.4 m maximum depth) 0.05 km^2 lake, situated 250 m above sea level and above the local marine limit.

The lake is < 2 km from Wolstenholme Fjord and ~ 50 km from the open waters of Baffin Bay. Secret Lake is currently precipitation fed by a 0.5 km^2 watershed. This catchment includes several small (1 m^2) connected pools along the main inflow NE of the lake, all of which are precipitation fed as well. The active layer of Thule's continuous permafrost is between 0 and 2 m (Bjella, 2013). Additionally, Secret Lake's small catchment is elevated well above local river systems (Fig. 3.1), precluding inputs from any other source, including outlet glaciers of the GrIS. Since regional deglaciation around 10.7 ka, there is no evidence that the ice sheet, now 13 km away, advanced far enough to enter the present day watershed (Corbett et al., 2015; Corbett et al., 2016). The lake is ice-covered for much of the year but overflows into a surface outflow stream during the ice-free summer months, including during our visits to the site in late August of both 2014 and 2015. All of these aforementioned catchment characteristics make Secret Lake an excellent candidate to reconstruct past isotopes of precipitation.

Table 3.1. Greenland lakes where surface sediments and lake-water were sampled in August 2014 or 2015.

Lake Name	Latitude (°N)	Longitude (°W)	Depth (m)	Surface Elevation (m a.s.l.)	$\delta^{18}O_{lake\ water}$	$\delta D_{lake\ water}$	$\delta^{18}O_{\ chironomids\ (0\text{-}1\ cm)}$
Secret Lake	76.580	–68.659	3.2	250	–18.5	–143.3	3.8
Stardam	76.665	–67.941	5.25	221	–19.2	–151.1	2.9
T1	63.757	–51.356	9	25	–15.2	–104.5	10.5
T2	63.757	–51.364	11	43	–15.3	–104.7	9.3

T1 and T2 are informal names. All lakes are isolated from glacial meltwater. $\delta^{18}O/\delta D$ values are reported in per mil, relative to VSMOW.

We recovered a 1.44 m sediment core (core 14-SEC-N1) from 3.36 m water depth in Secret Lake using a hammer driven Nesje piston system in August 2014. Coring stopped when we met

resistance and repeated hammering did not advance the core tube further into the sediment. We bagged the top 2 to 3 cm of sediment, including the sediment water interface while recovering the core in the field. Basal sediments are dense diatomaceous clay with abundant aquatic moss material. We also acquired an accompanying surface sediment sample (top 0-1 cm) using an Ekman dredge less than 2 meters from the core site.

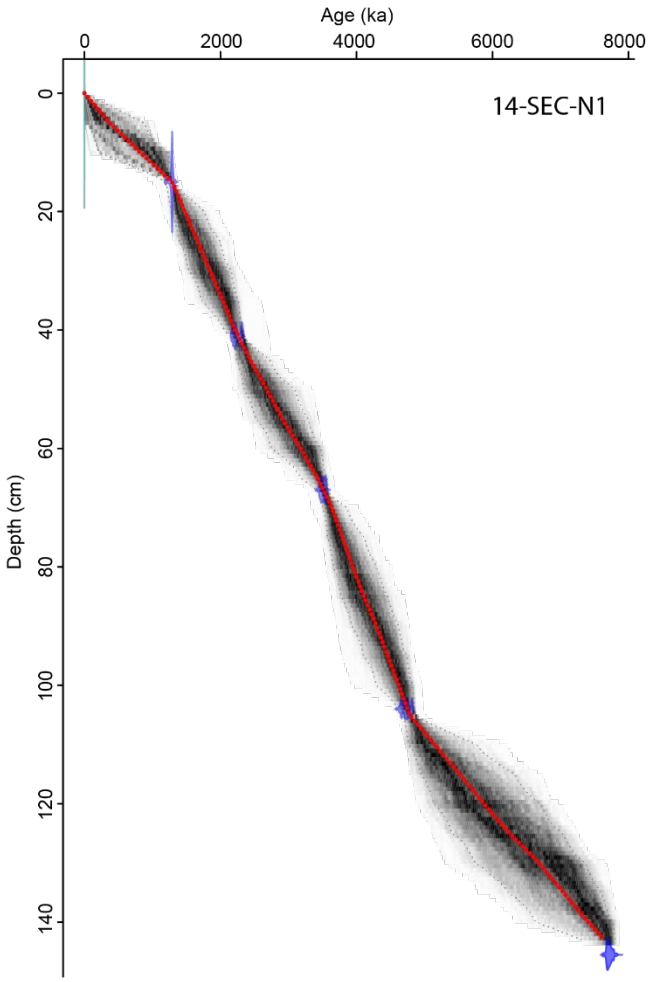

Figure 3.2. Age-depth model for 14-SEC-N1, with calibrated ^{14}C dates and their respective probability density functions (transparent blue) and inferred modern surface (green bar). Darker greys indicate more likely calendar ages bounded by 95% confidence intervals; the red curve shows the single 'best' model based on the weighted mean age for each depth.

Despite the shallow depth of the lake, and wind storms in excess of 70 knots that occurred less than 1 week prior to sampling, wave action does not appear to have disturbed surface sediments, as laminated stratigraphy is intact in the top 5 cm of a nearby surface core. Water column clarity measured shortly after the storm using a Secchi disk was ~ 3 m, further evidence that widespread suspension of sediments by wave action is not problematic even in this relatively shallow lake.

Secret Lake is less than 6 km distance and less than 100 m different in elevation from Thule Air Base (TAB), where long term historical climate monitoring provides valuable information for interpreting our modern and paleo $\delta^{18}O$ record. Daily temperatures, relative humidity and precipitation are available from the TAB meteorological station from 1951 to 2012. Mean annual air temperatures (MAAT), mean July temperatures (MJT) and mean annual precipitation (MAP) at TAB are –11 ± 1.3 °C, 6 ± 1.2 °C and 184 ± 56 mm mean water equivalent per year (mm w.e. yr^{-1}) respectively. Additionally, an International Atomic Energy Agency (IAEA) monitoring station at TAB collected monthly temperature and $\delta^{18}O$ / δD values of precipitation from 1966 to 1971, accessible through the IAEA's Global Network of Isotopes in Precipitation online portal (IAEA/WMO, 2015).

3.2.2. Geochronology

The 14-SEC-N1 chronology is based upon six AMS ^{14}C ages on cleaned, hand-picked aquatic moss remains. Ages were calibrated using Calib 7.1 and IntCal13 (Reimer et al., 2013; Stuvier et al., 2005). The age-depth model was developed with the Bacon package in R, which

uses Bayesian statistics to calculate probable sedimentation rates (Blaauw and Christen, 2011). The final age depth model output is produced using over 7 million iterations (Fig. 3.2).

3.2.3. Preparation of chironomids for $\delta^{18}O$ measurements

Two to four gram aliquots of bulk sediment, representing 0.5 to 1.5 cm of core depth, were deflocculated in a 10% KOH solution at 20 °C for 30 minutes. Processed sediment was thoroughly rinsed with DI water over a 150 micron sieve, and then chironomid remains were independently hand-picked, checked and cleaned of any remaining adhering sedimentary material. Wet remains were transferred to Nanopure water in pre-weighed and oven dried 3.2 x 4 mm lightweight Elemental Microanalysis ® silver capsules. Filled capsules were crimped gently, freeze dried for at least 5 days immediately prior to isotope measurements, and then reweighed to determine the dry sample mass. We picked 150 to 200 individual head capsules for each sample to obtain adequate mass (between 150 and 200 μg) for these analyses.

Hot acid and alkali baths (60 to 70 °C) proposed by Wang et al. (2009) have been shown to both preferentially remove the chitin and protein moieties from modern whole insects (including head capsules) during pre-treatment, and potentially induce oxygen exchange with laboratory water. This may result in erroneous oxygen isotope values depending on whether chitin or protein was removed during processing, or whether lab water oxygen was exchanged with cuticles (Verbruggen et al., 2009). In contrast, cool (20 °C) alkali baths were shown by Verbruggen et al. (2009) to not significantly affect the $\delta^{18}O$ values of head capsules.

To assess whether pretreatment to remove carbonate was needed for our samples, we analyzed subfossil head capsules at 7 levels (0, 10, 35, 55, 96, 118 and 143 cm) throughout the

core to check for the presence of adhering carbonates using Fourier Transform Infrared Spectroscopy (FT-IR). Head capsules were cleaned with KOH and DI water as described above, then 3 to 4 whole subfossils from each depth subsample were individually scanned using a Bruker Hyperion 2000 series FT-IR Microscope system between 600 and 4000 cm^{-1} at 32 times per 4 cm^{-1} resolution. Peaks at ~712, ~862 and ~1440 cm^{-1} are characteristic of carbonate and correspond to the in-plane bending vibration, the out-of-plane bending vibration and the asymmetric stretching of bonds in a CO_3^{2-} molecule, respectively (Liu et al., 2013; Reig et al., 2002; Xia et al., 2015). These characteristic carbonate peaks were not present in the spectra of any samples (representative spectrum are shown in Fig. 3.3). Geologic surveys of the area also indicate no carbonate bedrock in our study area (Dawes, 2006). Considering the results of visual and FT-IR inspection of head capsules, and the possible effects of acid pretreatment on chironomid exoskeletons, as suggested by Verbruggen et al. (2009), we did not treat chironomids with HCl.

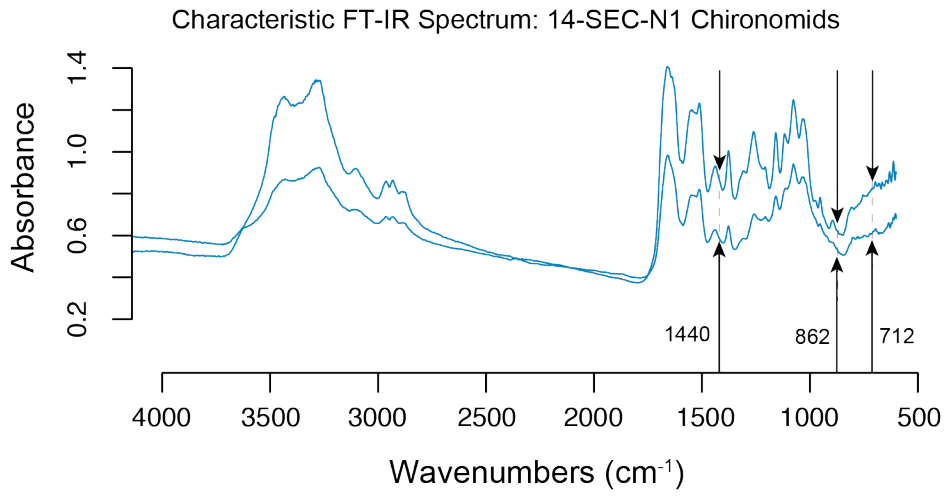

Figure 3.3. Fourier Transform Infrared Spectroscopy (FT-IR) spectrum characteristic of chironomid head capsules from the 14-SEC-N1 core. The absence of peaks at ~712, 862 and 1440 cm^{-1} indicate that carbonates are not adhering to head capsules prior to oxygen isotope analysis.

3.2.4. Preparation of aquatic moss for $\delta^{18}O$ measurements

Past studies exploring the relationship between aquatic plants and host waters have typically isolated the cellulose component from aquatic plant remains for $\delta^{18}O$ analysis (DeNiro and Epstein, 1981; Mayr et al., 2014; Sauer et al., 2001). Such extraction methods address the uncertainties that arise from different isotope effects in the various compounds that make up bulk plant material. Nonetheless, recent investigations into $\delta^{18}O$ values of bulk aquatic moss remains show strong correlations with isolated cellulose from the same sample, within ~1 ‰ (Jones et al., 2014; Zhu et al., 2014). Subfossil mosses (*Warnstorfia exannulata*) were picked from the Secret Lake core and thoroughly cleaned with DI water, then soaked in a 10% HCl solution at room temperature for 1 hour. We did not treat the samples with HF as described in Zhu et al. (2014) due to the demonstrated lack of carbonates in the watershed, but all samples were rinsed again with DI water, then inspected for any remaining adhering material under a 30 x dissecting microscope. Leaves were then removed manually, isolating 70 to 120 μg of stem for isotope analysis. Typically, a single stem section was used, however, in the upper 20 cm of the core, multiple stem remains were often required to achieve sufficient mass. Samples were then placed in water in silver capsules and freeze-dried as described for chironomid head capsules above.

3.2.5. $\delta^{18}O$ analysis

The oxygen isotope composition of chironomid head capsules and moss stems were measured using a Thermo Scientific™ High Temperature Conversion Elemental Analyzer (TC-EA) coupled to a Thermo Scientific™ Delta V Isotope Ratio Mass Spectrometer (IRMS). Standards of known oxygen isotopic composition (IAEA-CH3, IAEA-CH6, IU Benzoic acid,

NBS-127 and IAEA-SO5) were analyzed among all unknown sample runs. Additionally, we analyzed a previously unknown internal chitin standard, acquired from Sigma-Aldrich, due to its stoichiometric similarity to our unknown chironomid head capsules. Duplicate analyses of standards yielded analytical errors of 0.33 ‰ for the IRMS run in which we analyzed chironomid remains, and 0.41 ‰ for the run analyzing moss remains. Duplicate analyses of unknown materials down core yielded sample to sample errors of 0.52‰ for chironomids and 0.4 ‰ for the mosses. All $\delta^{18}O$ values are reported as per mil (‰) relative to VSMOW.

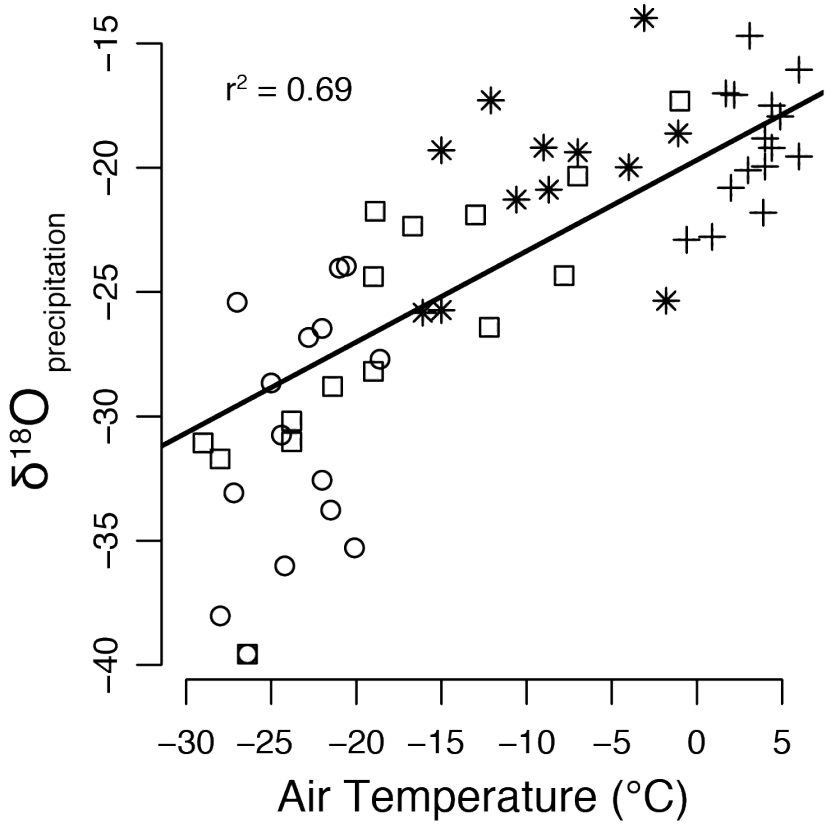

Figure 3.4. Monthly (1966 to 1971) $\delta^{18}O$ values of precipitation and temperature measurements for Thule from WMO - IAEA/GNIP. Open circles are winter (DJF) measurements, open squares are spring (MAM), cross symbols are summer (JJA) and stars are autumn (SON). The solid black line is a linear regression fit representing the annual $\delta^{18}O$ values of precipitation – temperature relationship, weighted to the amount of precipitation (0.46 ‰ $^{o}C^{-1}$).

Modern lake water and precipitation isotopes were analyzed with a Picarro L2130-*i* Analyzer. Field samples (taped 10 mL bottles with zero headspace) were transferred to septum-capped vials, injected into a heated vaporizer, and then analyzed via cavity ring-down spectroscopy (Gupta et al., 2009). Repeated (8x) 1.2 µL injections for standards across all runs yielded analytical uncertainties < 0.08 ‰, and unknown sample to sample errors of 0.17‰.

3.3. Results

3.3.1. Core description and geochronology

Core 14-SEC-N1 is composed of 144 cm of banded (1 to 3 cm bands) grey to light brown gyttja. Coarse plant remains are preserved throughout the core, but decrease in abundance towards the top 20 cm, which is also characterized by finer, darker laminae (< 0.5 cm). Plant material down core is dominantly aquatic moss stems. These subfossil plant remains as well as modern mosses acquired during the 2014 field season are *Warnstorfia exannulata*, common in high latitude Arctic lakes, often forming extensive mats across lake bottoms (Ole Bennike, pers comm; Guo et al., 2013).

The six AMS ^{14}C results provide a millennial scale age-depth model and sedimentation history. No ages were considered outliers and replicate basal moss samples yielded identical calibrated ages of 7,730 yr (Table 3.2). The mean sedimentation rate for Secret Lake is 50 yrs cm^{-1}. From 7.7 ka to 5 ka, rates are slightly lower at 75 yrs cm^{-1}. From 5 ka to about 1.8 ka, rates increase to between 30 and 40 yrs cm^{-1}. Rates once again decrease to 90 yrs cm^{-1} from 1.8 ka to the top of the core.

Table 3.2. Radiocarbon ages from Secret Lake

Core	Depth (cm)	Lab Number	Material Dated	Fraction Modern	$\delta^{13}C$ (‰ PDB)	Radiocarbon Age (^{14}C yr BP)	Calibrated Age (cal yr BP)
14-SEC-N1	15.5-16	OS-115371	Plant Macrofossils	0.8437 ± 0.0019	–29.6	1360 ± 20	1290 ± 10
14-SEC-N1	41.5-42.5	OS-115372	Plant Macrofossils	0.7558 ± 0.0017	–29.8	2250 ± 20	2250 ± 80
14-SEC-N1	68-68.5	OS-115478	Plant Macrofossils	0.6649 ± 0.0016	–31.0	3280 ± 20	3510 ± 40
14-SEC-N1	104-105	OS-115479	Plant Macrofossils	0.5943 ± 0.0016	–28.9	4180 ± 20	4730 ± 90
14-SEC-N1	146-147	OS-115480	Plant Macrofossils	0.4249 ± 0.0015	–28.5	6880 ± 30	7730 ± 65
14-SEC-N1	146-147	OS-125562	Plant Macrofossils	0.4239 ± 0.0012	Not reported	6890 ± 25	7730 ± 60

Calibrated ages are reported as the midpoint of the 2σ range ± ½ of 2σ range.

3.3.2. $\delta^{18}O$ values of Thule-region precipitation and lake water

The relationship between average annual $\delta^{18}O$ of precipitation and mean annual surface temperature calculated from several years of historical (1966-1971) IAEA GNIP monitoring at TAB is 0.44 ‰ $°C^{-1}$ (r^2 = 0.66) (Fig. 3.4; IAEA/WMO, 2015). Continuous meteorological monitoring at TAB from 1952 through 2012 indicates that 29 and 35% of annual precipitation in the Thule area falls during the summer and autumn months, respectively (Wong et al., 2015). When monthly precipitation amounts (and their corresponding isotope values) are weighted with respect to total annual precipitation, the slope is marginally steeper at 0.46 ‰ $°C^{-1}$ (r^2 = 0.69), reflecting the greater influence of summer and autumn precipitation. These local relationships from time series are more shallow than the global spatial relationship (0.67 ‰ $°C^{-1}$) documented by Dansgaard (1964). Previously estimated Greenland isotope-temperature relationships for precipitation over the last 9000 years, however, appear to be more comparable to what we observe for Thule GNIP samples than to the global spatial relationship. Studies comparing Greenland ice core $\delta^{18}O$ values with borehole temperature inversions from Greenland ice cores during the

Holocene, and gas occlusion based methods before the last glacial termination converge on a relationship between 0.44 and 0.53 ‰ $°C^{-1}$ (Buizert et al., 2014; Dahl-Jensen et al., 1998; Vinther et al., 2009). Seasonal relationships between temperature and $\delta^{18}O$ values of precipitation from the Thule IAEA data vary between 0.25 ‰ $°C^{-1}$ for autumn to 0.73 ‰ $°C^{-1}$ for winter (Table 3.3). Large seasonal changes in this relationship are expected in the high Arctic where the temperature and other climatic differences between winter and summer are more extreme than much of the world (Rozanski et al., 1993).

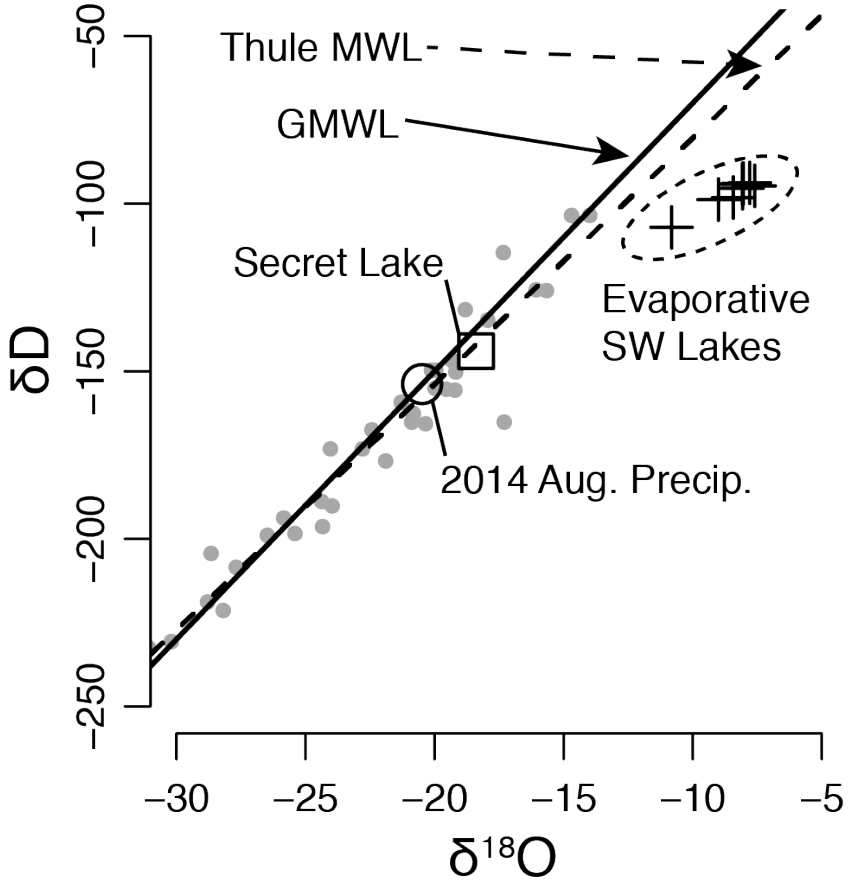

Figure 3.5. (previous page) Isotopes of Secret Lake (August 2014) lake water and August 2014 precipitation (a single snowstorm), compared with meteoric waters. Grey points are historical isotopes of precipitation from IAEA monitoring at Thule Air Base, 1966 - 1971; (WMO - IAEA/GNIP 2015), GMWL is the global meteoric water line (Craig, 1961); The Thule MWL is a linear regression from the IAEA historical monitoring. Crosses are July 2014 lake water from SW Greenland lakes near Kangerlussuaq at the head of Sondre Stromfjord, where lakes are known to experience significant evaporative enrichment in a relatively warm, dry summer climate (Leng and Anderson, 2003). $\delta^{18}O/\delta D$ values are reported in per mil, relative to VSMOW.

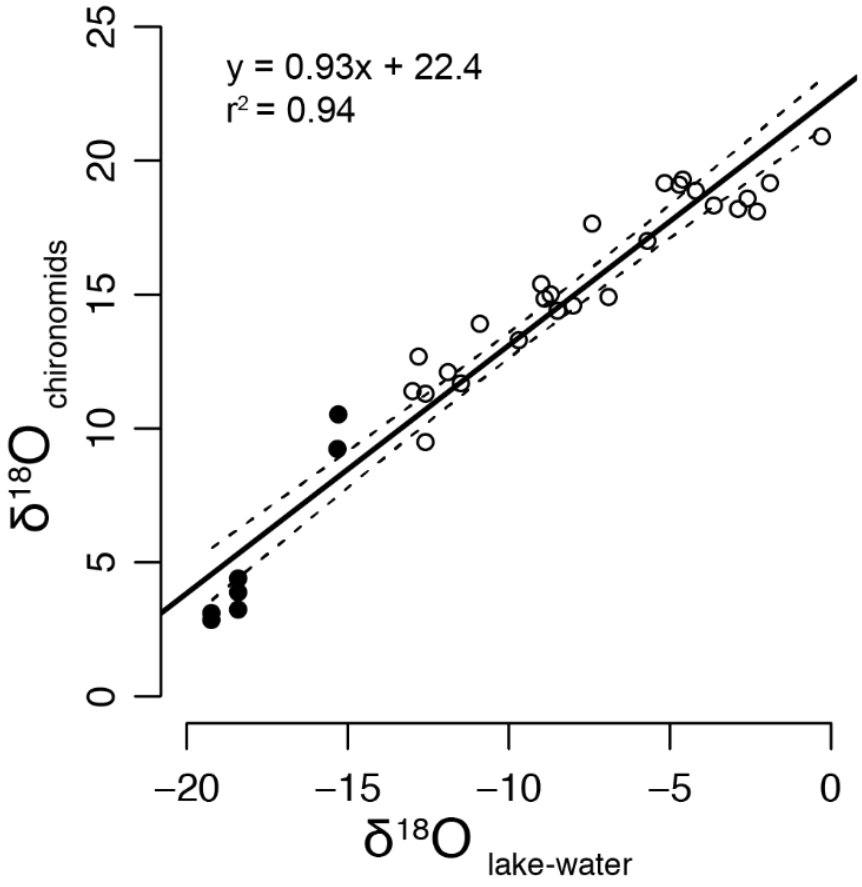

Figure 3.6. Global relationship between $\delta^{18}O$ values of chironomid head capsules and lake waters with 95 % confidence intervals. New data from Greenland surface sediments are plotted as solid circles. Previous field-based studies by Verbruggen at al., 2011 and Mayr at al., 2014 are plotted as open circles. Wooller et al. 2004 do not report lake water $\delta^{18}O$ values. $\delta^{18}O$ values are reported in per mil, relative to VSMOW.

Table 3.3. Mean seasonal $\delta^{18}O$ values of Thule meteoric waters collected by the IAEA (1966 – 1971) and slopes of the $\delta^{18}O$-temperature relationships (WMO - IAEA/GNIP 2015)

	Annual $\delta^{18}O$	Spring $\delta^{18}O$	Summer $\delta^{18}O$	Autumn $\delta^{18}O$	Winter $\delta^{18}O$
Average $\delta^{18}O$	–25.9	–25.9	–18.9	–21.1	–30.5
Max. $\delta^{18}O$	–14.0	–17.3	–14.7	–14.0	–24.0
Min. $\delta^{18}O$	–39.6	–39.6	–22.9	–25.8	–39.6
Seasonal T°C- ‰ Slope	0.44	0.57	0.59	0.25	0.73
Amount weighted T°C- ‰ Slope	0.46				

* Spring is MAM, summer is JJA, autumn is SON, and winter DJF. $\delta^{18}O$ values are reported in per mil, relative to VSMOW.

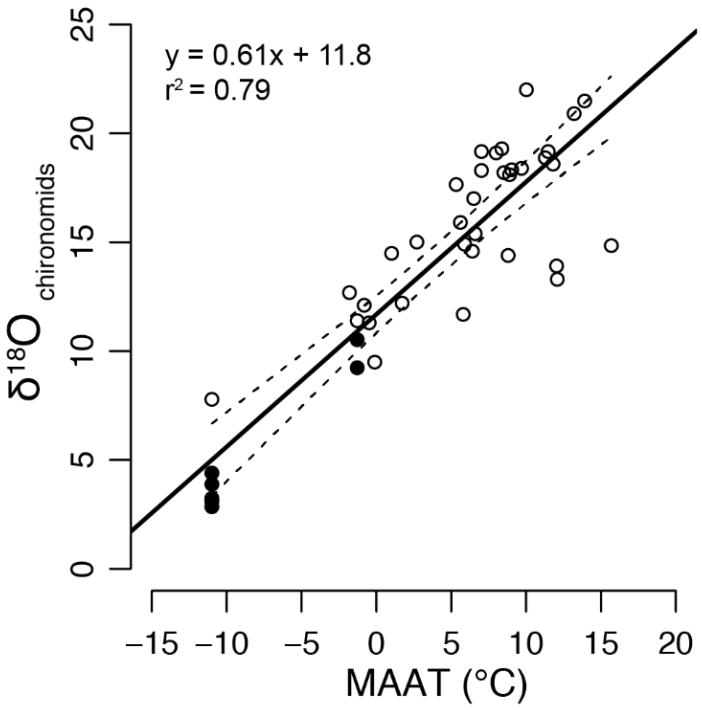

Figure 3.7. Global relationship between $\delta^{18}O$ values of chironomids in surface sediments and mean annual air temperatures (MAAT) for each lake with 95 % confidence intervals. New data from Greenland are plotted as solid circles. Previous field-based studies by Wooller et al., 2004, Verbruggen at al., 2011 and Mayr at al., 2014 are plotted as open circles. $\delta^{18}O$ values are reported in per mil, relative to VSMOW.

Modern lake water we collected in late summer from Thule-region lakes, including Secret Lake, is isotopically similar to both the mean historical (IAEA GNIP) summer precipitation and the 2014 summer precipitation sample that we collected from a single snowstorm. The measured $\delta^{18}O$ value of surface water from Secret Lake in August 2014 was –18.4 ‰, within 0.5 ‰ of mean historical summer (JJA) precipitation values (–18.9 ‰). Secret Lake surface water falls on the local meteoric water line as defined by available IAEA data (Fig. 5). The estimated lake volume is 93,000 m^3 fed by a 0.5 km^2 watershed. Annual precipitation of 184 ± 56 mm w.e. yr^{-1} from TAB meteorological records and compiled by Wong et al. (2015) suggest that (averaged since the start of the record in 1952) the Secret Lake watershed receives nearly 90,000 m^3 precipitation per year. Using these estimates, the mean residence time of lake waters in Secret Lake is approximately 1 year. Actual residence time presumably varies greatly throughout the year, with short effective residence time of cold-season precipitation during the rapid snowmelt period in spring (Woo, 1980).

3.3.3. $\delta^{18}O$ of modern chironomid remains

The $\delta^{18}O$ values of chironomid head capsules analyzed from surface sediments near Thule and Nuuk, paired with $\delta^{18}O$ values of modern lake water, have been added to a growing list of similar samples from around the world (Fig. 3.6). Combining our new data with the northern Europe (Verbruggen et al., 2011) and Patagonia data (Mayr et al., 2014), we calculate a biological fractionation factor (BFF) of 1.0224 – near identical to that calculated by Verbruggen et al. (2011) (1.0223) in 2011 but less than that estimated by early pilot studies (Wooller et al., 2004). Based on all available data including our new high Arctic sites, chironomids are 22.4 ± 1.3 ‰ higher

relative to the lake water in which they grow. The strong correlation between lake water and head capsule $\delta^{18}O$ ($r^2 = 0.94$) is based on multiple studies thus far examining 38 lakes spanning 36° of Northern Hemisphere (NH) latitude (4° in the southern hemisphere) and a 27°C range of mean annual surface temperature.

Given that chironomid head capsules consistently record lake water isotopic composition, and lake water (in appropriate settings) is influenced by the condensation temperature of watershed precipitation, oxygen isotopes measured in head capsules are a potential proxy for paleotemperature in lakes not greatly affected by evaporation (Wooller et al., 2004). Wooller et al. (2004) found that MAAT is highly correlated with the $\delta^{18}O$ values of chironomid head capsules in surface sediments of their four study lakes ($r^2 = 0.98$), with a slope of 0.65 ‰ $°C^{-1}$. The weaker relationship between $\delta^{18}O$ values of chironomids and MAAT found in all comparable data worldwide ($r^2 = 0.79$) likely reflects the differing, complex controls on oxygen isotopes of precipitation and ultimately lake water between sites (Fig. 3.7).

3.3.4. Analysis of downcore organic materials

$\delta^{18}O$ values of Secret Lake chironomids decreases by ~2 ‰ from the beginning of our record after 8 ka to the present, from an average of 5.5 to 3.8‰ (Fig. 3.8D). From 7.7 ka to around 4 ka, values are between 7 and 4.5‰ and then decrease gradually into the late Holocene. The lowest $\delta^{18}O$ values measured in the Secret Lake record occur between 1.2 ka and the present. The difference between the highest values and lowest values between 7.7 ka and 1.2 ka is just over 3 ‰. Downcore analysis of $\delta^{18}O$ values from *Warnstoria exannulata* stems yields a more variable record, but indicates a trend towards 2 ‰ lighter values after 4 ka (Fig. 3.8C). Although the $\delta^{18}O$

values of the *Warnstorfia exannulata* exhibits more sample-to-sample variability and a less coherent trend than chironomid $\delta^{18}O$, mean values after 4 ka are consistently lower. We can assume that the aquatic mosses lack significant lignin (Sculthorpe, 1967) and are composed mainly of cellulose, and assume a cellulose - growth water fractionation of ~28 ‰ (Mayr et al., 2014; Sauer et al., 2001; Zhu et al., 2014). Thus, our macrophyte data indicate a drop in average lake water $\delta^{18}O$ values from a maximum of -17 at the start of our record at 7.7 ka to –21 ‰ in the Neoglacial. As discussed above, chironomid head capsules are higher by 22.4 ‰ relative to growth water, so chironomids and mosses yield very similar reconstructed lake water composition throughout the Holocene. This lends confidence to reconstructions of both absolute lake water composition and the magnitude of the overall isotopic shift from early to late Holocene (Fig. 3.8F).

We place conservative constraints on temperature change based upon Secret Lake chironomid $\delta^{18}O$ by applying and comparing three $\delta^{18}O$ - temperature relationships: the global spatial relationship (Dansgaard, 1964), the Thule IAEA GNIP historical relationship (annual amount-weighted from 1966 to 1971), and the summer (JJA) relationship from the IAEA collections at Thule. These three estimates of the precipitation-temperature relationship (0.46 to 0.67 ‰ $°C^{-1}$) yield estimated temperature differences of 7 to 4.2 °C between the warmest and coldest parts of the past 7.7 ka. Relative to modern (i.e. the temperature inference from surface sediments), the isotopic data suggest that during the warmest period from 7.7 to 6 ka temperatures were 2.5 to 4°C warmer than present, and during the last 1.2 kyr, the coldest period in our record, temperatures were 1.5 to 3 °C cooler than present (Fig. 3.9). As we describe in the Discussion below, these estimates are likely maximum constraints on the amplitude of temperature change experienced over these time periods.

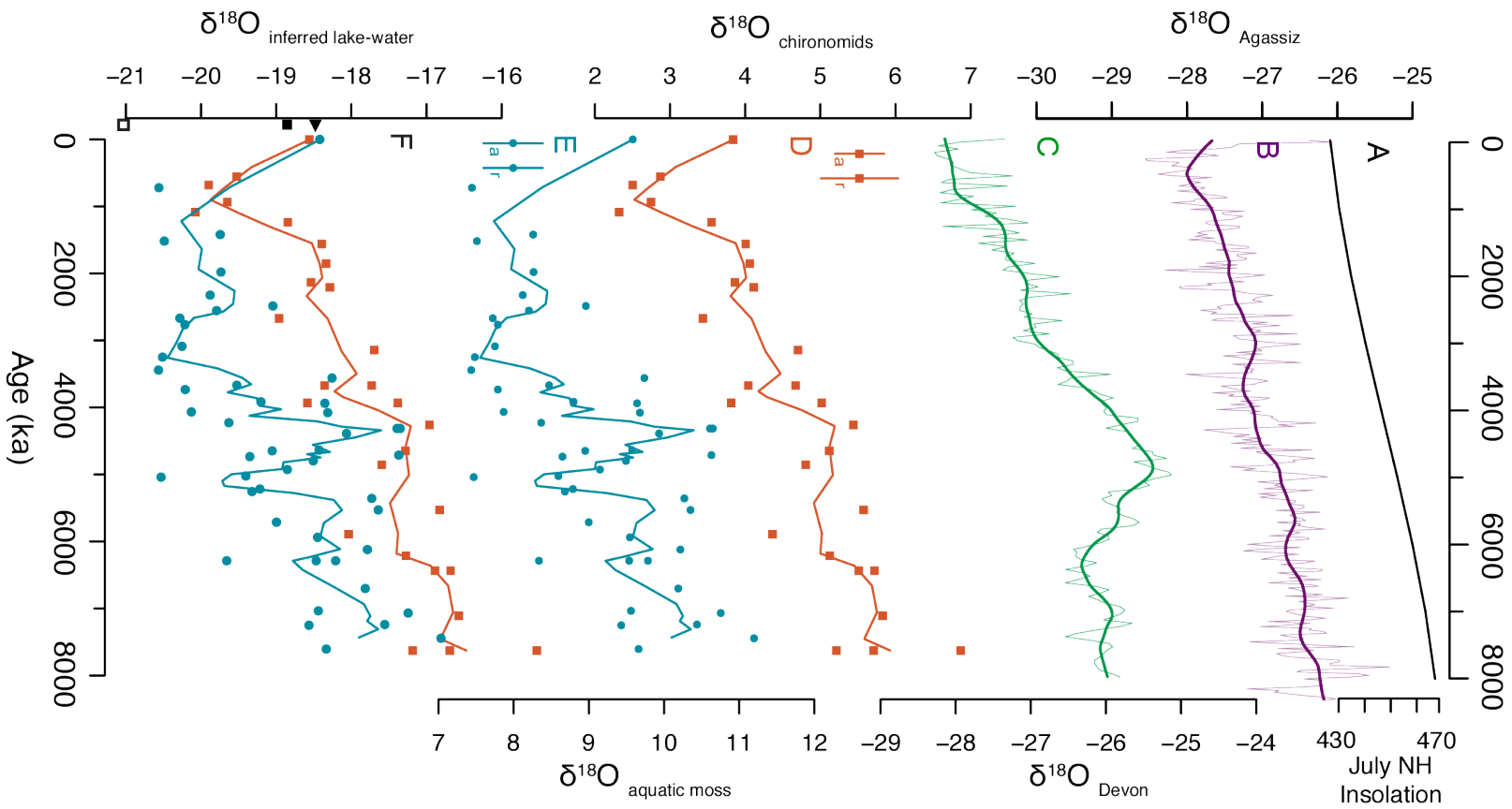

Figure 3.8. Downcore results from Secret Lake and climate data from northwest Greenland. A: Northern Hemisphere July insolation in Wm^{-2}. B: Elevation corrected $\delta^{18}O$ from Agassiz Ice Cap (Lecavalier et al., 2017). C: $\delta^{18}O$ values from Devon Ice Cap (Koerner, 1977). D: $\delta^{18}O$ values of chironomid head capsules from Secret Lake with a 3-point moving average. The uppermost measurement at 0 yr is from a separate surface (0-1 cm) sample. E: $\delta^{18}O$ values of aquatic mosses from Secret Lake with a 3-point moving average. F: Inferred lake water from chironomid $\delta^{18}O$ (red points) and aquatic moss $\delta^{18}O$ values (blue points); shown on y-axis are measured August 2014 lake water (triangle) and mean historical summer and autumn precipitation (closed and open squares respectively (1966-1971; WMO - IAEA/GNIP 2015). Analytical and replicate 1σ errors for measured materials in D and F are denoted 'a' and 'r' respectively. $\delta^{18}O$ values are reported in per mil, relative to VSMOW.

3.4. Discussion

3.4.1. Modern observations of chironomid oxygen isotope composition

Data from this study combined with published research comparing lake water and modern chironomid $\delta^{18}O$ values around the world demonstrate the utility of oxygen isotopes measured in chironomid head capsules as a proxy for lake water oxygen istotopes. We find that $\delta^{18}O$ values of chironomid head capsules in Greenland lake surface sediments are higher relative to host waters by 22.4 ‰, consistent with enrichment factors elsewhere in the world. The 22.4 ‰ enrichment in head capsules from growth (lake) water shown by the aggregated global surface sediment dataset is consistent regardless of the many factors that can influence the isotopic composition of lake water, and the wide diversity of climate at the study sites, which span 27 ºC MAAT and 20 ‰ in lake water $\delta^{18}O$ values. Unlike carbonate or diatoms (Leng and Henderson, 2013), chironomids may maintain a constant fractionation factor regardless of host water temperature (and presumably a correspondingly wide range of species assemblage composition), as demonstrated by our data and available literature.

As chironomid remains are widely preserved in lakes around the world, this proxy may prove valuable for reconstructing past lake water compositions in locations unsuitable for other isotope based methods, e.g. carbonate (Heiri et al., 2012; Heiri et al., 2009). In addition to their widespread preservation, chironomid head capsules also have the advantage that they can be confidently isolated in a straightforward fashion, compared for example to diatoms (Leng and Henderson, 2013). As lacustrine species are obligate aquatic organisms, there is little concern about terrestrial contamination, compared for example to isolating cellulose. Chemically gentle sediment treatment protocols such as the method outlined above do not appear to alter the isotopic

composition of the head capsule and are simpler than other methods, e.g. cellulose extractions. Care should be taken when working in watersheds containing carbonate bedrock, as precipitation of crystals may occur on the chironomid subfossils. For detailed discussion of treatment protocol experiments, see Verbruggen et al. (2009).

While recent data largely support fractionation effects independent of temperature, controlled laboratory culturing experiments could further enhance our understanding of any isotope effects during head capsule synthesis. Genus or species dependent effects have currently been quantified for carbon isotopes (van Hardenbroek et al., 2014), but it has not been fully explored whether this may be an issue with oxygen. In spite of these potential issues, there is great promise for this proxy to expand lake water isotope reconstructions to the many regions where chironomids are preserved, and in so doing, to allow for more widespread paleoclimate reconstructions.

3.4.2. Interpreting chironomid and lake water $\delta^{18}O$ values at Secret Lake

Given the hydrology and setting of Secret Lake, we have argued that its lake water isotopic composition primarily reflects the isotopic composition of precipitation, which in turn is strongly correlated with surface air temperature in northwest Greenland. We have also proposed that lake water at this site is summer and autumn biased, meaning that downcore trends dominantly reflect shifts in summer and autumn precipitation, with a lesser signal from winter and spring. This is in part because precipitation amount throughout the year (at least in the instrumental dataset) is weighted toward summer and autumn, with 64% of precipitation falling during the summer and autumn. Additionally, hydrologic inputs and outputs to the lake should essentially shut down

during the long ice-covered period from mid-autumn through late spring. Upon thawing of ice cover, cold-season precipitation enters the lake mostly during the rapid spring melt (when residence time should be shorter than the annual average) and summer precipitation likely lingers in the lake throughout the subsequent long, hydrologically inactive ice-covered season (Woo, 1980).

Lake water $\delta^{18}O$ samples collected in August 2014 have values indiscernible from mean historical (1966-1971) summer precipitation values for the Thule area (IAEA/WMO, 2017) (Tables 3.1 and 3.2, Fig. 3.5). Importantly, the relationship of the modern lake water to the meteoric water line (Fig. 3.5) suggests minimal enrichment from lake water evaporation in this through-flowing lake, even at the end of summer when evaporative influences likely peak just before lake ice cover resumes. Permafrost in the Thule area and in the vicinity of Secret Lake also limits groundwater flow within the small watershed, particularly from mid-autumn to early summer. In warmer south Greenland, freezing of the active layer by mid-September essentially halts any subsurface inputs to lakes (Leng and Anderson, 2003). These observations support the interpretation that lake water oxygen isotopes at this site primarily reflects contemporaneous precipitation isotopes. $\delta^{18}O$ values of lake water inferred from chironomid head capsules in Secret Lake surface sediments are comparable to both historical summer lake water $\delta^{18}O$ values (Fig. 3.8F), and from that of snow collected in late August 2014. Combined, these observations indicate that $\delta^{18}O$ values of chironomid head capsules at Secret Lake are best interpreted as a summer and early autumn-biased proxy for oxygen isotopes of precipitation, provided the amount and seasonality of precipitation falling within the watershed and entering the lake has been relatively stable through the Holocene.

The 3 ‰ decline between early and late Holocene in $\delta^{18}O$ values of chironomids from Secret Lake is larger than observed in the ice core record from Agassiz ice cap, Ellesmere Island 400 km to the W-NW (Fig. 3.8B). Isotopic shifts in Secret Lake more closely resemble the ice core record from Devon ice cap, Devon Island (Fig. 8E) (Koerner, 1977). $\delta^{18}O$ values in Agassiz ice cap declines by ~2 ‰ from 7.7 ka to present, interpreted as a cooling of 4 °C (Lecavalier et al., 2017). The $\delta^{18}O$ record from the Devon ice cap (not corrected for isostatic uplift) shows a 2.2 ‰ shift towards lower values after 5 ka. Our reconstruction of oxygen isotopes of precipitation in northwest Greenland suggests a greater positive temperature anomaly during the HTM than in these other records. This further supports our assertion that the Secret Lake chironomid $\delta^{18}O$ record is largely recording the warmest part of the year, since declining summer insolation was the dominant change in forcing at these latitudes through the Holocene.

Inferred lake-water reconstructions from moss and chironomid data are largely in agreement for the entire record. As noted in section 4.4.2, the moss $\delta^{18}O$ values exhibit greater variability than chironomids between 8 and 4 ka, followed by more consistent $\delta^{18}O$ trends thereafter. Aquatic moss samples were measured on 3 to 5 mm sections of multiple stems for each sample. Aquatic moss growth is seasonal and can be rapid, growing between 2 and 12 cm in high Arctic lakes during a summer (Guo et al., 2013). Our sampling of such small stem sections potentially captures only a portion of the growth season, and much less than the 25-50 years likely represented from chironomid data points, which may explain the greater sample-to-sample variability exhibited in the moss $\delta^{18}O$ data. Divergence between the moss and chironomid data could be due to enhanced summer cooling or increased winter temperatures (i.e. decreasing seasonality) through the Holocene.

Factors other than insolation-driven local surface temperature also play a role in determining precipitation and lake water isotopic composition over time. For example, marine sediment cores recovered in northern Baffin Bay indicate that sea ice cover and duration were reduced during the HTM (Ledu et al., 2008; Levac et al., 2001). Ice-free conditions from ~7 to 3.6 ka persisted for 4-5 months per year, compared with 1 to 2 months from 3.6 to the pre-industrial era (Levac et al., 2001). Less sea ice cover during the warmer earlier Holocene could conceivably have multiple effects. Higher regional temperatures from sea ice feedbacks over Baffin Bay, combined with an enhanced local precipitation source, could result in higher mean annual precipitation $\delta^{18}O$ values. Conversely, it has also been argued that reduced sea ice cover can enhance winter snowfall, delivering isotopically lower precipitation as an annual average (Thomas et al., 2016). Shifting dominant storm tracks through the Holocene could also play a role. The historical IAEA monitoring data from TAB reveal a pronounced decrease in $\delta^{18}O$ values of precipitation during March every year, and Osterberg et al. (2015) have documented that major shifts in regional storm tracks occur at that same time of year. This effect is also evident in other high Arctic sites such as Barrow, Alaska (Rozanski et al., 1993).

Changes in evaporative enrichment of lake water in a changing climate would also overprint the primary precipitation signal. For example, if warmer summers during the HTM caused more evaporation of lake water, that would cause an enhanced positive anomaly in lake water isotopic composition despite evidence that evaporation has a minimal effect on modern lake water. We suggest that the isotopic changes recorded through the Holocene at Secret Lake most likely place upper bounds on the amplitude of temperature changes over that period. This would be the case if warmer summers in the study area were accompanied by greater evaporative

enrichment of lake water, as has been inferred elsewhere in Greenland for the early to middle Holocene (e.g. Anderson and Leng, 2004; Balascio et al., 2013), and/or characterized by a more proximal moisture source related to decreased sea ice.

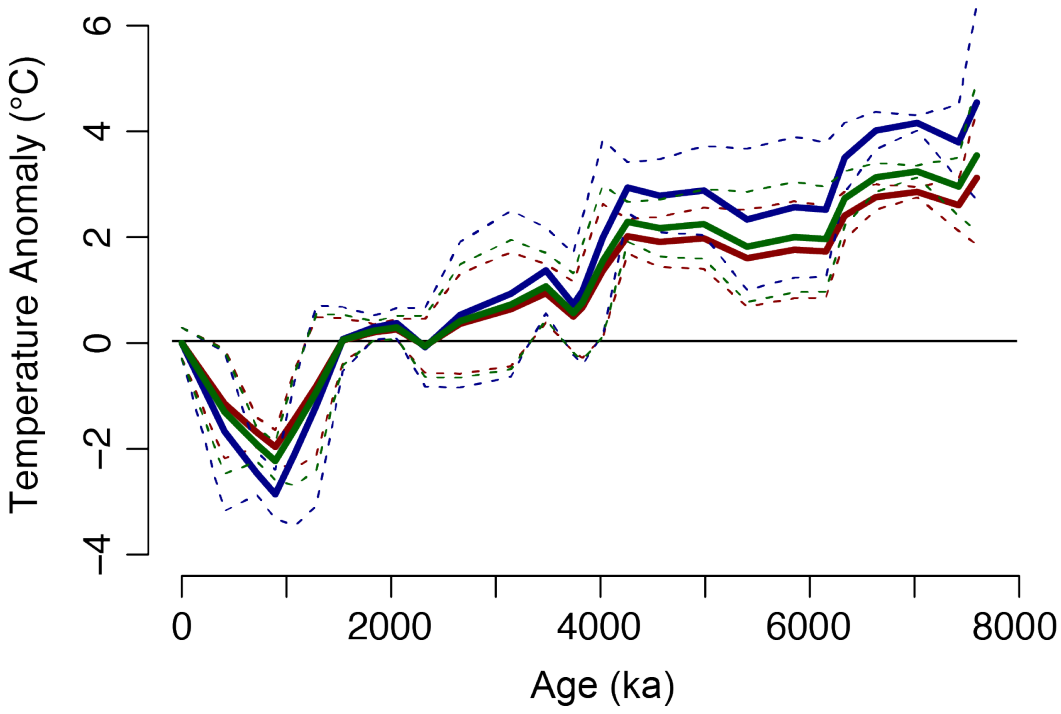

Figure 3.9. Isotope-inferred temperature anomaly from Secret Lake using the local summer precipitation $\delta^{18}O$ – temperature relationship of 0.59 ‰ $^{o}C^{-1}$ (green), the local annual amount weighted relationship of 0.46 ‰ $^{o}C^{-1}$ (blue), and the global relationship of 0.67 ‰ $^{o}C^{-1}$, (red). All estimates are bounded by ± 1σ. As discussed in the text, we view these estimates as upper bounds on the amplitude of past summer-biased temperature changes.

$\delta^{18}O$ values of chironomid head capsules suggest upper bounds of HTM temperatures (represented as anomalies relative to modern from a 3-point moving average of the data) up to 2.5 to 4 °C warmer until ~6 ka (Fig 3.9). A marked change in the climate regime around 4 ka is

recorded by drops in $\delta^{18}O$ values of both chironomids and aquatic moss stems, although the latter yields a much more variable record overall.

Our upper estimates of the HTM temperature anomaly, in excess of 3 °C warmer than present, are inferred using the (1966-1971) local annual amount weighted $\delta^{18}O$ – temperature gradient for TAB of 0.46 ‰ $°C^{-1}$. This slope is within the range of reported Holocene relationships estimated across Greenland from ice cores (Buizert et al., 2014; Dahl-Jensen et al., 1998; Vinther et al., 2009). However, as discussed above, Secret Lake and other lakes in the region appear biased towards summer and autumn $\delta^{18}O$ of precipitation values. The summer season $\delta^{18}O$ – temperature slope in Thule is 0.59 ‰ $°C^{-1}$, and the global spatial slope is 0.67 ‰ $°C^{-1}$. Given uncertainty regarding what slope is most applicable to a Holocene reconstruction, we place conservative constraints on paleotemperatures by applying all three slopes to generate our temperature reconstruction (Fig. 3.9). We conclude that HTM warm-season temperatures were between 2.5 to 4 °C warmer than present from 7.7 (the beginning of the record) to 6 ka. Summer temperatures decreased further ~4 ka and then throughout the late Holocene, with the coldest inferred temperatures occurring after 1.2 ka.

3.4.3. Regional Holocene climate history

We find summer temperatures as much as 2.5 to 4 °C warmer than present during the HTM, based upon $\delta^{18}O$ values of aquatic chironomid larvae remains in a northwest Greenland lake. As the sediment core we recovered from Secret Lake is younger than 8 kyr, this record does not capture the onset of Holocene warmth, and may not capture the warmest part of the Holocene. Continual cooling after 4 ka led to coldest temperatures after 1.2 ka, with temperature anomalies

2 to 3 °C below present. Below we compare this reconstruction with inferences from different archives and proxies throughout the region.

The warmest summer temperatures inferred from our isotope record are comparable in timing to peak August sea surface temperatures (SST) estimated in northern Baffin Bay, where warmer than present conditions prior to 4 ka have been attributed to greater insolation and persistent incoming warm water via the West Greenland Current (Ledu et al., 2008; Levac et al., 2001). 50 to 100% of the Agassiz Ice cap is composed of melted ice layers during the early Holocene, declining to < 10% around 4 to 5 ka (Fisher et al., 1995). Closer to our study site, peat deposits on an island offshore of northwest Greenland suggest warmer-than-present summers from the early Holocene through ~5.1 ka (Bennike et al. 2008). Warm indicator beetle and fish remains in northwest Greenland record a warmer early Holocene from 8.8 to 7.5 ka, overlapping briefly with the Secret Lake record (Fredskild, 1985). The geographically closest quantitative temperature reconstruction is inferred from aggregated pollen records across north Greenland and indicates warmest July temperatures (~1 °C warmer than present) between 7 and 5 ka (Gajewski, 2015). We must look farther afield for additional quantification of HTM warmth: Approximately 1000 km to the south, a 2 to 3 °C July temperature anomaly (relative to present) between 6 and 5 ka was reported based upon chironomid assemblages near Illulisat and Jakobshavn (Axford et al., 2013). Across Baffin Bay on northeastern Baffin Island, HTM summer temperatures were an estimated ~5 °C warmer than the pre-industrial late Holocene and 3.5 °C warmer than present, based upon chironomid assemblages (Axford et al., 2009b; Thomas et al., 2007). Both of the chironomid-based estimates are within (on the low end to middle of) the range of HTM temperature anomalies we reconstruct based upon oxygen isotopes.

Cold spells, the development of more extensive sea ice cover in Baffin Bay (Levac et al., 2001), and a decrease in sedimentation at Kap Inglefield Sø (250 km N of Thule) (Blake et al., 1992) after 4 ka are coincident with the gradual cooling recorded in the Secret Lake isotope record and presumably driven by summer insolation trends. Multiple high latitude climate records from Greenland and Arctic Canada synthesized by Briner et al. (2016) show a general regional shift to cooler conditions after 4 ka. A 3500-yr late Holocene record from Greenland's northernmost lake indicates coldest conditions there from 2.4 ka until the last century, in agreement with the timing of coldest conditions at Secret Lake (Perren et al., 2012b). A cooling trend over the last two millennia of the pre-industrial Holocene has been widely documented across the Arctic (e.g. Kaufman et al., 2009).

Glacial geological evidence in the form of subfossil plants found in a nearby North Ice Cap shear plane dating to 5.53 ka suggest that the ice cap (40 km north from Secret Lake) was less extensive than present prior to that time (Goldthwait, 1960), with subsequent Neoglacial re-advance. Low LGM $\delta^{18}O$ values indicative of Pleistocene conditions have not been found along the eastern North Ice Cap and the western Tuto Ice Cap margins (Fig. 3.1), also supporting regional early Holocene ice retreat behind present-day margins (Reeh et al., 1990). Summer temperatures > 2.5 °C warmer than present would presumably have driven significant retreat of these ice masses. Additional and more detailed glacial geologic investigations around the margins of North Ice Cap and the GrIS are currently underway (Kelly et al., 2015).

Improved constraints on the timing and magnitude of HTM warmth around Greenland can provide better input and tests for ice sheet sensitivity models. The HTM is a useful, albeit imperfect, recent analog for potential 21st Century warming. Following deglaciation, the GrIS

retreated behind its present margins (by as much as 20 to 60 km in some parts of Greenland) during the HTM (Larsen et al., 2015b; Young and Briner, 2015). Recent model experiments have imposed a hypothetical HTM temperature anomaly, in recognition that the isotope records from central Greenland ice cores did not yield reliable estimates of peak Holocene warmth (Lecavalier 2014, Simpson 2009). HTM temperatures inferred from ice core records were scaled up by 1 to 2 °C between 9 and 5 ka to maximize the fit between model results and observations of glacial advance and retreat across Greenland. However, the response of the ice sheet in the proximity of Camp Century (~ 200 km from Thule) is still not well represented with temperature parameterizations (Lecavalier et al., 2017; Lecavalier et al., 2014). Warmer summers in the early Holocene than those imposed, such as the middle to upper end of the 2.5 to 4 °C summer temperature anomaly suggested by our dataset from northwest Greenland, could help account for the differences between the model and observed relative sea level change in the northwest. The recently revised $\delta^{18}O$ inferred temperature record from the Agassiz Ice Cap is in agreement with our temperature anomalies between 7.7 and 4 ka, with even warmer temperatures prior to 7.7 ka (Lecavalier et al., 2017). Our results may provide further insights on the elevation history at Camp Century and the resulting ice core $\delta^{18}O$ record.

3.5. Conclusions

This study builds upon previous methodological work by further demonstrating the utility of chironomid $\delta^{18}O$ values as a proxy for lake water $\delta^{18}O$ values and past climate change. $\delta^{18}O$ values of chironomid remains in surface sediments are higher by a consistent amount relative to modern lake waters across Europe, South America and, as we demonstrate, a range of latitudes in

Greenland. The widespread preservation of chironomid remains in lakes worldwide can help expand reconstruction of lake water isotopes beyond sites where carbonate materials are preserved.

Oxygen isotopes measured in the subfossil remains of both chironomids and aquatic plants from a 7.7 kyr sediment record recovered from Secret Lake record a 3 ‰ decline in lake water $\delta^{18}O$ values between the early and late Holocene, with most of the decline occurring after ~4 ka. We argue that this isotopic shift provides a summer- and early autumn-biased maximum estimate of Holocene temperature changes over northwest Greenland. Inferred warm-season temperatures were 2.5 to 4 °C warmer than present from at least 7.7 ka to 4 ka, and the coldest part of the Holocene, after 1.2 ka, was 1.5 to 3 °C colder than present. The ranges of these estimates reflect uncertainty in the isotope-temperature relationship for precipitation through the Holocene. Due to the possible overprinting effects of enhanced evaporation and reduced sea ice in Baffin Bay (and thus a closer moisture source) during the HTM, the estimated anomaly of 2.5 to 4 °C between 7.7 and 4 ka is likely an upper limit, which (along with its summer bias) may explain why this estimate is slightly higher than from some other proxy records from the northern Baffin Bay region. The timing of temperature shifts at this study site in northwest Greenland appears consistent with published marine and terrestrial records from the surrounding region.

Peak Holocene warmth inferred from Secret Lake is also coincident with the documented retreat of regional glaciers, followed by readvance in the late Holocene. Additional ongoing paleoclimate and glacial investigations along the margin of the GrIS and local ice caps in northwest Greenland will further advance our understanding of ice sheet sensitivity to warming, and thus help to improve model capabilities in predicting future contributions of the GrIS to sea level rise.

Acknowledgements

Funding for this research was provided by National Science Foundation Grants PLR-1108303 and 1107411, the National Geographic Society (for sampling in southwest Greenland), a Geological Society of America Graduate Research Grant, the American Association of Geographers Marcus Fund, and the Institute for Sustainability and Energy at Northwestern. We thank A. Masterson, M. Osburn and K. Dutta for assistance with stable isotope analysis, G. Schellinger-Harrington and P. Kotecki for assistance with isolating chironomids for isotope analysis, O. Bennike for assistance identifying plant remains, N. Blair for assistance with FT-IR analysis, staff at LACCORE for core processing and WHOI-NOSAMS for radiocarbon analysis and two anonymous reviewers for helpful comments that improved the manuscript. Water isotopes were measured in the Osburn lab at Northwestern University. Field logistics were coordinated by Polar Field Services, particularly K. Cosper and J. Hurley. G. Bromley, L. Farnsworth, M. Jackson and A. Taylor assisted with field work. We thank the people and Government of Greenland (export permit 028/2014) and Thule Air Base for site access, and Air Greenland and the U.S. Air Force for transportation support.

CHAPTER 4:

Holocene climate and environmental development in Southwest Greenland

Abstract

Terrestrial temperature reconstructions from the ice-free margins of Greenland are critical for constraining the sensitivity of the ice sheet to past climate change. The glacial history of southwest Greenland is well understood thanks to numerous investigations in recent decades, however, very few regional quantitative temperature records exist with which to contextualize changes in the cryosphere. This chapter examines sedimentary records from two lakes south of Nuuk, Greenland (T1 and T2) and investigates millennial scale Holocene climate change using a multi-proxy approach. Changes in T1 X-Ray Fluorescence Spectroscopy (XRF), $\delta^{15}N$, $\delta^{13}C$ and biogenic silica data mark the transition from a marine environment to an isolated lake as relative sea level fell in the early Holocene. $\delta^{18}O$ values of subfossil insects (chironomids) from lakes T1 and T2 decrease by ~ 2 to 3 ‰ from ~ 9 ka (the onset of lacustrine sediment deposition in lake T2; ka = thousands of years before present), and 1 ka. Existing isotope-independent temperature reconstructions from the west coast of Greenland suggest that changes in $\delta^{18}O$ values of this magnitude correspond to gradual cooling of 2 to 4 °C, consistent with decreasing summer insolation trends. There is widespread regional evidence that cooling of this magnitude resulted in progressive regrowth of local ice caps, and readvance of regional mountain glaciers and the ice sheet. Furthermore, the regional consensus on the magnitude of temperature change indicates that the local, modern modeled temperature - precipitation $\delta^{18}O$ relationship cannot be used to infer temperature changes throughout the Holocene. Future studies utilizing $\delta^{18}O$ based proxies to infer temperature change should carefully assess local spatio – temporal isotope sensitivity.

4.1. Introduction

A growing dataset of millennial to centennial scale terrestrial climate records on the west coast of Greenland is improving our understanding of climate trends over the last 10,000 years (e.g. Sundqvist et al., 2014). General Holocene cooling is evident over much of Greenland, the result of declining summer insolation in the Northern Hemisphere, however regional scale modulation of climate and localized asynchronous responses is increasingly apparent (Briner et al., 2016; Marcott et al., 2013). At present, west Greenland has vast de-glaciated coastal areas, hosting large local ice caps (e.g. Sukkertoppen Iskappe). Glacial investigations to date have focused on reconstructing past ice sheet margin changes and ice cap and glacier behavior along the western coast (Larsen et al., 2017; Lesnek and Briner, 2018; Levy et al., 2017; Schweinsberg et al., 2017; Schweinsberg et al., 2018; Young and Briner, 2015). The western flank of the Greenland ice sheet as well as local ice caps are thought to have responded strongly to peak insolation in the early to mid-Holocene. The region around Nuuk is estimated to have de-glaciated between 10.7 ± 0.6 and 10.1 ± 0.4 ka, with ice retreating rapidly (est. 167 m a^{-1}) up to or beyond the present-day ice margin (Larsen et al., 2014). Relative sea level (RSL) model estimates suggest a local marine limit of about 80 m a.s.l., meaning that much of the low coastal landscape that exists today was glacially depressed and submerged below sea level immediately after de-glaciation. Isostatic rebound in the vicinity of Nuuk is thought to have reached near equilibrium by about 4 ka (Woodroffe et al., 2014). This time also coincides with the earliest archaeological evidence of human settlement of the Nuuk area. The Saqqaq culture settled much of the west coast of Greenland, but most densely areas near Disko Island and Nuuk until 2.8 ka. Following the Saqqaq, the Dorset people are also thought to have settled much of the island until 2.2 ka, followed by the

brief Norse settlement, and later the Thule people, ancestors of the present-day Greenlandic Inuit (Grønnow and Sørensen, 2004).

It is estimated that the ice sheet margin near Nuuk retreated between 60 and 200 km inboard of the present day ice margin during a warmer Holocene Thermal Maximum (HTM), subsequently re-advancing up to or slightly beyond its present day margin as insolation declined through the late Holocene (Larsen et al., 2015a; Lecavalier et al., 2014; Weidick et al., 2012). Quantitative estimates of HTM warmth are not yet available for the Nuuk region, but in central west to southwest Greenland HTM temperatures have been inferred from chironomid assemblages near Illulisat (Axford et al., 2013), and highly variable temperatures are also reconstructed from an alkenone record near Kangerlussuaq (D'Andrea et al., 2011). Marine records around the west coast of Greenland are relatively abundant with respect to quantitative terrestrial temperature records

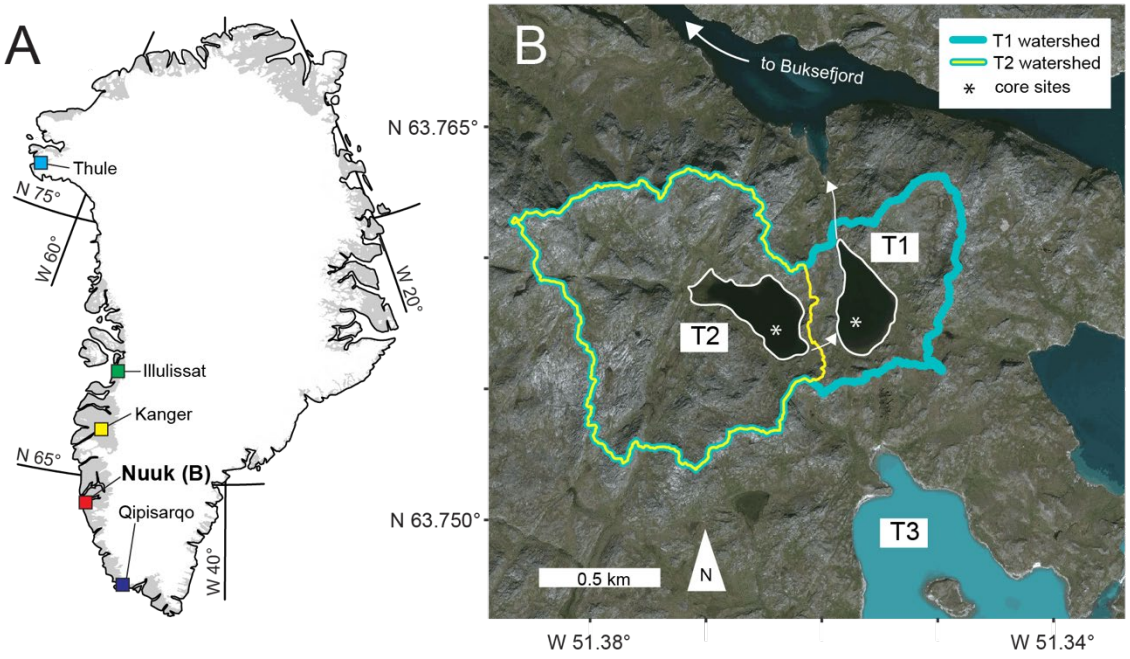

Figure 4.1. A: Locations around Greenland discussed in the text, including location (in red) of inset panel showing our study site near Nuuk. B: Study area, with catchment outlines of lakes T1 and T2 and the locations of the 15-T1-U4 and 15-T2-U3 core sites. Lake T3 outlet and inlet(s) are southwest of the inset map area.

and many document the Holocene marine evolution of Baffin Bay (Erbs-Hansen et al., 2013; Krawczyk et al., 2017; Moros et al., 2016; Perner et al., 2012; Seidenkrantz, 2013; Sha et al., 2017). Other millennial scale records of terrestrial climate are found in the far north of west Greenland at Secret Lake and Wax Lips Lake near Thule (Lasher et al., 2017; McFarlin et al., 2018), and in the far south at Lake Qipisarqo (Frechette and de Vernal, 2009; Wooller et al., 2004) (Fig. 4.1). However, a spatial gap remains in the terrestrial Holocene climate history of southwest Greenland, which we fill with a new oxygen isotope ($\delta^{18}O$) record from two lakes near Nuuk, Greenland. We also aim to further constrain probable $\delta^{18}O$ – temperature relationships at our site by comparing our temperature reconstructions with recent modeled temperature output from around Greenland.

4.2. Study site and methods

Three lakes adjacent to Buksefjord and the Tasisarsuaq embayment were sampled for modern water, surface sediment, and sediment cores during the 2015 summer, hereafter referred to as lakes T1, T2 and T3 (Fig 4.1). T1 and T2 are small (< 0.1 km^2) precipitation fed lakes, and T3 is a large (~ 2 km^2) lake currently receiving meltwater from local mountain glaciers and a regional ice cap between 15 and 30 km west. T2 is a headwater lake meaning it only receives inputs from precipitation falling over its 0.65 km^2 watershed and has one surface outflow which feeds directly into T1. T1 has a relatively small direct watershed (~ 0.35 km^2), though receives input from T2 and its watershed. T1 has one main outlet, which flows directly from the lake to the Tasisarsuaq embayment. Mean annual temperatures at Nuuk are -0.8 ± 6 °C and mean monthly precipitation (1958 to 2017) is 95 ± 99 mm (Fig 4.2) (Cappelen, 2017). The lakes are located less

than 10 km from the outer coast of west Greenland / Baffin Bay, and lie on glacially scoured Archean orthogneiss that is granodioritic to tonalitic in composition (GEUS, 2018). Lake water and precipitation samples were collected in 30 mL HDPE Nalgene bottles, taped to prevent evaporation, and later analyzed on a Picarro L2130-i analyzer at Northwestern University.

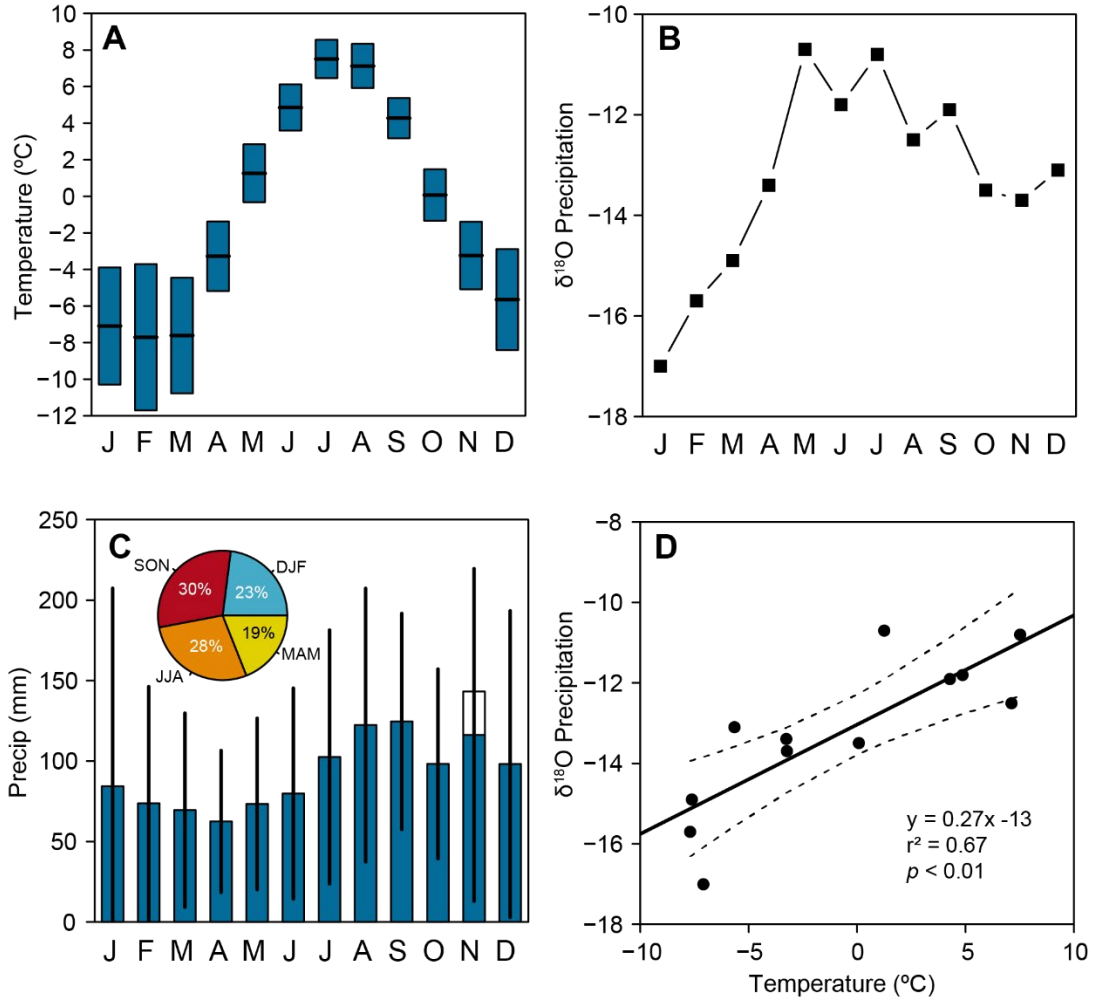

Figure 4.2. Climate and isotope data from Nuuk, Greenland. A: Measured average temperatures and standard deviation by month at Nuuk, Greenland (Menne et al., 2012). B: Modeled monthly precipitation isotopes at Nuuk (Bowen, 2018). C: Measured mean precipitation amounts (bars) and standard deviation (lines) at Nuuk, Greenland (HCDN, 2018), and proportion of precipitation by season. One value was excluded from the November data as it greatly skewed the relative contribution of autumn precipitation. D: Modeled monthly precipitation $\delta^{18}O$ plotted against average monthly temperatures at our study site (Bowen, 2018).

Cores 15-T1-U4 (178.5 cm) and 15-T2-U3 (163 cm) were recovered from lakes T1 and T2, respectively, using a Universal check-valve (piston-free) lightweight percussion coring system. Coring stopped when it was estimated that the 2 m tubes were mostly full but retained enough headspace to ensure the sediment water interface remained intact. Remains of plant and wood fragments (n = 6, from lacustrine sediments) and coral and bivalve remains (n = 2, from basal marine sediments) were collected from the T1 core, and plant and wood fragments (n = 5) were collected from T2 for AMS ^{14}C analysis, detailed in Table 4.1. Age depth models for each core were developed using the rbacon package in R (Fig. 4.3) (Blaauw and Christen, 2018). All terrestrial material was calibrated using IntCal13, while the two marine samples (coral and bivalve - likely *Mytilus edulis*) were calibrated using the Marine13 curve (Reimer et al., 2013). Assuming the deposition environment for these organisms was a shallow marine environment, in proximity to the rapidly melting GrIS, we apply a ΔR of -9 ± 66 years, the average of the nearest available comparable samples from the Marine Reservoir database (n = 6) (Reimer and Reimer, 2001).

A suite of sedimentary proxies was analyzed on the split 15-T1-U4 core: Magnetic susceptibility (MS) was measured using a Barrington MS2E sensor mounted to a Geotek MSCL at Northwestern's GeoCAL laboratory. Elemental composition was analyzed using an Olympus DELTA Professional X-Ray Fluorescence (XRF) detector (Rh anode X-Ray source) which automatically converts counts to estimated abundance (also mounted to the Geotek MSCL). XRF data was collected every 0.5 cm down the core with 30 second dwell times. Biogenic silica (weight percent, bioSiO_2) was measured at Northwestern's Quaternary Sediment Lab following the methods of Mortlock and Froelich (1989). Percent carbon and nitrogen (%C, %N) as well as isotope values ($\delta^{13}C$, $\delta^{15}N$) were measured on bulk sediment samples using a Costech 4010

Elemental Analyzer (EA) coupled to a Thermo Scientific Delta V-Plus Isotope Ratio Mass Spectrometer (IRMS) at Northwestern's Integrated Laboratories for Earth and Planetary Sciences The associated uncertainties for $bioSiO_2$, %C, %N, $\delta^{13}C$ and $\delta^{15}N$ are ±3.1%, ±0.02%, ±0.001%, ±0.45‰, and ±0.24‰, respectively. Samples for carbon and nitrogen analysis were not acidified prior to analysis after coulometry analysis of exploratory sediment samples in the T1 and T2 cores indicated negligible carbonate content.

$\delta^{18}O$ was measured on samples of ~50-100 isolated chironomid head capsules from both cores. Samples were prepared following the methods of Lasher et al. (2017) and analyzed on a Thermal Conversion Elemental Analyzer (TC/EA) coupled to a Thermo Scientific Delta V-Plus IRMS (analytical uncertainty = ±0.4‰) Exploratory sampling of the core indicated low chironomid head capsule concentrations in the top 70 cm of the core. 8 cm^3 sediment samples spanning 2 cm of depth were collected at 5 cm intervals throughout the cores. Subsampled sediment was deflocculated in a 10% KOH solution at room temperature (20 °C) with the use of a magnetic plate stir rod assembly for 30 minutes. This solution was then rinsed thoroughly with DI water, sieved over a 125-micron mesh into large centrifuge tubes, then stored in a minimal amount of Nanopure water at 4°C until ready for sorting. Individual head capsules from each depth were then picked into lightweight (~ 7 mg) silver capsules and freeze dried for a minimum of three days, and up to a week prior to isotope analysis.

Chironomid $\delta^{18}O$ reliably archives the $\delta^{18}O$ values of chironomid growth water, and in certain lakes can therefore be a proxy for paleo precipitation $\delta^{18}O$ values (Lasher et al., 2017; van Hardenbroek et al., 2018; Verbruggen et al., 2011; Wang et al., 2009; Wooller et al., 2004). Our study lakes are small open basins with estimated residence times of ~ 1 year. We assume that the

Table 4.1. Radiocarbon ages from T1 and T2.

Core	Depth below sed surface (cm)	Lab ID	Material	^{14}C Age (uncalibrated)	Calibrated age (cal yr B.P.)	Fraction Modern	Calibration Curve Utilized	δ^{13}C
15-T1-U4	15.5	OS-135046	Plant/Wood	1910 ± 20	1860 ± 35	0.788 ± 0.0021	IntCal13	-24.03
15-T1-U4	52	OS-125559	Plant/Wood	4540 ± 20	5200 ± 120	0.5681 ± 0.0014	IntCal13	Not measured
15-T1-U4	84.5	OS-125586	Plant/Wood	6360 ± 30	7340 ± 100	0.4529 ± 0.0016	IntCal13	Not measured
15-T1-U4	86	OS-125558	Plant/Wood	6440 ± 20	7375 ± 50	0.4486 ± 0.0012	IntCal13	Not measured
15-T1-U4	104-105	OS-135047	Plant/Wood	7690 ± 35	8860 ± 130	0.3714 ± 0.0065	IntCal13	-21.37
15-T1-U4	128	OS-125585	Plant/Wood	8060 ± 20	9010 ± 15	0.3667 ± 0.0018	IntCal13	Not measured
15-T1-U4	177-178	OS-125545	Coral	8550 ± 30	9240 ± 150	0.3449 ± 0.0016	Marine13	Not measured
15-T1-U4	177-178	OS-125526	Bivalve	8460 ± 25	9150 ± 150	0.3489 ± 0.0011	Marine13	Not measured
15-T2-U3	16.5	OS-135044	Plant/Wood	2230 ± 20	2240 ± 85	0.7575 ± 0.0021	IntCal13	-25.92
15-T2-U3	28.5	OS-125544	Plant/Wood	3090 ± 30	3300 ± 75	0.68110 ± 0.0025	IntCal13	Not measured
15-T2-U3	54	OS-135045	Plant/Wood	5490 ± 25	6300 ± 85	0.5049 ± 0.0017	IntCal13	-25.83
15-T2-U3	84.5	OS-125652	Plant/Wood	7690 ± 140	8585 ± 390	0.37140 ± 0.0065	IntCal13	Not measured
15-T2-U3	93.5	OS-125655	Plant/Wood	8870 ± 190	9965 ± 440	0.33160 ± 0.0079	IntCal13	Not measured

Calibrated ages are reported as the midpoint of the 2σ range ± ½ of 2σ range.

major hydrological input at present (and presumably since isolation from the marine environment between 8 and 9 ka) is precipitation. Some lakes on the west coast of Greenland are hydrologically connected (Osburn et al., 2017), and so groundwater seepage may account for a small amount of water flux in our watersheds, but we have no firm estimates or constraints on these quantities. The lakes (T1 and T2) were through-flowing in August of 2015, and modern lake water in August 2015 fell on/near the GMWL, supporting our observations of minimal evaporative effects even in late summer. Precipitation amounts are fairly evenly divided throughout the year, though slightly

biased toward summer and autumn (Fig. 4.2C). $\delta^{18}O$ values measured from chironomids at T1 and T2 should therefore be a proxy for mean annual precipitation $\delta^{18}O$ over the Holocene sedimentary record.

4.3. Results

4.3.1. Modern water $\delta^{18}O$

Lake water samples collected from T1 and T2 in August 2015 fall on the Global Meteoric Water Line (Fig. 4.5). Precipitation was collected during two rain showers during the field season. The $\delta^{18}O$ values from these rain events also fall on the GMWL (Dansgaard, 1964). As no long-term precipitation monitoring station is located near Nuuk, we estimate the area's monthly precipitation $\delta^{18}O$ values from the model outputs of the Online Isotopes of Precipitation Calculator (OIPC) for our study site's location. The modeled local meteoric water line (MLMWL) has a shallower slope (6.7x) than the GMWL (8.0x), though modeled mean annual precipitation $\delta^{18}O$ with modeled errors overlaps with measured lake water $\delta^{18}O$ values from T1 and T2. Multiple precipitation samples collected from a single rain storm, but at two times during the storm potentially demonstrates the progressive distillation of heavy $\delta^{18}O$ as the storm progressed over the T1/T2 study site. Over a 30-minute time period, precipitation $\delta^{18}O$ values become heavier by ~ 2 ‰, from -14.5 to -12.5 ‰, while differing little with respect to d-excess. Lake water $\delta^{18}O$ values from the nearby T3 lake, a distally fed glacial lake also fed by local precipitation, is 3.5 ‰ more negative. Also sampled was the water from the Tasisarsuaq Bay (-6.5 ‰), presently hydrologically connected to Baffin Bay via Buksefjord, but also receiving meltwater from the distal regional ice caps and mountain glaciers via Lake T3's outlet river.

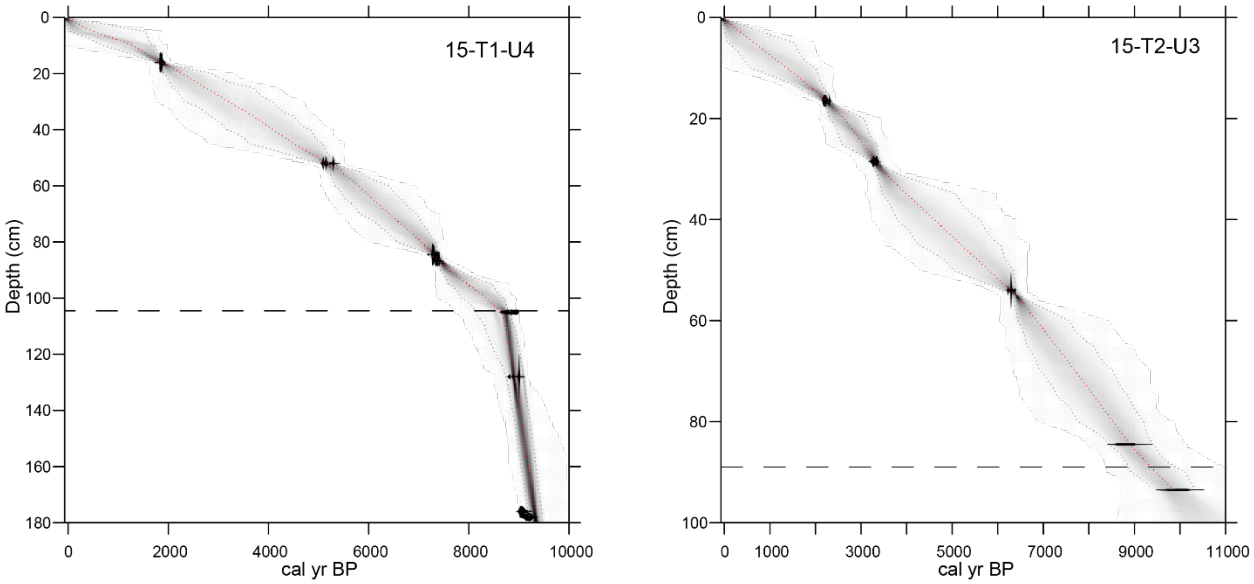

Figure 4.3. Age-depth models for 15-T1-U4 (left) and 15-T2-U3 (right), with calibrated ^{14}C dates and their respective probability density functions (black). Darker greys indicate more likely calendar ages bounded by 95% confidence intervals; the red curve shows the single 'best' model based on the weighted mean age for each depth. The dashed line represents the transition from marine to lacustrine deposition in each lake.

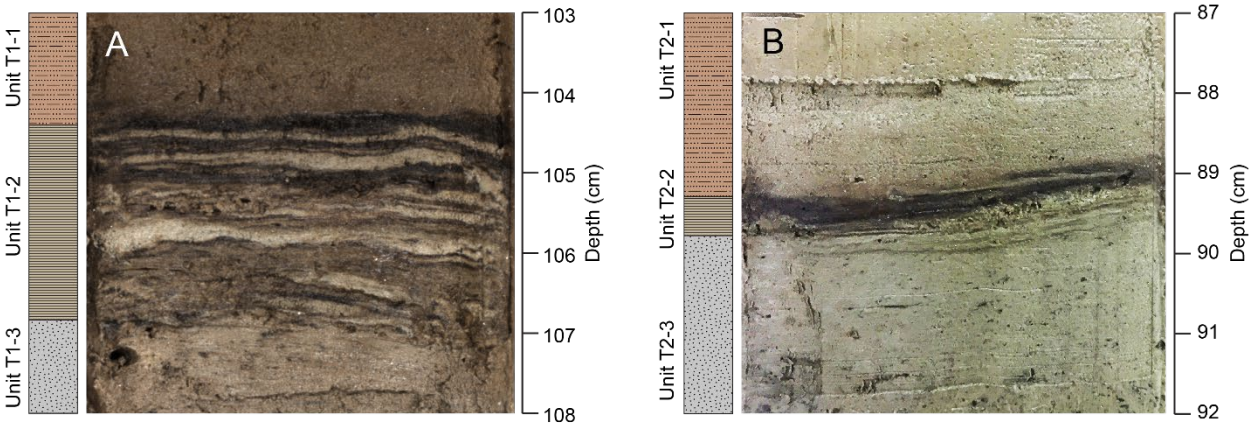

Figure 4.4. A: Photo of the meromictic marine to lacustrine transition unit in core 15-T1-U4. Unit T1-1 in is comprised of massive to coarsely banded gyttja. Unit T1-2 represents the characteristic contact found in many isolation basins around Greenland (Long et al., 2011). Unit T1-3 is characterized by glacio-marine sediments. B: same as in A, but for core 15-T2-U3. Depths are cm below the sediment water interface in each lake.

4.3.1. Core visual description and geochronology

Core 15-T1-U4 is 178.5 cm long and contains three distinct lithostratigraphic units (Fig. 4.6). All ages discussed are given in thousands of calibrated years before present (ka), except where specific age control is noted. The bottom unit (unit T1-3) is dense gray clay and contains mollusk and coral fragments at 177-178 cm dating to 9195 ± 150 cal yr BP (Table 4.1). This clay unit was deposited rapidly, (up to 0.5 cm yr^{-1}) and abruptly ends at 107 cm core depth, transitioning to a finely laminated black, brown and gray clay gyttja unit (unit T1-2; Fig. 4.4A) 3 cm thick dated to 8570 ± 110 cal yr BP from a radiocarbon age directly above unit T1-2. The uppermost 104.5 cm of core is brown, massive organic gyttja (unit T1-3), and accumulated slowly at about 0.1 mm yr^{-1} (Fig 4.3). An intact sediment water interface was captured; therefore, the top of the core represents 2015 C.E.

Core 15-T2-U3 (163 cm) exhibits the same sedimentary progression. Light gray clay at the base transitions to dark gray clay (collectively unit T2-3), terminating in a 1 cm finely laminated clay gyttja unit from 89 - 90 cm depth (unit T2-2; Fig. 4.4B). No material was available for radiocarbon analysis at the base of the core, and the deepest material (plant fragments) sampled just below the transition dates 9965 ± 400 cal yr BP. We do not extrapolate below this age; however regional deglaciation estimates date to ~10.7 ka (Larsen et al., 2014). A sample of plant and wood fragments sampled above unit T2-2 dates to 8835 ± 395 cal yr BP. These two bottom-most ages constrain the timing of the T1-3 and T1-2 boundary at 9390 ± 210 cal yr BP. Dense clay-rich gyttja is present above the laminated unit T2-2, transitioning into light and dark brown horizontally banded organic gyttja in the upper 40 cm of the core. Like in T1, the gyttja unit in T2 (unit T2-1) accumulated slowly at an average rate of 0.1 mm yr^{-1}. The break in sedimentation rate in the T1

core occurs at the T1-3 to T1-1 boundary, conterminous with the greatest change in sedimentary properties. 6 cm of gyttja were also captured at the base of the T2 core, however an inverted ^{14}C age (7450 ± 110 cal yr BP) on the bulk sediments confirmed our suspicion that young sediment from unit T2-1 was likely drawn into a gap at the base while the core was being recovered. Therefore, no data are reported here from the basal 6 cm of the core, and the bottom of unit T2-3 is treated throughout this paper as the base of the core.

4.3.2. Sedimentary characteristics

Magnetic susceptibility (MS) averages between 12 and 24 x 10^{-5} SI in the basal clay unit (T1-3), then transitions to consistent very low values above unit T1-2 (Fig. 4.6). XRF measured elemental composition displays similar trends to the MS, with Ti, S, Ca, transitioning from high to low concentration (or below detection limits) at the T1-3 to T1-2 transition at ~ 8.6 ka. %C is low in unit T1-3 (~ 4%,) then increases rapidly above unit T1-2 (10 to 13%) for ~1500 years, then decreased gradually to an average of 7.5% over the last 7000 years (Fig. 4.6). %N is similarly low in unit T1-3 (< 0.5%), then increases above unit T1-2 to 1.25%, before decreasing to values between 1% and 0.5% over the last 7000 years. C:N (percent weight) begins low, < 9 in the unit T1-3 (Fig. 4.7, 4.8). This increases to ~ 9% above the transition between 8250 and 7000, then continues increasing monotonically to 14 at the surface top of Unit T1-1. $\delta^{13}C$ values are low in unit T1-3, between -23 and -20 ‰. Above unit T1-2 at ~ 8.6 ka, values are variable, though generally decrease from -18 ‰ to more negative values between -21 and -20 ‰ after the transition to unit T1-1. $\delta^{15}N$ values begin relatively high, between 4 and 7 ‰ in unit T1-3, then transition to values between 1 and 3 ‰ between 8570 and the present (units T1-2 and T1-3). $BioSiO_2$ was

measured at coarse resolution throughout the core, also clearly marking the transition from massive clay (T1-3) to gyttja (T1-1). Low bioSiO_2 (1.4 to 2.2%) is present in unit T1-3, then increases rapidly to 19 to 26% above unit T1-2 in unit T1-1 (Fig. 4.6).

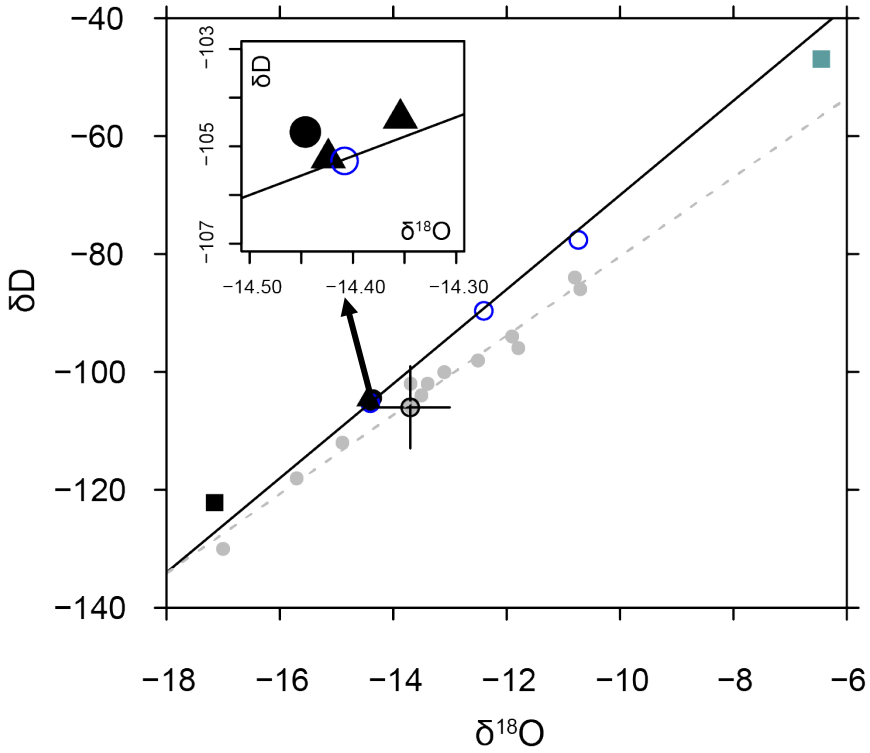

Figure 4.5. Isotopes of precipitation, lake and marine waters near our study site. Samples collected in August 2015: the black square is glacially fed lake T3, the blue square is glacially influenced seawater from a local embayment, the black triangle and black solid circles are lake water of T1 and T2, respectively, and the blue open circles are modern precipitation (two separate rainstorms, and two collections 0.5 hrs apart within a single rain event). The solid black line is the Global Meteoric Water Line (Craig, 1961). Light gray points, and the light gray dashed line are modeled monthly isotopes of precipitation and the modeled local meteoric water line over the lake site) from the OIPC calculator, and the open black circle with 1σ error bars is the modeled mean annual precipitation value the T1/T2 lake site (Bowen, 2018).

4.3.4. Chironomid $\delta^{18}O$ inferred lake water and temperature inferences

$\delta^{18}O$ values were measured from chironomid head capsules in the gyttja units of lake T1 and T2 (units T1-1 and T2-1). Head capsules were not present in either the clay basal unit (T1-3),

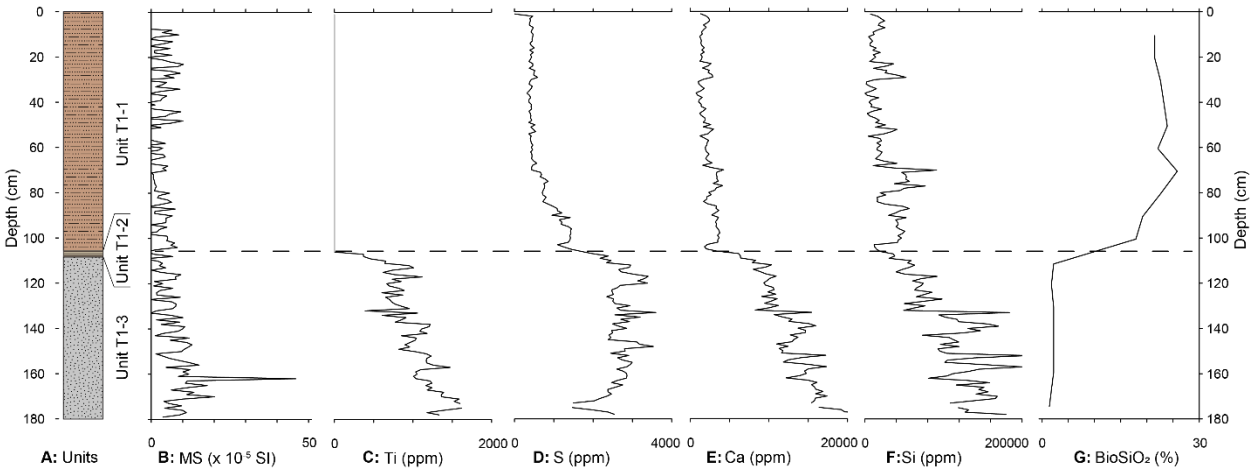

Figure 4.6. Sediment composition from lake T1 plotted vs depth. A: Lithostratographic units, B: Magnetic susceptibility (MS), C-F: titanium, sulfur, calcium and silica concentrations, G: Biogenic silica concentration. The dashed line represents the transition from a glacio-marine to lacustrine environment in T1 at ~ 8.6 ka.

or the meromictic layer in both cores (T1-2 and T2-2). Values from both cores are variable but decrease gradually up the core (Fig. 4.8). The resolution of values in the upper 70 cm of both cores is low, due both to low sediment accumulation rates and low concentrations of head capsules. 2 cm sections of core were sampled for sieving to collect enough head capsule mass for isotope analysis. A result of the abundance and low accumulation rate is that each $\delta^{18}O$ value measured is an average of potentially one to multiple centuries of recorded lake water. Fig. 4.8 shows both the analytical error from replicate standards analyzed amongst unknown chironomid samples (1σ = 0.4 ‰) as well as age uncertainties associated with 2 cm thick sediment samples, calculated using rbacon (Blaauw and Christen, 2018).

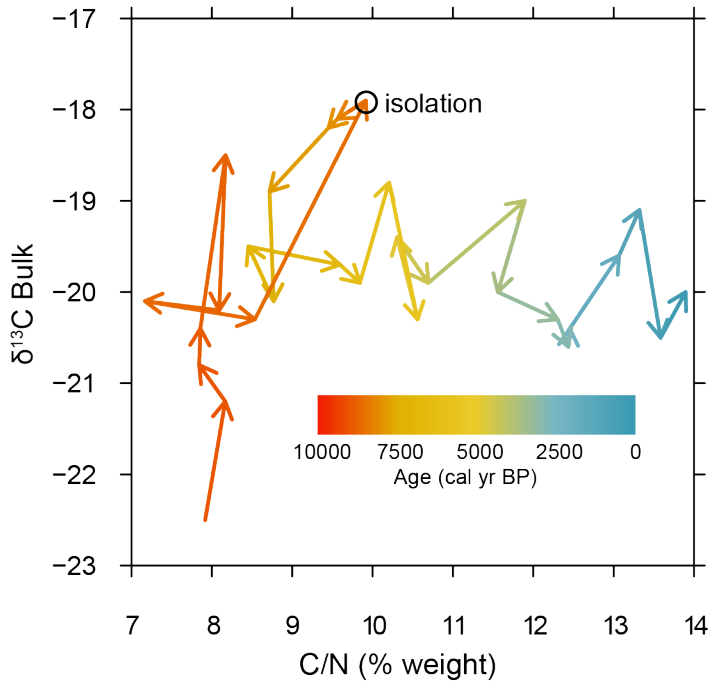

Figure 4.7. Biplot of $\delta^{13}C$ versus C/N in the T1 core.

In core T1, values between 14 and 14.5 ‰ were present between 8.5 and 7.8 ka. Between 7.8 and 2 ka, values became more variable, ranging from 13 to 15 ‰, though generally decreased through time. Relatively low values characterized the time between ~1.5 and 0.2 ka, ranging from 12.7 to 13.3 ‰. Overall, values decreased by about 1.25 ‰over 8000 years, or 0.16 ‰ per thousand years.

$\delta^{18}O$ values from T2, exhibit similar variability and greater value ranges than T1, but also decrease through time. Values ranged between 14 and 16.1 ‰ from 9 ka (right above unit T1-2 and T2-2) to 7 ka. Between 7 and 2.5 ka, values ranged between 15.9 and 11.9 ‰, but averaged 14 ± 0.8 ‰. The lowest values in the T2 core were present 2.5 and 0.5 ka and averaged 12.1 ± 0.8 ‰. The general trend for the T2 core is a decrease of 2.6 ‰ over 9000 years, or 0.3 ‰ per thousand years. Considered together, both lake records record a decrease in $\delta^{18}O$ values of 2.46 ‰ from ~ 9 to 1 ka, or 0.23 ‰ per thousand years. High values in both cores interrupted a decreasing trend

at 6 ka. As described in section 4.3.1, no long term simultaneous $\delta^{18}O$ precipitation – temperature data have been collected from Nuuk. Historical temperature measurement at Nuuk from the Global Historical Climate Network (Menne et al., 2012) paired with modeled monthly precipitation $\delta^{18}O$ values from the OIPC suggest a modern local $\delta^{18}O$ – temperature relationship of 0.27 ‰ $°C^{-1}$ (Fig. 4.2) and support that warmer temperatures in this region will generally be associated with higher precipitation $\delta^{18}O$ values. However, applying this relationship to interpret the paleo-isotope record results in an inferred general 5 to 6 °C cooling trend over the last 9000 years at our study sites. This magnitude of Holocene temperature change far exceeds any other estimate from southern Greenland or nearby regions (e.g., Briner et al. 2016). In contrast, applying instead the global spatial $\delta^{18}O$ – temperature relationship (0.67 ‰ $°C^{-1}$; Dansgaard (1964)) results in an inferred 2 to 4 °C of cooling over the same period, more in line with other published proxy-based estimates. As described in the Discussion, we view these estimates as providing constraints on past temperature

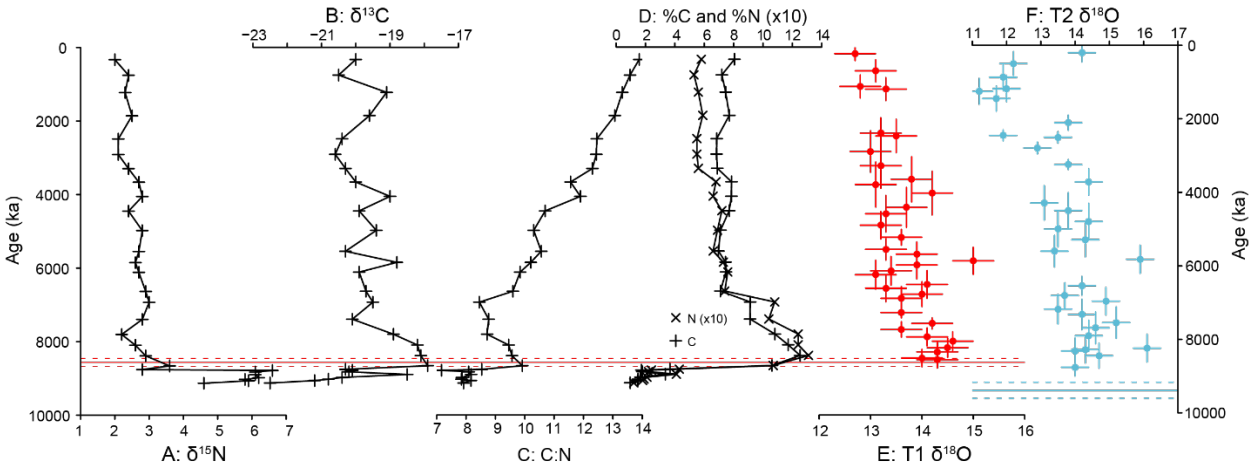

Figure 4.8. Bulk sediment composition and chironomid $\delta^{18}O$ from lake T1 and T2 plotted versus age. From Lake T1: A: $\delta^{15}N$, B: $\delta^{13}C$, C: C:N (weight percent) from T1, D: %C and %N, E: Chironomid $\delta^{18}O$. From lake T2, F: Chironomid $\delta^{18}O$. The red line represents the transition from a glacio-marine to lacustrine environment in T1 (i.e. boundary between units T1-3 and T1-2) at ~ 8.6 ka. The blue line represents the same transition in T2 at ~9.4 ka.

changes but – given the demonstrated uncertainty of isotope-temperature relationships over time at this site – not quantitative temperature estimates.

4.4. Discussion

4.4.1 Regional deglaciation and lake isolation

Regional cosmogenic ^{10}Be and ^{14}C evidence from molluscs and lakes, including from the Buksefjord area, indicates that the Greenland Ice Sheet retreated from the present-day coastal shelf near Nuuk beyond its present-day margin rapidly (Larsen et al., 2014; Winsor et al., 2015). These studies suggest our site should have been ice free by ~10.7 ka. Since our study lakes are below the local marine limit (~80 m; Long et al. (2011)), they were submerged below sea level after deglaciation, due to the residual isostatic depression effects of the GrIS. The sedimentological and geochemical properties of the basal clay units in both cores (units T1-3 and T2-3) reflect a marine depositional environment. C:N values < 9 suggest either marine or freshwater algae or particulate organic carbon sources, though δ^{13}C values between -16 and -23 ‰ are more reflective of marine organic matter than freshwater (Fig. 4.7) (Leng and Lewis, 2017). As the land rebounded following deglaciation, T2 and T1 emerged and became discrete basins with T2 (currently at 40 m a.s.l.) isolating first. The banded clay gyttja isolation contact (unit T2-2), characteristic of lake emergence and temporary meromictic conditions (Long et al., 2011) is evident in the visual stratigraphy (Fig. 4.4) and marks T2's transformation to a lake at 9390 ± 210 cal yr BP. Lake T1, (currently 17.5 m a.s.l.) located adjacent to (~140 m away) but below T2, isolated about 800 years later at 8570 ± 110 cal yr BP. Similar isolation lakes cored near Nuuk by Kobbefjord at 38 to 34 m a.s.l. record the marine to non-glacial lacustrine transition at ~ 8.7 and 8.5 ka respectively, in agreement with our regional isolation estimates at comparable altitudes (Larsen et al., 2017).

The presence of non-laminated clay rich gyttja (unit T2-1) above the marine-lacustrine transition (unit T2-2) in T2 suggests that some glacial influence was present in the watershed upon this lake's relatively early isolation. Initially high Ti and Si in the basal (marine) unit T1-3 of T1 also suggests regional glacial activity in the coastal fjords or shallow coastal environments at our site between 10.7 and approximately 8.5 ka. However, high Ca and S concentrations and the absence of visible sand/coarse grains (ice rafted debris) within the marine units at both lakes indicate the site experienced minimal distal glacier influence, at least after 9.1 ka (Fig. 4.6). By the time T1 and the nearby Kobbefjord lakes became isolated between 8.7 and 8.5 ka, local glacial runoff did not reach lakes T1 and T2.

4.4.2. Timing of Holocene climate and environmental change

After isolation, $\delta^{13}C$ of bulk sediment remained elevated for ~1000 yrs, suggesting relatively brief elevated inorganic C deposition relative to what came after, presumably from freshly comminuted glacio-marine deposits covering the catchment (Anderson et al., 2018). A slow decline of S and Ca content following isolation supports the idea that residual marine sediments blanketing the watershed were transported into the lake in the early centuries of lake development, or at least that there was a lingering marine influence, perhaps from sea spray (Fig. 4.6D) (Wagner and Bennike, 2012). Elevated %C and %N immediately above the meromictic isolation transition (i.e., the boundary between units T1-1 and T1-3) are indicative of a productive lake environment between 8.5 and 7 ka. While inorganic C deposition was likely elevated, the paired increase in and extended duration of both %C and %N also points to relatively high organic productivity, supported by high $biSiO_2$ (19 – 26%) (Fig. 4.6). C:N remains < 10 until ~7 ka,

indicative of high aquatic productivity dominated by algae or invertebrates and/or a possible lingering marine influence (Leng et al., 2012).

More positive $\delta^{18}O$ values from both T1 and T2 during the first 2000 years of lacustrine deposition (~9 to 7 ka) indicate that this high productivity may have been associated with warmer temperatures in the region (Fig. 4.8). The local HTM (period of peak Holocene temperatures) at our study site near Nuuk overlaps with this period, although we cannot evaluate whether climate prior to that (during the period of glaciomarine deposition at our sites) was as warm or even warmer. Warm growing season temperatures near our site are also inferred from pollen assemblages from lakes around Nuuk between 9 and 8.5 ka (Fredskild, 1983), and warm indicator statoblasts present in lakes sediments near the present day Sisimiut coast (370 km to the north) suggest warmer than present conditions between 10.2 and 4.7 ka (Wagner and Bennike, 2012). High chlorophyll-*a* and *β* carotene values at coastal lakes near Sisimiut also suggests higher lake productivity, presumably driven by warmer temperatures between 9 and 5.6 ka (Law et al., 2015; Perren et al., 2012a). Farther afield of our site, relatively warm summer temperatures, analogous to the present day coastal climates of south Greenland are inferred from terrestrial leaf wax $\delta^{2}H$ at Lake N3 (~ 550 km N near Illulisat) between 8 and 5 ka (Fig. 4.9D), particularly in the first 1000 years of the record (Thomas et al., 2016). Chironomid inferred July temperatures from North Lake (also near Illulisat) show warmer than present conditions from 7.1 (though possibly earlier, as this is the beginning of this sediment record) to 2.6 ka (Fig. 4.9C) (Axford et al. 2013). The North Lake study and interpretation of inland lake level changes near Kangerlussuaq (Aebly and Fritz 2009) suggest peak Holocene warmth ~2-4 degrees warmer than present between ~6 and 4 ka. Additional lake studies around the Kangerlussuaq area also suggest similar arid conditions between 7 and 5.6

ka (Anderson and Leng, 2004; McGowan et al., 2003). We note however that a strong precipitation gradient currently exists between the coast near Sisimiut, and the inland Kangerlussuaq area (Curtis et al., 2018). It is therefore possible that past arid conditions at inland sites was a relatively local phenomenon. Farther south at Qipisarqo Lake near Kangilinnguit, peak July temperatures are inferred from pollen assemblages between 7.5 and 6.5 ka (Frechette and de Vernal, 2009), while in contrast at the same site chironomid inferred temperatures from $\delta^{18}O$ and assemblages indicate earlier peak warmth between 9 and 7 ka (Fig. 4.9F) (Wooller et al., 2004). Based on these terrestrial records, generally warm temperatures around southwest Greenland occurred between 9 and 5 ka. Although there is less consensus on a specific duration of peak warmth across the region, many studies suggest that maximum Holocene temperatures occurred relatively early within this time window (~8.5 to 7 ka).

In addition to a strong response of the GrIS margin in southwest Greenland to high summer insolation in the early Holocene (Fig. 4.9A), glaciologically separate ice masses in the vicinity of our site also support peak warmth prior to 8 ka. Larsen et al., (2017) studied three glacial threshold lakes near Nuuk and reconstructed the glacial history of nearby ice caps. The Qasigiannguit Ice Cap (currently 680 – 1000 m a.s.l.) near Nuuk survived following deglaciation of the region ~ 10.7 ka but disappeared by ~7.9 ka. Two other local, higher altitude ice caps also retreated significantly or vanished altogether before 8 ka. Larsen et al., 2017 proposed that these ice caps near Nuuk are sensitive to and respond to changes in temperature on the order of centuries. For the ice caps to have melted out of the lake watersheds by 7.9 ka, it is conceivable that peak warmth in this region preceded locations farther north up the coast, initiating retreat of the Nuuk ice caps a few centuries before glacially influenced sediment disappeared from the lake record.

Following peak warmth, the climate gradually deteriorated and the environment around our study site stabilized beginning at 7 ka. As %C decreased after 7 ka, bioSiO_2 increased up to 26% and C:N values gradually increased to the range of 10 to 15, indicating increasing terrestrial input to the lake from the watershed (Fig. 4.8) (Leng and Lewis, 2017) albeit with continued algal contributions. Relatively stable %C and %N between 7 ka and the present, as well as a progressive trend towards more negative $\delta^{13}C$ values likely reflects ontogeny processes in the form of declining lake productivity and the establishment of stable oligotrophic conditions (Law et al., 2015). $\delta^{18}O$ remained variable, though more negative than the first 1500 years. The gradual trend towards more negative values between 7 and 1 ka was interrupted by anomalously high $\delta^{18}O$ values recorded in both cores at ~ 6 ka. More positive temperatures are also inferred around this time from alkenones at Braya Sø near Kangerlussuaq (D'Andrea et al., 2011) and may indicate a transient warm event on the west coast of Greenland. Regionally warm conditions are also inferred from extra-limital taxa preserved in lake sediments between 7 and 6.5 ka (Bennike et al., 2010), overlapping with decreased lake water levels and inferred arid conditions at multiple inland lakes between 7.4 and 6 ka (Anderson and Leng, 2004; Bennike et al., 2010).

Progressive cooling in the region after 7 ka is supported by the regrowth of the Nuuk area ice caps. The earliest evidence of these ice caps reforming is at ~ 5.5 ka, when glacial melt from the highest altitude ice cap re-entered the watershed of a threshold lake (Larsen et al., 2017). Snow-line lowering / expansion of the larger Sukkertoppen Iskappe north of these more local ice caps near Nuuk is also documented at ~4.3 ka following a few thousand years of diminished extent (Schweinsberg et al., 2018). Continued lowering of ice cap equilibrium line altitudes on the west coast of Greenland is marked by glacial sediment re-appearing in progressively lower elevation

lake records between 3.6 to 3.5 ka, and later between 1.6 and 0.8 ka (Larsen et al., 2017). Similarly dated periods of enhanced ice cap advance from Sukkertoppen is noted at ~1.8, 1.2 and 0.7 ka (Schweinsberg et al., 2018). In addition to gradually decreasing insolation, these ice cap advances roughly correspond to a postulated slowdown of the West Greenland Current which could have enhanced cooling off the west Greenland coast (Perner et al., 2012). Increased sea ice, coinciding with reduced meltwater input is described not long after the WGC slowdown in Ameralik Fjord at ~3 ka (~ 50 km N of our study site) (Moller et al., 2006). Episodes of late Holocene glacial advance farther north at Sukkertoppen have also been loosely linked to increased volcanic activity and resulting sea-ice/ ocean feedbacks (Schweinsberg et al., 2018), similar to other snow-line lowering events documented across Baffin Bay (e.g. Miller et al., 2012). The resolution of our new dataset largely precludes making such conclusions about centennial to decadal climatic variability due to volcanic activity or other short-term internal feedbacks. However, sub-millennial changes in ocean dynamics off the west coast of Greenland may have modulated or enhanced regional cooling in the late Holocene. Millennial scale differences between the timing of maximum warmth in proxy records around west Greenland, Baffin Bay and Baffin Island over the last 9000 years likely reflects ocean or residual ice sheet / meltwater modulation of regional to local climates.

That our record shows the warmest conditions prior to 8 ka and thus earlier than described in a limited number of climate records farther north on the west Greenland coast could be due to a number of factors. First, the apparent conundrum may exist because many west Greenland lake records that explicitly reconstruct temperature do not extend back to the early Holocene (before 8 ka) and may therefore not capture peak warmth. The North Lake temperature record near Illulisat shows a warming trend from the beginning of the record at 7.1 ka, reaching peak temperatures

later at 6 ka (Fig. 4.9C) (Axford et al., 2013). This contrasts with a separate lake record that shows a general monotonic decrease in terrestrial δ^2H values from ~ 8 to 1 ka, possibly representative of relative summer temperature change (Fig. 4.9D) (Thomas et al., 2016). If delayed warming did characterize the Baffin Bay region north of the Davis Strait, one hypothesis is that residual cold water from the rapidly retreating Laurentide Ice Sheet (LIS) and GrIS occupied Baffin Bay and muted the effects of early Holocene peak summer insolation (Kaufman, 2004). This hypothesis is now supported by a multi-proxy marine record from Disko Bay indicating both cold bottom water and cold freshwater at the surface from at least 8.3 to 7.5 ka (Moros et al., 2016). The effects of residual GrIS meltwater cooling in Baffin Bay could also have been localized north of the Davis Strait. Additional marine records documenting the early to mid-Holocene are sparse south of the Davis Strait and off the coast of Nuuk near our study site, but there is some evidence of regional sea surface temperature heterogeneity between Baffin Bay and the Labrador Sea (Ouellet-Bernier et al., 2014). While warmer temperatures were not present north of the Davis Strait until ~7.5 ka, elevated sea surface temperatures were found in the northern most Labrador Sea prior to 7.6 ka (Gibb et al., 2015). Warmer sea surface temperatures attributed to a strong, retroflected West Greenland Current were also documented in the northwest Labrador Sea between 8.6 and 7.4 ka (Lochte et al., 2019). Presently, a significant proportion of the warmer (and denser/deeper) Irminger Current component of the WGC is diverted west, then south to mix with the Baffin Current south of the Davis Strait (Schmidt and Send, 2007; Seidenkrantz, 2013). A similar hydrographic configuration of the current could have limited the warming effects of the WGC near Disko Bay during the early Holocene. Proximity to the GrIS in the early Holocene could also have modulated local climates. Early Holocene margins of the inland ice in the vicinity of our site were

up to and possibly over 100 km distant, diminishing ice sheet climatic influences near Nuuk (Larsen et al., 2014), but were likely an order of magnitude less up the coast where possible delayed warming occurred (Briner et al., 2010).

One goal of reconstructing past climates over Greenland is improving the spatial and temporal resolution of data used to force ice sheet models. Constraining the sensitivity of the ice sheet to past temperature shifts is critical to improving estimates of ice mass loss in the near future. Our new isotope inferred temperatures estimates may assist in both explaining past model shortfalls and improving future model results. Levy et al. (2017) noted discrepancies between GrIS extent estimates from the Huy3 model in the early to mid-Holocene and measured observations of ice retreat behavior in SW Greenland. The Huy3 model both delays the timing of early Holocene retreat, and overestimates mid Holocene retreat distance slightly north of our study site (Lecavalier et al., 2014). As our isotope record suggests, peak warmth prior to 8 ka may have aided the rapid and significant retreat of the ice margin past its present-day location by 10.4 to 10.7 ka around Nuuk. Gradually declining regional temperatures after 8 ka could have slowed retreat rates in the middle Holocene. This revised temperature history in southwest Greenland – which differs from the central GrIS ice core derived temperature history used in deglaciation models could help account for the apparent overestimated maximum retreat north of Godthabsfjord (Levy et al., 2017).

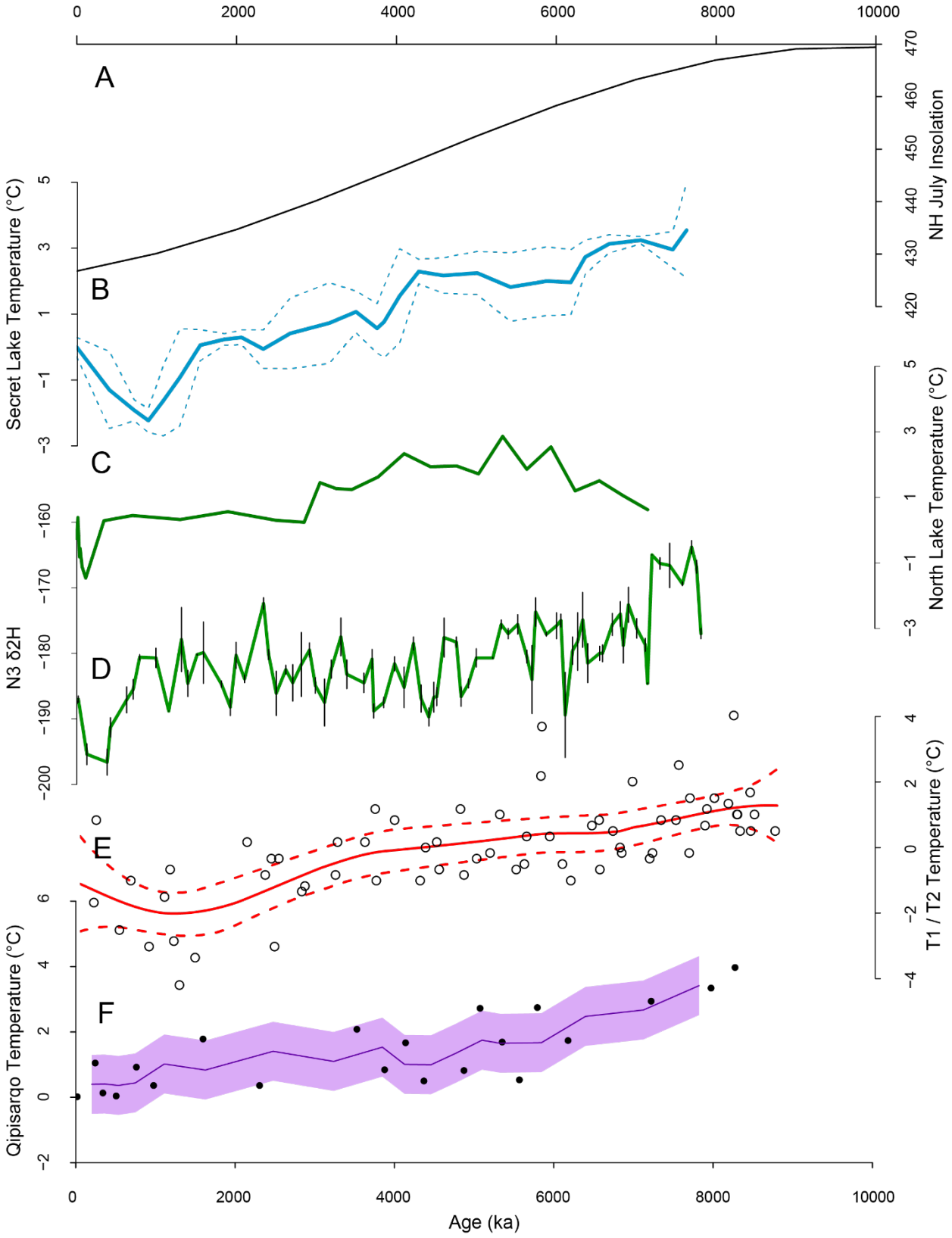
A
B
C
D
E
F
0
2000
4000
6000
8000
10000
NH July Insolation
420
430
440
450
460
470
Secret Lake Temperature (°C)
−3
−1
1
3
5
North Lake Temperature (°C)
N3 δ2H
−200
−190
−180
−170
−160
T1 / T2 Temperature (°C)
−4
−2
0
2
4
Qipisarqo Temperature (°C)
−2
0
2
4
6
Age (ka)

Figure 4.9. (previous page) Comparison of temperature proxy data from the west coast of Greenland. A: Northern Hemisphere summer insolation at 65N (W m-^{2}). B: $\delta^{18}O$ inferred temperature anomaly at Secret Lake near Thule (Lasher et al., 2017). C: Chironomid assemblage inferred temperature anomaly at North Lake near Illulisat (Axford et al., 2013). D: $\delta^{2}H$ from N3 near Illulisat (Thomas et al., 2016). E: Combined $\delta^{18}O$ inferred temperatures from T1 and T2 (assuming temperature – $\delta^{18}O$ relationship of 0.67 ‰ °C^{-1}), fitted using a generalized additive model in the R package gratia (Simpson, 2019). F: $\delta^{18}O$ inferred temperatures from Qipisarqo Lake in south Greenland (Wooller et al., 2004)

4.4.3. Assessing the magnitude of Holocene temperature change and isotope-temperature relationships

Existing terrestrial temperature records from the west coast of Greenland largely converge on 3 to 4 °C of cooling from maximum HTM warmth to minimum Neoglacial cold over the Holocene (Fig. 4.9). Temperatures inferred from chironomids at North Lake near Illulisat were between 2 and 3 °C warmer than present, and experienced ~ 4 °C of absolute cooling over the Holocene (Axford et al., 2013). Chironomid assemblage inferred temperature change from a south Greenland lake (Qipisarqo) shows summer cooling of ~2 °C over the Holocene, comparable to chironomid $\delta^{18}O$ inferred changes that show slightly greater mean annual temperature cooling on the order of 3 to 4 °C (Wooller et al., 2004). A later pollen reconstruction, also from Qipisarqo, suggests July air temperatures cooled by ~4 to 5 °C over the Holocene (Frechette and de Vernal, 2009). Greater magnitude Holocene temperature changes are documented elsewhere on Greenland and across Baffin Bay, likely due to differing regional responses to insolation forcing and associated feedbacks (Axford et al., 2009b; Axford et al., 2017; Lasher et al., 2017; McFarlin et al., 2018).

To estimate the change in temperature at our study site from the chironomid $\delta^{18}O$ values, we can use a temperature – $\delta^{18}O$ relationship. If we apply the modern temperature – $\delta^{18}O$

relationship calculated at our site using the online isotope of precipitation calculator (0.27 ‰ °C-1; Bowen, 2018) to interpret our Holocene precipitation isotopes reconstruction, the resulting temperature reconstruction suggests over 10 °C of absolute temperature change over the last 9000 years. This magnitude of change greatly exceeds most existing proxy records mentioned in the previous paragraph that cover the same time span around west Greenland, Baffin Bay and eastern Arctic Canada (Axford et al., 2009b; Axford et al., 2013; Frechette and de Vernal, 2009; Lasher et al., 2017; McFarlin et al., 2018; Wooller et al., 2004). Even using an average Greenland-wide Holocene temperature – $\delta^{18}O$ relationship of 0.36 ‰ $°C^{-1}$ (Kobashi et al., 2017) to interpret our results from lakes T1 and T2 suggest overall Holocene temperature change greater than any independent proxy record. This implies that neither of these isotope-temperature relationships was consistently applicable over time at our study sites throughout the Holocene. Simulated isotope sensitivity at ice core sites during the last glacial period indicates that the temperature - $\delta^{18}O$ relationship at the Dye-3 ice core site (the closest ice core to our study site) is significantly different from other ice core sites farther north (e.g. GISP2) (Sime et al., 2019). Though the results of this last glacial period modeling study are not directly comparable to our Holocene record, the estimated mean sensitivity at the Dye-3 site was 0.63 ‰ $°C^{-1}$, much closer to the modern day global and high latitude marine sites relationship. Interpreting our isotope data using the observed global spatial or high latitude marine sites spatial relationships - 0.67 to 0.71 ‰ $°C^{-1}$ - (Arppe et al., 2017; Dansgaard, 1964) results in inferred average temperature changes at T1 and T2 of ~ 2 to 4 °C over the last 9000 years (Fig. 4.9E). This range overlaps with the independent proxies summarized above, and with recently modeled annual temperature output near Nuuk (Buizert et al., 2018).

Since surface air temperature exerted a strong influence on other regional proxy records (Axford et al., 2013) and local glaciers and ice caps (Larsen et al., 2017), it was likely a primary control on precipitation $\delta^{18}O$ at our site through the Holocene. However, other factors may have also influenced $\delta^{18}O$ of precipitation and lake water isotopic composition over time at our site. In addition to the role of ocean currents in modulating coastal air temperatures and precipitation condensation temperatures in around Baffin Bay, sea ice may have a large impact on both temperature and moisture availability/moisture source. For example, different sea ice conditions in northern Baffin Bay in the early to mid-Holocene may have influenced $\delta^{18}O$ values documented in chironomids at Secret Lake near Thule (Lasher et al., 2017). Between ~7 and 3.6 ka, ice-free conditions persisted in northern Baffin Bay for 4-5 months per year, compared with the 1 to 2 months common in over the last 3000 years (Ledu et al., 2008; Levac et al., 2001). Enhanced moisture availability from a local precipitation source (e.g. an ice-free northern Baffin Bay) would result in higher precipitation $\delta^{18}O$ values (Faber et al., 2016; Malmierca-Vallet et al., 2018). Reduced sea ice cover has also been shown to change the temperature – $\delta^{18}O$ relationship, resulting in a steeper slope (Faber et al., 2016). However, we suggest that the impacts of sea ice on $\delta^{18}O$ values of precipitation at our site in southwest Greenland are likely less than farther north in Baffin Bay. Sea ice is usually only present for 1 to 2 months of the year near Nuuk (Fetterer et al., 2019) and the duration of sea ice cover in southern Baffin Bay was further reduced in the mid Holocene (de Vernal et al., 2013; Sha et al., 2017). The resulting absolute change in annual moisture availability would presumably have been less than further north, minimizing possible changes in $\delta^{18}O$ attributable to sea ice conditions on millennial time scales.

4.5. Conclusions

Multiple proxies analyzed from two isolation basins in southwest Greenland track millennial scale climate change through the Holocene. Following deglaciation of coastal southwest Greenland c. 10.4 ka, lakes T1 and T2 emerged from the sea between 9.4 and 8.5 ka as the landscape rebounded and relative sea level fell. More positive $\delta^{18}O$ values measured in chironomid head capsules suggest peak warmth in the region occurred in the early Holocene between 9 and 7 ka, coincident with elevated C concentration. $\delta^{18}O$ values gradually decreased by 2 to 3 ‰ from 7 ka into the late Holocene, which we interpret at least partly as a response to insolation driven cooling also evidenced by the local glacial history. This inferred gradual cooling drove progressive lowering of snow lines on regional ice caps between 5.5 and 0.6 ka. Ocean currents, particularly the West Greenland Current likely contributed to sub-millenial scale modulation of the southwest Greenland climate. Paired $\delta^{13}C$ and C:N values shows an evolution from early to late Holocene towards oligotrophic lake conditions and stabilization of the surrounding catchment as temperatures decreased.

We argue that $\delta^{18}O$ values of chironomids are a strong proxy for precipitation $\delta^{18}O$ at our site. However, the temperature – $\delta^{18}O$ relationship in southwest Greenland through the Holocene is uncertain, and the modern relationship seems inadequate to explain the likely $\delta^{18}O$ inferred temperature range, limiting our confidence in inferring absolute temperature change. Independent estimates of temperature change from the west coast of Greenland suggest that the 2 to 3 ‰ shift in chironomid $\delta^{18}O$ values at our study sites probably corresponds to ~ 2 to 4 °C of cooling between 9 and 1 ka. Additional independent local reconstructions of temperature over the Holocene will be

critical to understanding the spatio – temporal changes in the temperature – $\delta^{18}O$ relationship in west Greenland.

Acknowledgments

This project was made possible by a National Geographic Society grant awarded to Y. Axford, and a Northwestern University Undergraduate Research Assistant Program grant. I thank M. Osburn, A. Masterson, G. Schellinger, P. Puleo, and C. Lee for lab access and assistance; Woods Hole Oceanographic Institution–National Ocean Sciences Accelerator Mass Spectrometry facility (Woods Hole, Massachusetts, USA) for radiocarbon analysis; Y. Axford, S. Ólafsdóttir and B. Gray for field assistance and T. Axford for building field equipment. We thank the people and Government of Greenland, Ilisimatusarfik (University of Greenland) and M. Rosen for field support.

CHAPTER 5:

Medieval climate at the Norse Eastern Settlement in Greenland

This chapter of research originally appeared in: Lasher, G.E., Axford, Y., 2019. Medieval warmth confirmed at the Norse Eastern Settlement in Greenland. Geology. https://doi.org/10.1130/g45833.1

Abstract

Recent work has documented glacier advances in West Greenland coincident with the Medieval Climate Anomaly (MCA) and warmth across much of Northern Europe. The North Atlantic Oscillation (NAO) has been invoked to explain anti-phasing of temperatures between these North Atlantic regions. Historical and model observations suggest negative correlation between the mode of NAO and both temperature and $\delta^{18}O$ values of precipitation over much of Greenland. We test for a hypothesized positive NAO mode and associated cool conditions during the MCA in South Greenland within the Norse Eastern Settlement by reconstructing $\delta^{18}O$ values of precipitation at sub-centennial resolution over the past 3000 years using aquatic insect subfossils preserved in lake sediments. More positive $\delta^{18}O$ values are found between 900 and 1400 C.E., indicating a period of warmth in South Greenland superimposed on late Holocene insolation-forced Neoglacial cooling, and thus not supporting a positive NAO anomaly during the MCA. Highly variable $\delta^{18}O$ values record an unstable climate at the end of the MCA, preceding Norse abandonment of Greenland. The spatial pattern of paleoclimate in this region supports proposals that North Atlantic subpolar ocean currents modulated South Greenland's climate over the last 3000 years, particularly during the MCA. Terrestrial climate in the Labrador Sea and Baffin Bay regions may be spatially heterogeneous on centennial timescales due in part to the influence of the subpolar gyre.

5.1. Introduction and Motivation

Abundant evidence exists across much of northern Europe for warm conditions during the Medieval Climate Anomaly (MCA, ~ 950 to 1250 C.E.) (Solomina et al., 2016), however climate during this time was more variable elsewhere in the Northern Hemisphere (Consortium, 2013). This period is of interest in Greenland because favorable climate conditions are often associated with Norse settlement of the island at 985 C.E (Jones, 1986). Cooling and increased climate variability is conventionally implicated in the collapse of the Norse settlements ~1450 C.E., however, non-climatic explanations have also been proposed (Dugmore et al., 2012; Hartman et al., 2017). Data constraining local climate within the settlement areas during this period are limited, and it is unclear whether they support climatic explanations for Norse settlement history in Greenland.

Many glaciers around South and West Greenland and Baffin Island advanced after the MCA, reaching their maximum late Holocene extents during the Little Ice Age (LIA, ~ 1250 to 1850) (Larsen et al., 2016; Miller et al., 2012). In contrast, recent investigations also find mountain glacier advance comparable to the LIA between 975 and 1275 C.E. on Baffin Island and in West Greenland (Jomelli et al., 2016; Young et al., 2015). Marine records around Baffin Bay also give contrasting views of conditions for the last 2000 years. Some results indicate a warm MCA relative to the LIA (e.g. Perner et al., 2012), while others find expanded sea ice cover and cool sea surface temperatures (SST) during the MCA (Krawczyk et al., 2017; Sha et al., 2017). Quantitative proxy records of Greenland climate are sparse, and nearly all high-resolution records are from ice cores documenting conditions over the Greenland Ice Sheet (GrIS). Most terrestrial records from Greenland are too coarse to resolve the MCA and LIA, and those with adequate temporal resolution

suggest spatial heterogeneity in the climatic expression of these periods. For example, West Greenland lake records show pronounced cold conditions during the LIA (Axford et al., 2013), but 250 km south, temperatures are highly variable over the last 3000 years with no clear MCA or LIA expression (D'Andrea et al., 2011). The alkenone-based record of D'Andrea et al. (2011) was found to be anti-phased with a speleothem $\delta^{18}O$ record from Ireland, suggesting contrasting climates between West Greenland and Europe. If similar anti-phasing with Europe led to cool conditions in South Greenland (SGL) during Medieval times, this would contradict the hypothesis that climatic warming facilitated Norse settlement there.

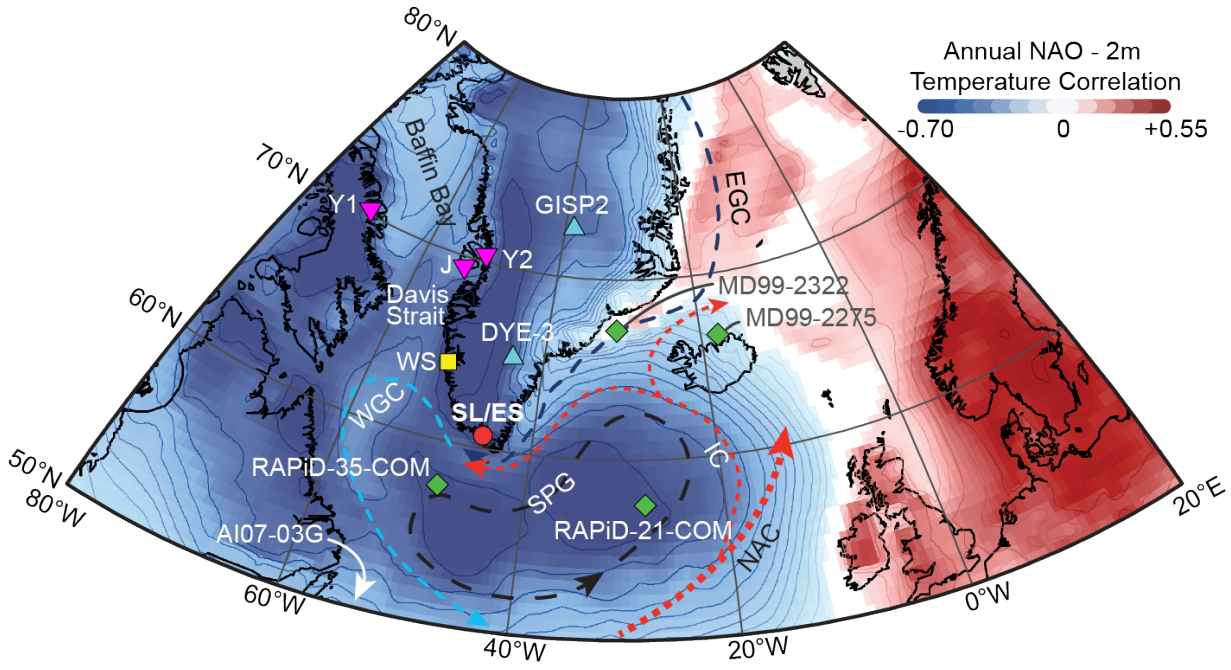

Figure 5.1. Sites, ocean currents and atmospheric patterns discussed in Chapter 5. SL/ES is Scoop Lake and the Norse Eastern Settlement). WS: Western Settlement, blue triangles: ice cores, green diamonds: marine records, and purple triangles: West Greenland and Baffin Bay moraine records from Young et al. (2015; Y1 and Y2) and Joemlli et al. (2016; J). NAC: North Atlantic Current, SPG: Sub Polar Gyre, EGC: East Greenland Current, WGC: West Greenland Current, and IC: Irminger Current.

One mechanism proposed to explain the MCA in Europe, and now too evidence for coeval anti-phased cooling around Baffin Bay, is the North Atlantic Oscillation (NAO). Based upon a tree ring and speleothem-based NAO reconstruction, (Trouet et al., 2009) hypothesized that a dominantly positive NAO (NAO+) mode persisted during the MCA, delivering warm air masses to Northern Europe. Observations of NAO variability suggest that a positive mode could result in cool conditions in South and West Greenland/Baffin Bay during the MCA and perhaps explain glacial advance there (Young et al., 2015). However, other studies contradict the notion of persistent NAO+ conditions throughout this time period (Ortega et al., 2015) (Fig. A1).

To test whether SGL experienced cold conditions during the MCA due to dominant NAO+ conditions, we reconstruct $\delta^{18}O$ of precipitation over the past 3000 years at a site within the western dipole of the NAO and within the Norse Eastern Settlement (Fig. 1). At our study site, both temperature and moisture sources are influenced by the NAO and both affect precipitation $\delta^{18}O$ values in the same direction, amplifying rather than obscuring the isotopic signature of warming or cooling.

5.2. Methods and Approach

We isolated and analyzed $\delta^{18}O$ of subfossil chironomids (the aquatic larvae of Insecta: Diptera: Chironomidae) preserved in lake sediments. Scoop Lake (SL) (N 60.697°, W 45.419°) is a 7 m deep, ~0.05 km^2 remote, non-glacial, through-flowing lake located at 477 m a.s.l. on sparsely to unvegetated granodiorite bedrock. We recovered a 156-cm long gyttja core (16-LOW-U2), with an intact sediment-water interface and intact horizontal stratigraphy throughout (Fig. A2), in August 2016 and analyzed the upper 80 cm of the core for a high-resolution late Holocene

sequence. Eight aquatic plant macrofossils were AMS ^{14}C dated from this zone (Table A1). Chironomid head capsules (CHCs) were prepared following the methods described in Lasher et al. (2017) and analyzed on a Thermal Conversion Elemental Analyzer coupled to an Isotope Ratio Mass Spectrometer.

$\delta^{18}O$ values of CHCs reflect that of the water they grow in (van Hardenbroek et al., 2018), and water source and lake hydrology determine growth water $\delta^{18}O$. SL water collected in late August 2016 plots on the global meteoric water line, indicating minimal evaporation (Fig. A3). The $\delta^{18}O$ value of CHCs in SL surface sediment, (0-1 cm) representing the last ~40 yrs, is 10.8 ± 1 ‰ (n = 3). Using the demonstrated CHC – lake water enrichment factor (+ 22.5 ‰) (van Hardenbroek et al., 2018), average lake water $\delta^{18}O$ over the last 40 years is –11.7 ‰. This value is near identical to mean measured precipitation $\delta^{18}O$ of summer precipitation collected over three weeks in August 2016 (–11.9 ‰), and to the amount-weighted annual average of historical (1961-1974) precipitation (–12.0 ‰) from Kangilinnguit, Greenland (150 km NW) (IAEA/WMO, 2017). Estimated residence time of water in SL is 1-3 years. Considering these factors, we argue that CHC $\delta^{18}O$ from SL is a strong proxy for annual precipitation $\delta^{18}O$ values over SGL.

$\delta^{18}O$ values of precipitation in the high latitudes are strongly correlated with surface air temperatures, and in SGL are also influenced by SSTs and moisture source (Bonne et al., 2014; Sodemann et al., 2008). In SGL, moisture source is strongly influenced by the configuration of the NAO. Models and observations suggest lower $\delta^{18}O$ precipitation values in SGL during NAO+ modes, due to higher latitude (and thus colder) air mass trajectories influencing condensation temperatures (Sodemann et al., 2008; Vinther et al., 2010). If the NAO was in a sustained positive mode during the MCA, CHCs should record more negative $\delta^{18}O$ precipitation values at our study

site. Reconstructed $\delta^{18}O$ at SL will record some combination of changing temperatures and prevalence of high-latitude air masses over time. Due to the meteorological setting of our site these signals are additive, so we interpret changes in $\delta^{18}O$ at SL as maximum constraints on mean annual temperature changes over time.

5.3. Results

Five ^{14}C ages were used to develop the age-depth model in rBacon (Fig. A1), after rejecting three outliers falling outside the 95% confidence intervals of a model containing all dates (Table A1). Given sedimentation rates, each 1-cm-thick sample integrates an average of 40 years. $\delta^{18}O$ values (reported as per mil [‰] relative to VSMOW, analytical $1\sigma = 0.4$ ‰) measured from CHCs decrease by 2.5 ‰ from the beginning of the record 3000 years ago to 900 C.E. (Fig 2A). This trend is interrupted at 900 C.E. when $\delta^{18}O$ values increase by 1.5 ‰. The period between 900 and 1400 C.E. is characterized by overall more positive $\delta^{18}O$ values than both the previous and following four centuries. A brief (<200 yrs) period of lower values is centered at 1150 C.E. The 15th Century marks the transition to overall lower values and exhibits the highest variability of the record. Low $\delta^{18}O$ values persist between 1500 and 1900 C.E. $\delta^{18}O$ values from surface sediments are 2 ‰ higher than average values between 1600 and 1900 C.E., indicating an increase in precipitation $\delta^{18}O$ values during the last century.

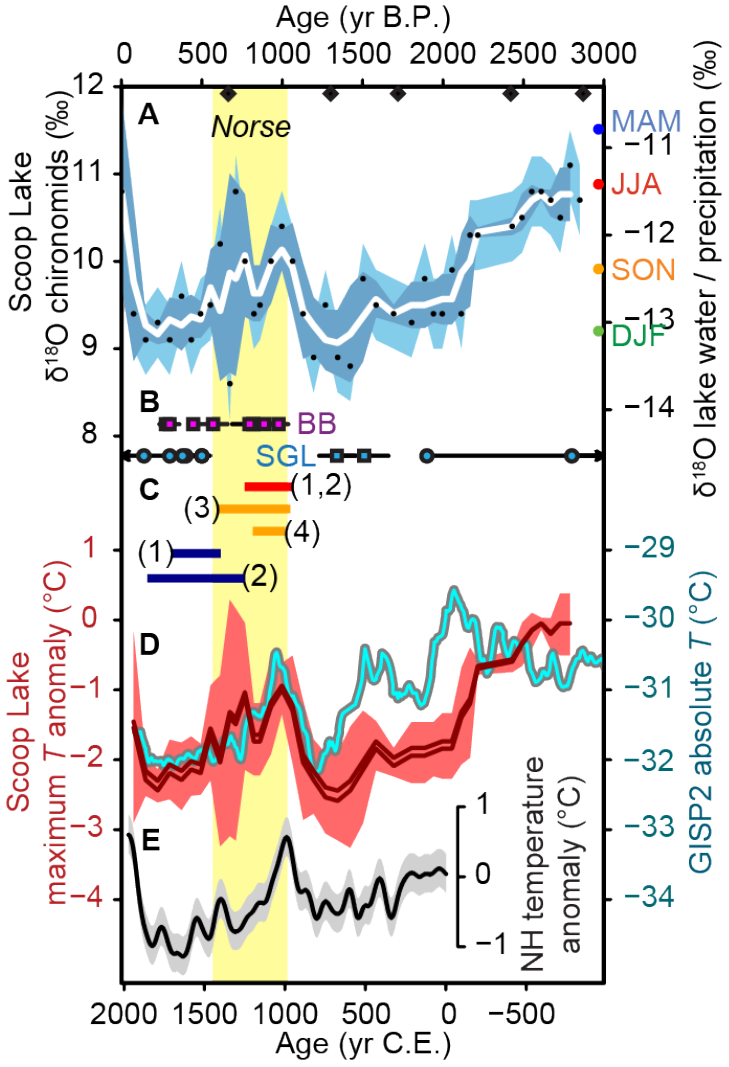

Figure 5.2. Results and temperature interpretations from Scoop Lake (SL), South Greenland. Norse settlement of Greenland bounded in yellow. A: $\delta^{18}O$ values of SL chironomids (light blue band: $\delta^{18}O$ analytical 1σ) and a 3-point moving average (dark blue band: moving average 1σ), right axis circles: 1961-1974 seasonal means of precipitation from South Greenland (IAEA/WMO, 2017). Top axis black diamonds: ^{14}C samples. B: South Greenland (SGL) and Baffin Bay region (BB) late Holocene maximum glacier extent. Circles: glaciers present in SGL lake watersheds (Larsen et al., 2016). Squares: ^{10}Be dated late Holocene glacial extent (Jomelli et al., 2017, Young et al., 2015 and Winsor et al., 2014). C: Durations of the MCA (red), LIA (blue) (1; Moffa-Sanchez and Hall, 2017) (2; Solomina et al., 2016). Peak SSTs (orange) off N. Iceland (3; Sicre et al., 2014) and S.E. Greenland (4; Miettenen et al., 2015). D: SL maximum temperature anomaly inferred from chironomid $\delta^{18}O$ (red), temperatures inferred at GISP2 (Alley, 2004). E: Extratropical NH temperature (Christiansen and Ljungqvist, 2012).

We estimate temperature from inferred precipitation $\delta^{18}O$ using two methods: the global $\delta^{18}O$ - temperature relationship of 0.67 ‰/ °C (Dansgaard, 1964) and a similar relationship observed at coastal high-latitude North Atlantic IAEA sites (0.71 ‰/ °C; Arppe et al. (2017)). These relationships translate into Neoglacial cooling of ~2 °C between 3000 and 1500 years ago (Fig. 2D). This cooling trend was interrupted by warming of ~1.5 °C between 900 and 1400 C.E., punctuated by a multi-decadal cooling event. Consistent LIA cooling, 1.5 °C colder than the preceding warmth, lasted between 1500 and 1900 C.E. and was followed by a warming of 2 °C to present.

5.4. Discussion

The hypothesized anti-phase cold expression over Greenland during the MCA from a dominant NAO+ configuration is not supported by our results. Neoglacial cooling in SGL is interrupted by warmer, albeit variable, temperatures between 900 and 1400 C.E. Ice core temperature reconstructions in central Greenland are similar in timing and magnitude to those at our site, particularly over the last 1000 years (Fig. 2D) (Alley, 2004). The magnitude of temperature shifts over South and central Greenland is generally higher than multi-proxy reconstructions of temperature for the whole Arctic (Christiansen and Ljungqvist, 2012), suggesting either amplified local temperature change or that isotopes here also reflect changes in dominant moisture source that accompanied past temperature changes. The timing of GrIS fluctuations around SGL agrees well with temperature trends at SL. Neoglacial advance nearby culminated by 1.8 ka, with subsequent retreat then advance at 500 C.E. (Larsen et al. 2016) (Fig. 2B). An outlet glacier near Narsarsuaq (50 km N of SL) reached its late Holocene maximum

between 500 and 800 C.E., coincident with inferred cool temperatures (Fig. 2B) (Winsor et al., 2014). However, across the broader western dipole of the NAO, proxy records paint a complex picture of MCA conditions. We propose and explore two explanations for these seemingly conflicting patterns:

(1) There was no prolonged, dominantly NAO+ configuration during the MCA. More positive water vapor/precipitation $\delta^{18}O$ values – such as those observed during most of the MCA at our study site – are delivered to SGL during NAO- configurations (Bonne et al., 2014). Additionally, while several mountain glacier records show LIA-comparable advance during the MCA, no centennially-resolved terrestrial proxy records from Greenland or Baffin Island show four centuries of cold Medieval conditions. The isotope record at SL shows 1.5 °C of warming beginning at 900 C.E. and a generally warm MCA, but with variable conditions including cooler decades around 1150 C.E. Brief cold spells during overall milder temperatures following 1500 years of insolation-forced Neoglacial cooling may have permitted LIA-equivalent advance of some sensitive mountain glaciers during the MCA. This explanation does not require that the NAO was in a dominant negative configuration during the MCA, but rather suggests that SGL warmed via another mechanism. Our results support a recent proxy-informed NAO model reconstruction that found no positive anomaly during the MCA (Ortega et al., 2015).

(2) Late Holocene climate in coastal SGL was modulated by subpolar gyre (SPG) circulation, which could explain warming there during the MCA. Enhanced Labrador Sea deep water formation associated with a strong SPG between 1000 and 1400 C.E. could have enhanced warm water delivery to coastal areas around SGL via the Irminger Current (IC), raising SSTs and coastal air temperatures. Coeval SST anomalies of approximately the same magnitude as

temperatures at SL are documented off the north Icelandic shelf and Southeast Greenland (Fig. 1, Fig. 2C) (Miettinen et al., 2015; Sicre et al., 2014). Cold-biased benthic foraminifera decrease between 1000 and 1300 C.E. in Igaliku fjord, <10 km from SL, providing local evidence for warm IC influence (Lassen et al., 2004).

Strong warming from changes in the SPG was likely localized around SGL and Iceland, with less influence north of Davis Strait and the Norse Western Settlement. Much of the warm IC component of the West Greenland Current, responsible for SGL's mild climate, is diverted south of Davis Strait (Seidenkrantz, 2013) (Fig. 1). This geographically variable influence of the West Greenland Current helps explain modern climatic heterogeneity in the region, and likewise could contribute to spatial variability in past climate trends. SST decreases off Labrador and indicators of Labrador Sea water south of Iceland support a vigorous SPG and enhanced cold Labrador Current during the MCA (Moffa-Sanchez and Hall, 2017; Sicre et al., 2014), which could have driven contrasting cool conditions favorable for glacier advance on Baffin Island.

5.5. Conclusions and Implications

We conclude from our reconstruction of oxygen isotopes of precipitation that the MCA in southernmost Greenland near the Norse Eastern Settlement was generally warmer between 900 and 1400 C.E., reversing 1500 years of Neoglacial cooling and overlapping with the arrival of Norse settlers at 985 C.E. (Jones, 1986). Cold conditions following the MCA began with a period of exceptional climate instability (the period of highest sample-to-sample variability in our isotope record) from 1350 to 1450 C.E. that preceded Norse abandonment ~1450 C.E. Multiple factors have been linked to Norse settlement and abandonment of Greenland, including climate change,

food shortages, and cultural dynamics (Dugmore et al., 2012; Hartman et al., 2017). Our results now provide direct evidence for major contemporaneous climate shifts within the Eastern Settlement.

The climate of SGL over the last 1500 years was largely in phase with Northern Europe and was probably strongly influenced by major subpolar ocean currents. Warm MCA temperatures in SGL, inferred here from a proxy sensitive to NAO-related changes in atmospheric circulation, do not support the hypothesis that the MCA was a period of dominantly positive NAO conditions. MCA glacier advances documented on the coasts of northern Baffin Bay may be compatible with warmth in SGL due to different effects of the SPG north of Davis Strait, or those advances could record regional short-term cooling superimposed over general MCA warmth. Additional studies reconstructing sub-centennial climate variations around Greenland and its coastal margins are needed to diagnose the complex mechanisms of climate change there. This is especially urgent given the critical role that this region, home to vulnerable components of the Atlantic overturning circulation and to a dynamic sector of the GrIS, will play in future global change.

Acknowledgments

This project was funded by U.S. National Science Foundation Polar Programs CAREER award 1454734, and a Northwestern University Undergraduate Research Assistant Program grant. We thank M. Osburn, A. Masterson, P. Puleo, and C. Lee for lab access and assistance; Woods Hole Oceanographic Institution–National Ocean Sciences Accelerator Mass Spectrometry facility (Woods Hole, Massachusetts, USA) for radiocarbon analysis; A. Hartz, G. Sinclair, and J. McFarlin for field assistance; T. Axford for building field equipment; and M. Chipman for manuscript improvement. We thank the people and Government of Greenland (license VU-00096,

export permit 009/2016), and Air Greenland, Polar Field Services, and J. Simund for field support. We thank two anonymous reviewers whose feedback improved this manuscript.

CHAPTER 6:

Late Holocene climate variability in the subpolar North Atlantic, Baffin Bay and Greenland

Abstract

Recent paleoclimate reconstructions from Greenland, Baffin Bay and the subpolar North Atlantic suggest that a spatially and temporally heterogeneous climate characterized the late Holocene. This chapter explores this regional heterogeneity using 29 centennially resolved temperature proxy records within the bounds of approximately 50° to 80° N latitude and 80° W to 20° E longitude. A composite temperature record from these sites show a general cooling trend over the last 3000 years driven by continued decreasing insolation in the late Holocene. Cooling in the region culminated by 1900 CE, coincident with widespread evidence for maximum glacier advance on Greenland, Baffin Island and Iceland. An increase in regional temperatures occurred in the 20th century. This progression of millennial scale cooling interrupted by warming during the industrial era is consistent with other spatially overlapping climate synthesis studies. Principal component analysis (PCA) was also performed on a subset of the temperature proxy records between 100 and 1900 CE. The first principal component (PC) explains 36% of the variance and shows a uniform cooling trend across much of the region. PC two explains 13% of the variance, and shows localized centennial scale warming around south Greenland and Iceland between 1000 and 1400 CE, superimposed on the insolation driven cooling trend. A comparison of the composite temperature reconstruction with a PCA analysis of ocean circulation proxy records from the subpolar North Atlantic suggest that the subpolar gyre (SPG) plays a critical role in modulating centennial scale climate change within the bounds of the study area.

6.1. Introduction

Recent Holocene paleoclimate data syntheses have produced expansive databases of proxy records at variable temporal resolutions (PAGES 2k Consortium, 2013; 2017; Sundqvist et al., 2014). Among syntheses and reviews relevant to the Arctic and subarctic are studies focused on the Western Hemisphere Arctic (Kaufman, 2004), Arctic Canada and Greenland (Briner et al., 2016), Fennoscandia (Sejrup et al., 2016), Beringia (Kaufman et al., 2016) and the Earth as a whole (Marcott et al., 2013) throughout the Holocene. By summarizing numerous, diverse proxy datasets, these studies have elucidated coherent trends and regional differences in what is inherently noisy paleoclimate data. In particular, the use of probabilistic principal component analysis of compiled proxy records has helped show second and possibly third order trends. For example, the role of orbitally forced insolation changes over the last 11,000 years in many Northern Hemisphere regions is now clear. Meanwhile, less obvious spatio–temporal patterns can now be better attributed to climatic influences such as ocean circulation or the effects of residual ice sheets from the Last Glacial Maximum (Briner et al., 2016; Sejrup et al., 2016).

These same Holocene scale synthesis studies have also identified sub-millennial, and occasionally sub-centennial, climate anomalies superimposed on multi-millennial trends. Within the last 3000 years, and within the North Atlantic region, the most common anomalies are the Roman Warm Period (RWP, ~-700 CE to 400 CE), the Medieval Climate Anomaly (MCA, ~ 950 to 1250 C.E.) and the Little Ice Age (LIA, ~1250 to 1850 CE). As is true with millennial scale climate change around the Arctic (e.g. the HTM or the onset of Neoglaciation), the timing and spatial coherence of these anomalies remains a matter of debate.

Clearly identifying the spatial and temporal extents of climatic events on a centennial time scale requires a more focused approach than the Holocene studies. The efforts of the PAGES 2k Consortium and others have resulted in a handful of higher resolution climate reconstructions, but these often explore only the last 2000 years (Christiansen and Ljungqvist, 2012; Consortium, 2013; Consortium, 2017; Kaufman et al., 2009; Mann et al., 2008). Paleoclimate research around Baffin Bay, Greenland, and the broader North Atlantic suggests that a highly heterogeneous climate characterized the last few millennia and that the causes of this heterogeneity are complex. For example, maximum late Holocene glacial advance in west Greenland and on Baffin Island (Jomelli et al., 2016; Young et al., 2015) occur at the same time as anomalously warm temperatures are recorded in south Greenland (Lasher and Axford, 2019). Warm sea surface temperatures near Iceland (Sicre et al., 2011) occur simultaneously with cooling off the Labrador coast (Sicre et al., 2014).

Considering such observations, this study is designed to explore three related questions: 1) What was the spatio-temporal pattern of century-scale climate change over the region spanning Baffin Bay and the Labrador Sea to the Norwegian Sea, encompassing Greenland and Iceland, over the last 3000 years? 2) How do the climate changes in this region compare with the conclusions of synthesis studies from other regions or wider areas? 3) What mechanisms are responsible for centennial climate change in this subpolar North Atlantic region? We investigate these questions by examining centennial scale climate trends in published proxy datasets from the North Atlantic region within the bounds of approximately 50° to 80° N latitude and 80° W to 20° E longitude.

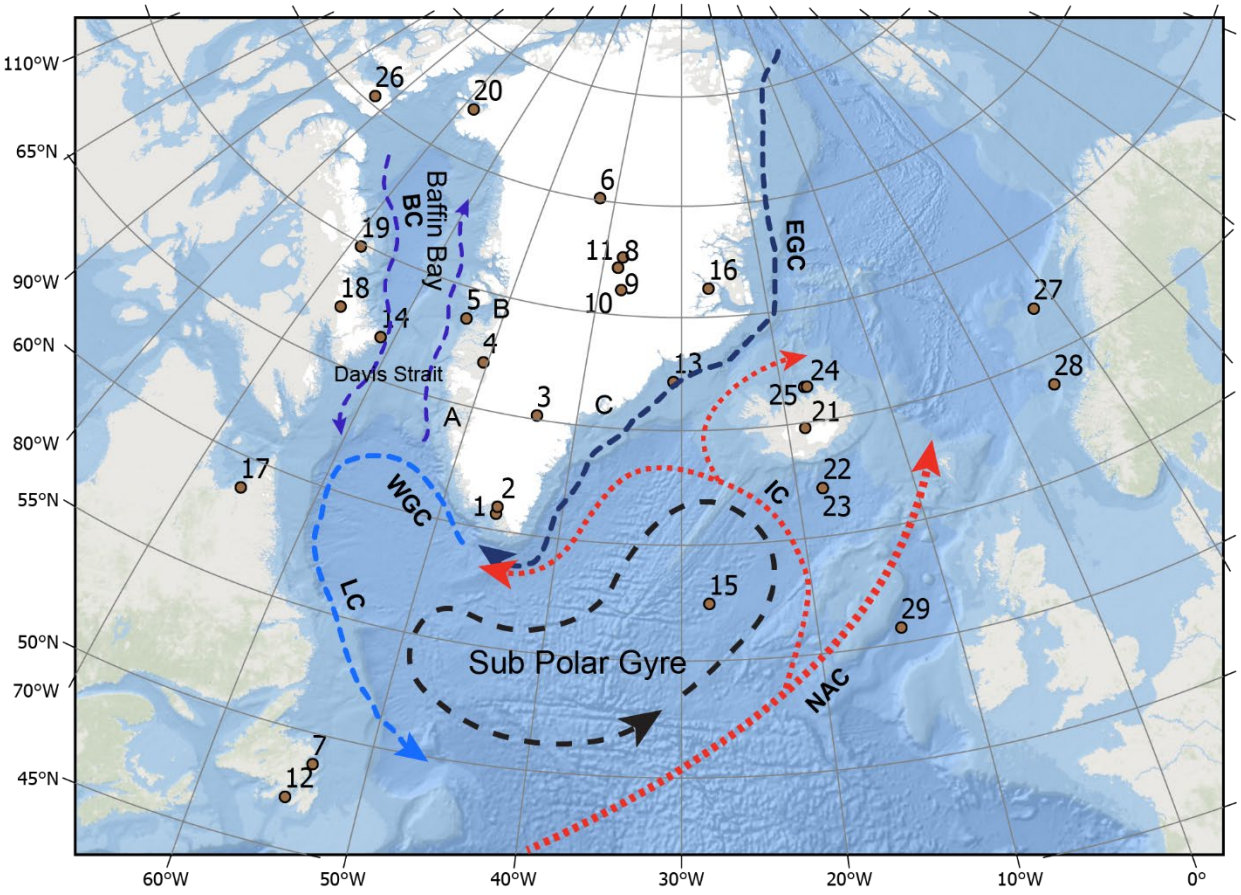

Figure 6.1. Map of the study region with the location of sites used, locations of interest, and major ocean currents (refer to Table 6.1 for additional information about each site). NAC: North Atlantic Current, EGC: East Greenland Current, WGC: West Greenland Current, IC: Irminger Current, BC: Baffin Current and LC: Labrador Current. A: Nuuk, B: Disko Bay / Jakobshavn Isbrae, C: Sermilik Fjord / Helheim Glacier.

6.2. Methods

6.2.1. Selection of proxy records

Twenty-nine paleoclimate proxy records are included in our analysis, representing nine different proxy types. All have temporal resolution fine enough to interpret temperature changes on the scale of 100 years (Fig. 6.1, Table 6.1.), and are documented as temperature sensitive; i.e.,

they are interpreted by the original producers of the data in terms of temperature (air temperature or sea temperature – both surface and near/sub surface). Most temperature sensitive proxy records utilized in this study are from the latest update of the PAGES 2k global proxy database (PAGES 2k Consortium, 2017); however we have included six additional records to improve spatial representation within the limits of our study area that 1) meet our temporal resolution requirements, and 2) are interpreted as temperature records in the associated original publications (Fallu et al., 2005; Krawczyk et al., 2017; Lasher and Axford, 2019; Miettinen et al., 2012; Miettinen et al., 2015; Sicre et al., 2014). Additionally, we include five records of ocean circulation, specifically indicating the strength of the subpolar gyre, to study the relationship between subpolar gyre strength and temperature (Moffa-Sanchez and Hall, 2017).

6.2.2. Statistical methods

Since these proxy records were all generated at variable temporal resolutions, each record was reduced to common time resolution. All proxy records were first converted to common era time (CE). The data were then binned into 100-year intervals averaging all values within a given time interval using the bin function in geoChronR, which calculates the mean of all values within a defined interval (Fig. 6.2) (McKay et al., 2017). As the focus of this study is the last 3000 years, our first bin averages all data from 2000 to 1900 CE, and is centered at 1950 CE in our figures. Preceding 100-year time bins up to -1000 CE (1000 BCE) are similarly averaged and centered.

Table 6.1. Proxy records used in the study.

Site no.	Site name	Lat	Lon	Archive	Proxy	Param	Season	Ref.
1	Scoop Lake	60.7	-45.42	Lake	Chironomid $\delta^{18}O$	Temp	Ann	(Lasher and Axford, 2019)
2	Igaliku	61	-45.43	Lake	Pollen	Temp	JJA	(Massa et al., 2012)
3	Dye3	65.18	-43.83	Ice Core	$\delta^{18}O$	Climate	Ann	(Vinther et al., 2010)
4	Braya So	67	-50.42	Lake	Alkenone	Temp	JJA	(D'Andrea et al., 2011)
5	MSM343310	68.65	-53.82	Marine	Diatom	Temp	July	(Krawczyk et al., 2017)
6	NGRIP	75.1	-42.32	Ice Core	$\delta^{18}O$	Climate	Ann	(Vinther et al., 2006)
7	AI07-03G	48.73	-53.48	Marine	Alkenone	Temp	JJA	(Sicre et al., 2014)
8	GISP2	72.1	-38.08	Ice Core	Inferred	Temp	Ann	(Alley, 2004)
9	GISP2	72.1	-38.08	Ice Core	$\delta^{15}N$	Temp	Ann	(Kobashi et al., 2017)
10	Crete	71.12	-37.32	Ice Core	$\delta^{18}O$	Climate	Ann	(Vinther et al., 2010)
11	GRIP	72.58	-37.64	Ice Core	$\delta^{18}O$	Climate	Ann	(Vinther et al., 2010)
12	AI07-12G	47.13	-54.55	Marine	Alkenone	Temp	JJA	(Sicre et al., 2014)
13	MD99-2322	67.14	-30.83	Marine	Diatom	Temp	aSST	(Miettinen et al., 2015)
14	Donard Lake	66.73	-61.35	Lake	Varves	Temp	JJA	(Moore et al., 2001)
15	RaPID-21-3k	57.45	-27.90	Marine	Alkenone	Temp	JJA	(Sicre et al., 2011)
16	Renland	71.27	-26.73	Ice Core	$\delta^{18}O$	Climate	Ann	(Vinther et al., 2008)
17	K2	58.73	-65.93	Lake	Chironomid	Temp	JJA	(Fallu et al., 2005)
18	Penny	67.25	-66.75	Ice Core	$\delta^{18}O$	Climate	Ann	(Fisher et al., 1998)
19	Big Round Lake	69.87	-68.83	Lake	Varves	Temp	JAS	(Thomas and Briner, 2009)
20	Camp Century	77.16	-68.13	Ice Core	$\delta^{18}O$	Climate	Ann	(Dansgaard et al., 1969)
21	Iceland Document	64.77	-18.37	Historical	Documents	Temp	Ann	(Bergthórsson, 1969)
22	RaPID-21-COM	62.08	-17.82	Marine	Diatom	Temp	JJA	(Miettinen et al., 2012)
23	RaPID-12-1k	62.08	-17.82	Marine	Mg/Ca	Temp	JJA	(Thornalley et al., 2009)
24	MD99-2275[1]	66.55	-17.7	Marine	Diatoms	Temp	JJA	(Jiang et al., 2005)
25	MD99-2275[2]	66.55	-17.42	Marine	Alkenone	Temp	JJA	(Sicre et al., 2011)
26	Devon	75.33	-82.5	Ice Core	$\delta^{18}O$	Temp	Ann	(Fisher et al., 1983)
27	Voring Plateau	66.97	7.64	Marine	Diatom	Temp	JJA	(Berner et al., 2011)
28	Storegga Slide	63.76	5.26	Marine	$\delta^{18}O$	Temp	JJA	(Sejrup et al., 2011)
29	Feni Drift	55.65	-13.98	Marine	Mg/Ca	Temp	JJA	(Richter et al., 2009)

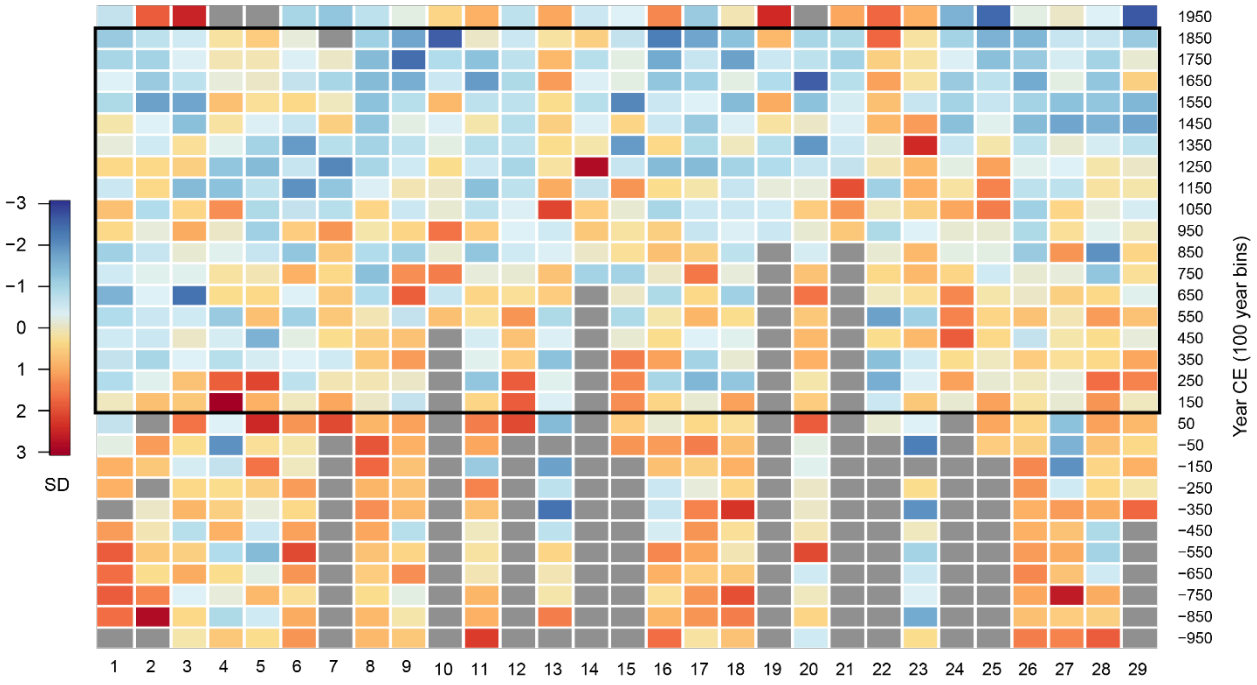

Figure 6.2. Heat map of temperature sensitive proxy records utilized in the study, binned in 100-year intervals, and standardized to variance of ± 1SD. Positive SD values indicate warm temperatures, while negative SD values indicate cold temperatures. Complete records within the black box were used to conduct a PCA between 100 and 1900 CE.

While some records include data after 2000 CE, many of the selected proxy studies do not. 25 out of 29 records had complete or near complete 100-year averaged data over the last 2000 years. One site (AI-07G) had missing values for one time interval centered at 1850 (Sicre et al., 2014). This gap was filled using the pcaMethods package in R, which combines an expectation maximization approach with a probabilistic model to fill the missing data (Stacklies et al., 2007). 4 records were missing data that could not be interpolated in this way; e.g. they were missing the most recent data centered at 1950, or they began after 1000 BCE, and we did not forward or back-project values. A composite relative temperature reconstruction was compiled from the 29 sites over the last 3000 years by taking the mean of binned site z scores (Fig. 6.3). Sites discussed in

the text included in Table 6.1 are annotated with parentheses referring to the site number (e.g. Scoop Lake (1)).

A principal component analysis was completed using 25 of the binned/averaged records using the vegan package in R on normalized data (Okasanen et al., 2018). Because missing values were not forward or back projected (i.e. binned data was missing in the final century for some records and in early centuries for several others), to include as many records as possible the PCA was conducted for the period of maximum data coverage, i.e., from 100 to 1900 CE. PCA scores for each site were then used to create a spatially interpolated representation of the first two principal components across our study area using an inverse distance weighting method in ArcPro. Additionally, a PCA was conducted on the five North Atlantic marine records that were recently discussed as indicators of SPG strength (Moffa-Sanchez and Hall, 2017). PC scores from these records were then compared with the composite temperature record.

Additionally, to assess how widespread the impacts of certain climate mechanisms are (e.g. the SPG), Pearson correlation coefficients were calculated amongst available proxy sites. First, correlation coefficients were calculated between sites used in the PCA analysis between 100 and 1900 CE, as well as all sites in Table 6.1 between 900 and 1900 CE. Correlation coefficients from these sites between 100 and 1900, and 900 and 1900 CE were then compared and mapped against coefficients from a recently published South Greenland terrestrial temperature record. (Lasher and Axford, 2019). This record was chosen for comparison because it is in the middle (longitudinally) of the SPG, is located relatively close to ice core and marine records and provides a chance to explore the coherence of SPG impacts on different climate archives and environments.

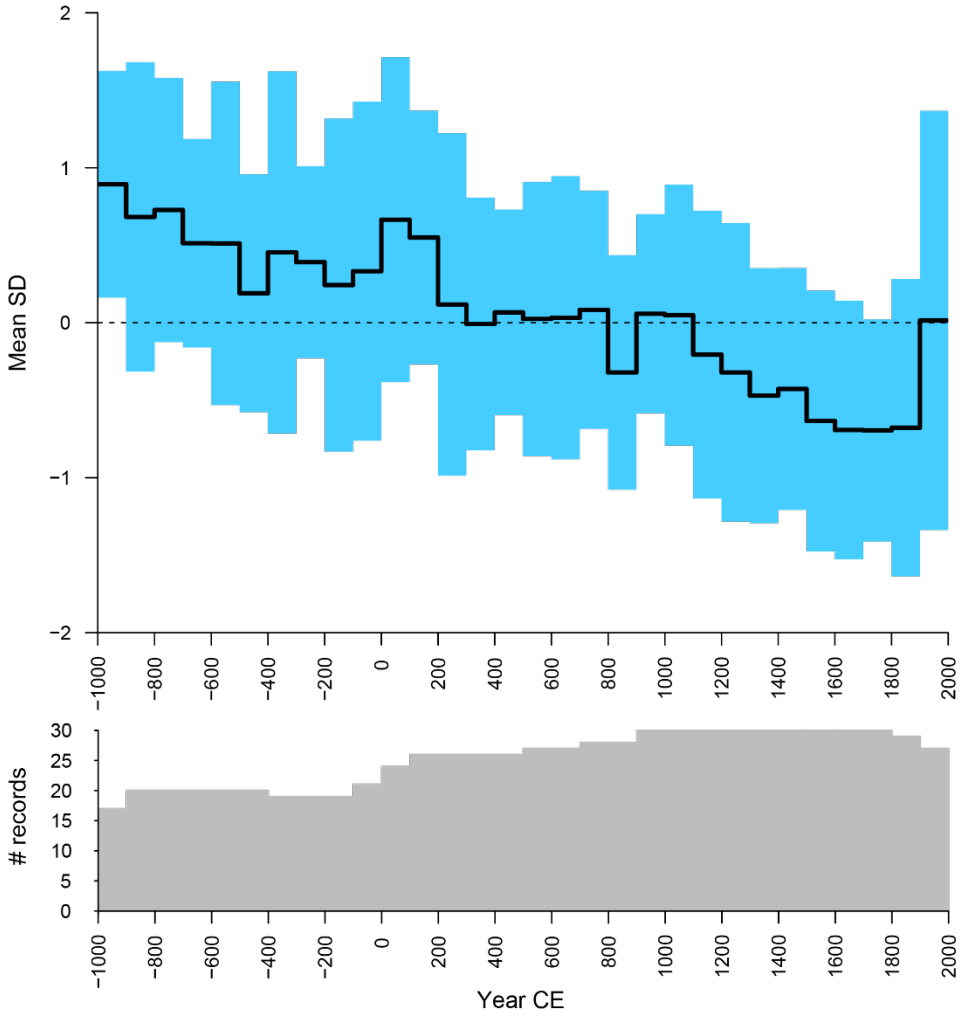

Figure 6.3. Top: Composite temperature record from the 29 proxies listed in Table 6.1. based on the mean of SD values in Figure 6.2, ± 1σ of available studies. Bottom: Total number of records available for each time bin.

6.3. Results

The composite relative temperature record for the North Atlantic shows general cooling over the last 3000 years (Fig. 6.3). Temperatures within the study area were warmer than the 20th century CE in parts of the first millennium, then dropped ~200 CE. Relatively stable temperatures characterized the centuries between 200 and 1100 CE, followed by strong cooling from 1100 to

1900 CE. The coldest centuries of the record occur between 1500 and 1900 CE, and the 20th century was the warmest of the last eighteen Centuries. The magnitude of temperature change is greatest between the 19th and 20th centuries CE, which is notably the period of global industrialization.

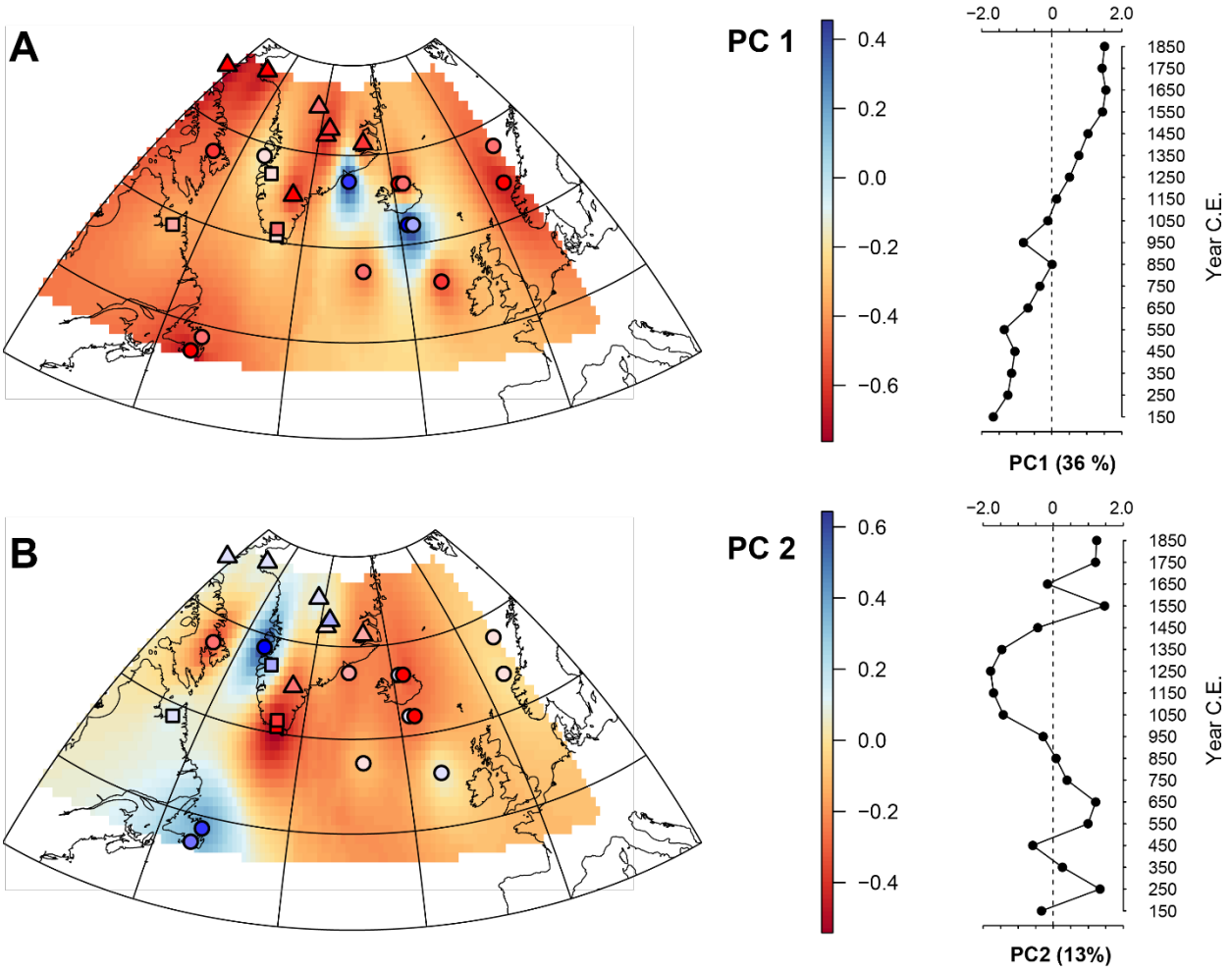

Figure 6.4. A: (left) Sites and loadings for PC1, (right) PC1 scores over the last 2000 years. B: (left) Sites and loadings for PC2, (right) PC2 scores over the last 2000 years. Triangles on the map are ice core records, squares are lake records and circles are marine records. Ages on the right plots are the center of 100-year bins.

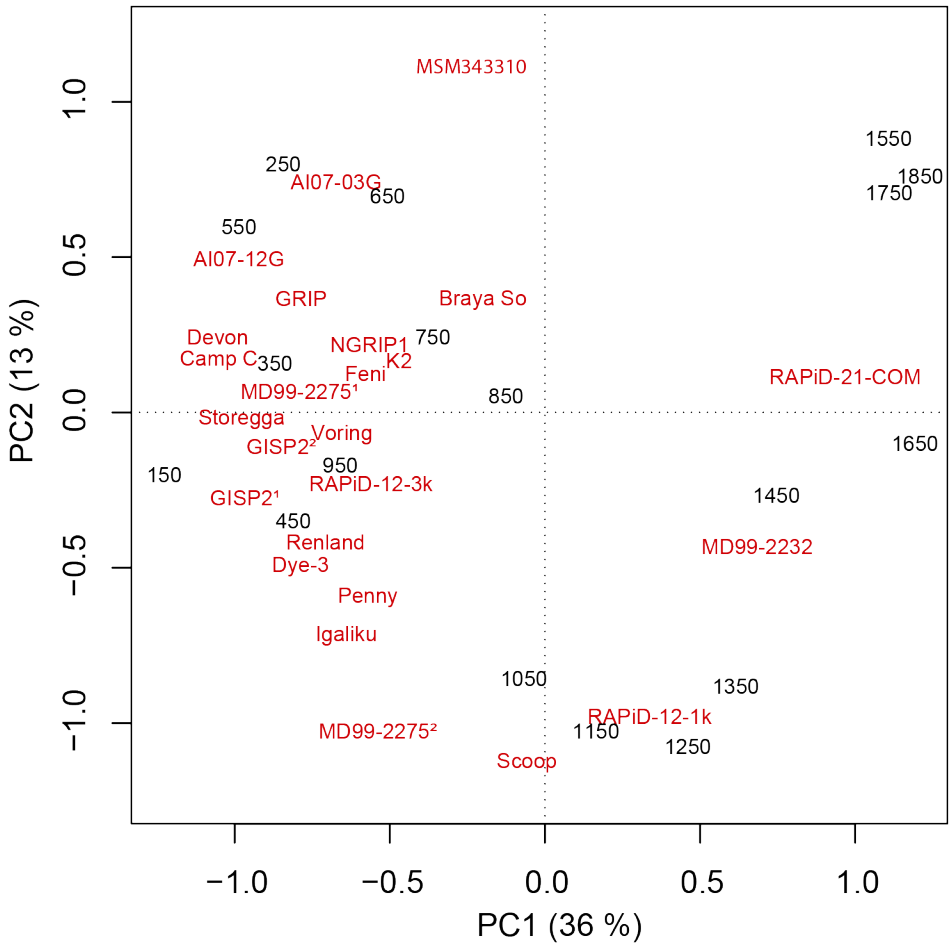

Figure 6.5. Species (study sites - red) and site (center age of 100-year bins - black) scores from principal component analysis (PCA) between 100 and 1900 CE. Axis labels include percent variance explained.

The first principal component (PC1) of the temperature time series accounts for 36% of the total variance in the dataset and shows a strong first order trend over the last two millennia (Fig. 6.4A, Fig 6.5). A reversal of the declining trend between 900 to 1000 CE may indicate brief warming. All but three of the temperature sensitive sites record either strong cooling, or little to no change between 100 and 1900 CE. For example, ice core records from the Greenland Ice Sheet

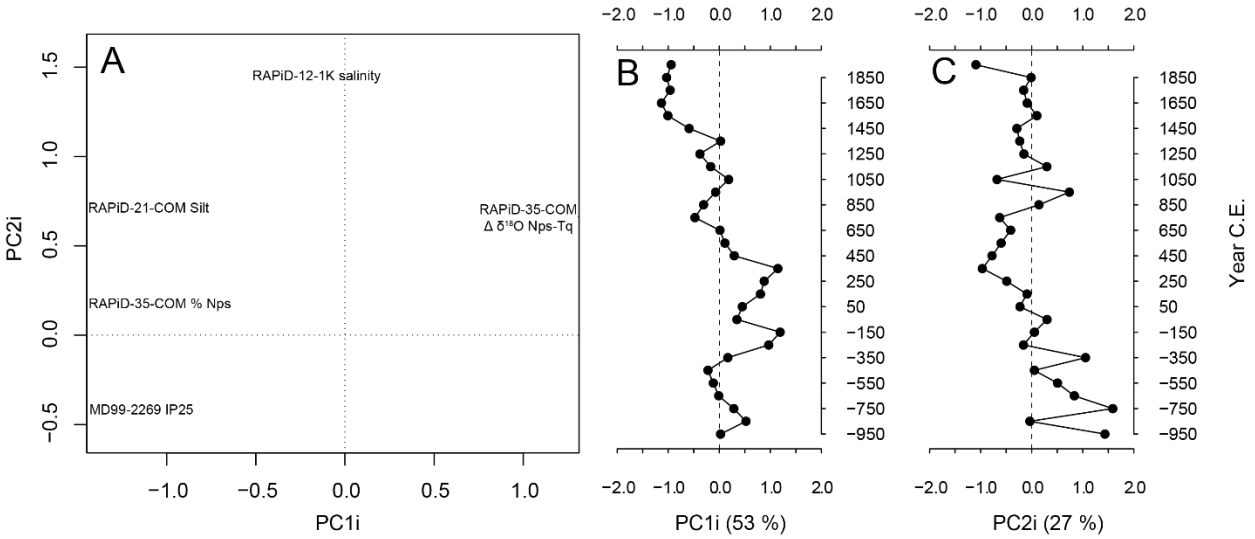

Figure 6.6. A: PCA biplot of centennially binned sub polar gyre strength indicator proxy data discussed in (Moffa-Sanchez and Hall, 2017). B and C: PC1i and PC2i scores of the same proxy data.

as well as Baffin and Devon Island ice caps all have negative loadings for PC1, associated with a Neoglacial cooling trend throughout the late Holocene (Fig. 6.4). Two diatom-based records, one off the SE coast of Greenland (Miettinen et al., 2015) and one off the southern coast of Iceland (Miettinen et al., 2012), indicate the opposite trend, suggesting warming, as does a Mg/Ca record also off south Iceland (Thornalley et al., 2009). Two sites on the west coast of Greenland, one marine diatom record (Krawczyk et al., 2017) and one lacustrine alkenone record, (D'Andrea et al., 2011), show large sub-millennial variability, but no strong long term cooling trend over the last 2000 years.

Principal component two (PC2), accounting for 13% of the variance, shows a more complex spatial and temporal pattern over the last 2000 years than PC1 (Fig 6.4B). The most notable feature is a period between ~1000 and 1400 CE when relative warmth, superimposed on the overall cooling trend demonstrated in PC1, is expressed over the central North Atlantic including south and east Greenland, Iceland and surrounding seas. This contrasts with relatively

cool temperatures during this time over west and possibly central Greenland and in the western Labrador Sea.

The first principal component (PC1i) of SPG circulation indicators discussed in (Moffa-Sanchez and Hall, 2017), responsible for 53% of the variance, shows a general trend towards more negative scores over the last 3000 years (Fig. 6.6). Values increase between 700 and – 400 CE, and again between 900 and 1400 CE. Periods of high PC1i scores correspond to periods of enhanced reconstructed SPG strength, which in turn delivers warmer waters to the coastal environments around Iceland, southern Greenland and potentially northwestern Europe (Moffa-Sanchez and Hall, 2017). Principal component two of these same indicators (PC2i) accounts for 27% of the variance, also largely tracks the strength of the SPG, but appears more sensitive to changes in salinity from the RAPiD-12-1k core south of Iceland (Fig. 6.6A) (Thornalley et al., 2009). PC2i scores generally decrease for the first 2000 years, exhibit variability between 700 and 1200 CE, then vary little until the last century. A comparison of the PC1i scores with the composite temperature record shows a strong linear relationship, and a strong correlation ($\rho = 0.64$) (Fig. 6.7). The relationship with PC2i is less robust.

Correlation coefficients between temperature proxy data at Scoop Lake (Site 1, Fig. 6.1) (Lasher and Axford, 2019) in south Greenland and temp-sensitive proxy data at other sites used in the PCA show a spatial pattern over the last 2000 years remarkably similar to the results of PC2 (Fig 6.7A). Sites that correlate with Scoop Lake are generally located in south Greenland and to the east, with the exception of the Penny Ice Cap $\delta^{18}O$ record on Baffin Island (Fisher et al., 1998). Sites negatively or weakly correlated with Scoop Lake are located around Baffin Bay, and along the coast of Labrador. Distal sites near the coast of Sweden and off the coast of Ireland also show

weak or negative correlations, as do central Greenland and high-latitude ice cores. Over the last 1000 years only, most sites show stronger correlation to Scoop Lake, with two exceptions on Baffin Bay (Thomas and Briner, 2009) and a SST reconstruction off the southern coast of Iceland (Miettinen et al., 2012) (Fig. 6.7B).

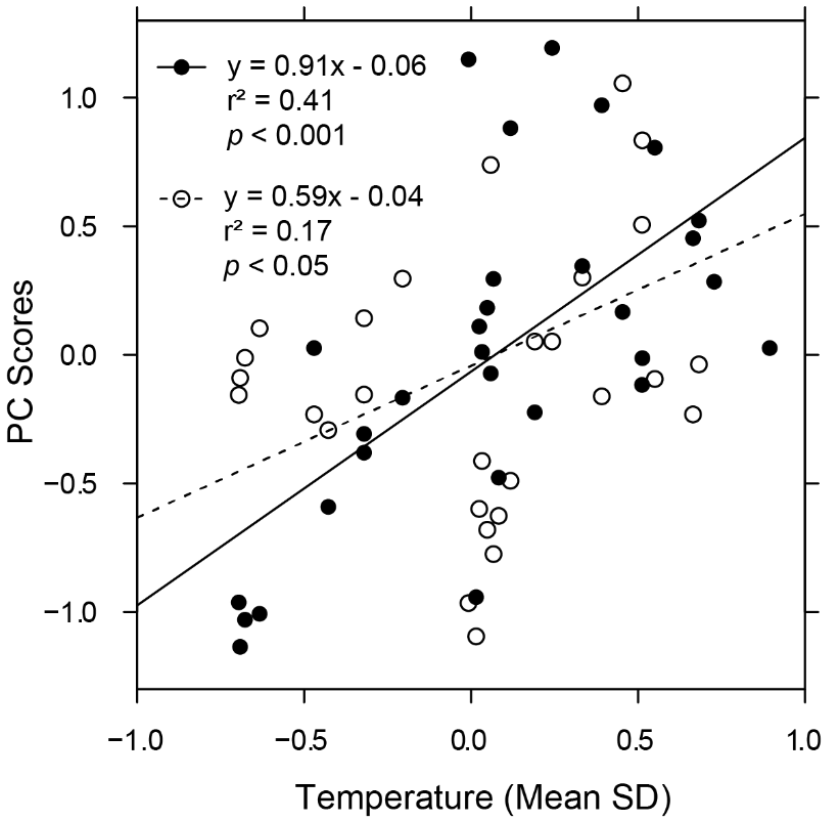

Figure 6.7. Linear regression between average 100 year values of the composite temperature record from Fig. 6.2, and PCi scores of the SPG indicator proxies from Fig. 6.6 (Moffa-Sanchez and Hall, 2017). The solid black line and filled points are the PC1i scores, whereas the dashed line and open points are the PC2i scores.

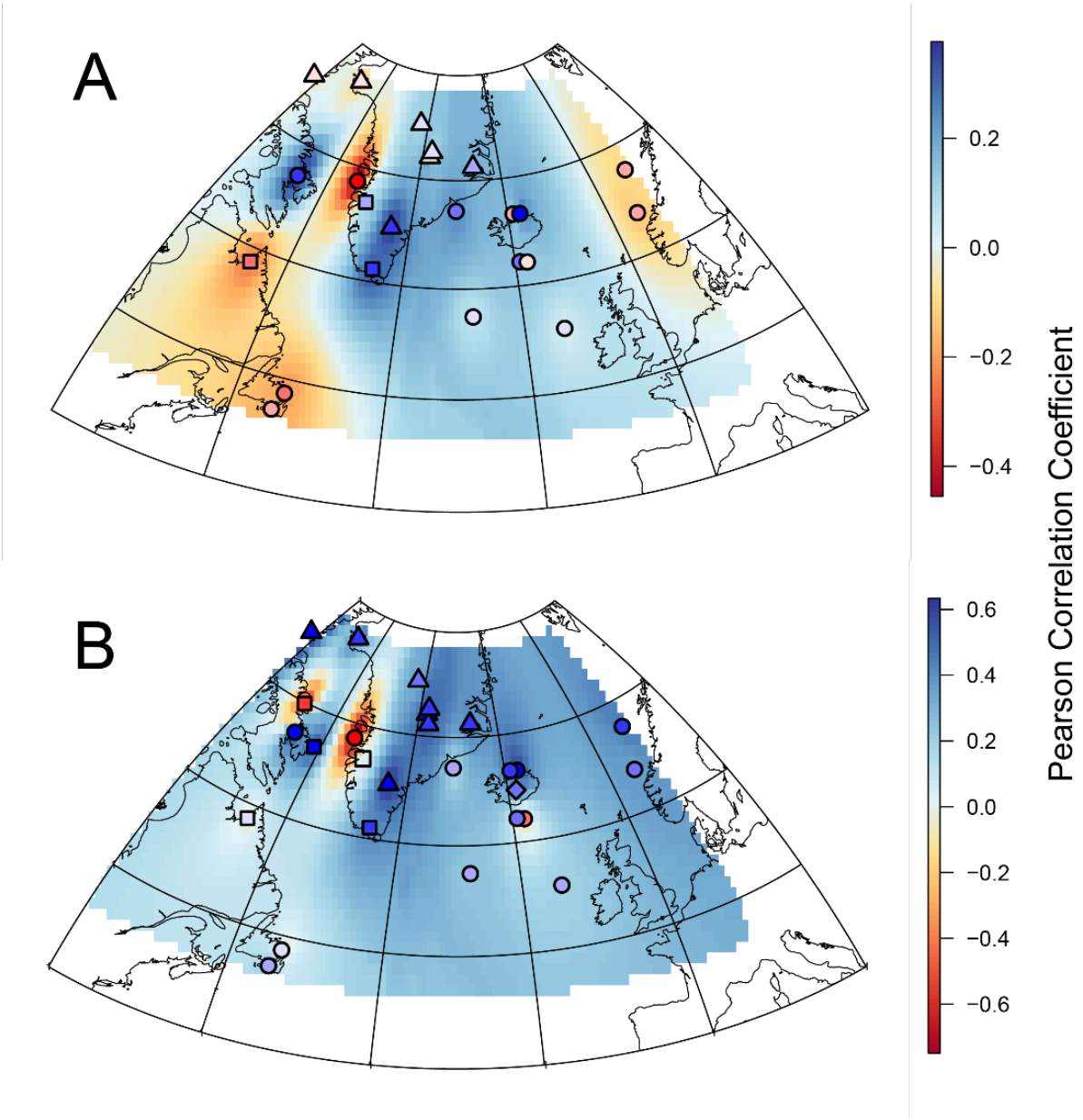

Figure 6.8. A: Pearson correlation coefficients calculated between temperature reconstructions at Scoop Lake in south Greenland and other temperature-sensitive proxy data at the other 24 sites used in the PCA analysis between 100 and 1900 CE. B: Same as in A but includes all sites from Table 6.1 between 900 and 1900 CE, excluding Scoop Lake. Triangles on the map are ice core records, squares are lake records, circles are marine records and the diamond is a compilation of historical documents.

6.4. Discussion

6.4.1. Proxy differences

At three locations, multiple records were used: specifically, at the MD99-2275 (24, 25), RAPiD-12-1k (23) and RAPiD-21-COM (22) marine core sites, and the GISP2 (8, 9) ice core site. PCA scores at these sites for PC1 are very similar, indicating that different proxies or methods from the same location both support the same first order trend over the last 2000 years. For PC2, these sites show less agreement, possibly due to different proxies used at the sites. Off the north coast of Iceland at MD99-2275, sea surface temperatures are reconstructed using a diatom transfer function (Jiang et al., 2005) (24) and using an alkenone based method (Sicre et al., 2011) (25). The diatom-based study is explicitly reported as a summer SST reconstruction and while the alkenone record does not discuss the seasonality of the record, it too is likely summer biased. South of Iceland, we note similar differences in PC2 site scores from a Mg/Ca study (Thornalley et al., 2009) (23) and a diatom-based study at the same location (Miettinen et al., 2012) (22). Unlike the two north Icelandic records, these two reconstructions use proxies that record climatic conditions at different depths in the water column, and thus differences in temporal trends could indicate different sub-millennial ocean temperature trends at different depths. This phenomenon has been previously documented and reproduced in Holocene syntheses and the CCSM3.0 model of North Atlantic Ocean temperatures at different depths in the water column (Andersson et al., 2010; Sejrup et al., 2016). Ultimately, differences at these sites can probably be attributed to complex seasonal influences on growing seasons and differing habitats of these proxies within the water column (Andersson et al., 2010; Jansen et al., 2008).

Difference in proxy types may also explain spatially contrasting trends in PC1 over the last 2000 years. Warming over the last 2000 years is evident off the south coast of Iceland (RAPiD-12-1k and RAPiD-21-COM) (23, 22) and southeast Greenland (MD99-2232) (13). Sea surface temperatures are reconstructed at both MD99-2232 (13) and RAPiD-21-COM (22) (Miettinen et al., 2012; Miettinen et al., 2015). RAPiD-12-1k (23), located at the same core site as RAPiD-21-COM (22), records near-surface conditions, and both reconstructions show general warming over the last 2000 years, albeit with some centennial scale variability. Surface (and long-term sub-surface) warming south of Iceland, which contrasts with most marine, terrestrial and ice core cooling trends in the region over the last 3000 years remains difficult to explain. One hypothesis is that declining insolation trends resulted in increasing Atlantic Meridional Overturning Circulation (AMOC) and enhanced ocean heat flux to the area south of Iceland (e.g. Hofer et al., 2011). A second hypothesis is that a gradual late Holocene slowdown of the SPG reduced cold water delivery from the Labrador Sea via the southern arm of the gyre into the region around the Reykjanes Ridge, resulting in gradually increasing temperatures there (Quillmann, 2014). Warming off the southeast coast of Greenland (Miettinen et al., 2015) (13) may also reflect enhanced warm water delivery via one of these mechanisms, but it is difficult to reconcile with the nearby records north of Iceland that show cooling during the same time period. More likely, the general warming trend at the MD99-2322 (13) off southeast Greenland reflects the decreasing influence of the nearby GrIS during the late Holocene, or a decrease in the influence of the cold East Greenland Current during the last l000 years (Justwan and Koç, 2016). While proxy type (especially differences in proxy seasonality and proxy depth in the water column) may be partially responsible for different climate trends among sites in PC1, it also seems likely that complex

spatial variability in ocean heat transport around the sub-polar North Atlantic over the last 3000 years explains some of the contrasting trends documented there.

6.4.2. Millennial scale late Holocene climate trends

Over the last 3000 years, warm temperatures (relative to the most recent decade in our composite: 1990 to 2000 CE) fluctuated until 1000 CE when accelerated cooling occurred (Fig. 6.2). The results of PC1, which are limited to the last 2000 years, shows a trend similar to the composite temperature reconstruction (Fig. 6.3). Comparable first order cooling trends are documented across the Arctic (Briner et al., 2016; Kaufman et al., 2009; Sejrup et al., 2016), and are largely attributed to declining summer insolation. In our analysis, this signal is most evident in the ice core records from Greenland and eastern Arctic Canada, though cooling is also evident in a number of marine records from the western Labrador Sea (Sicre et al., 2014) (7, 12) to the coasts of Scandinavia (Berner et al., 2011) (27). Proxy records from lake cores in Greenland (D'Andrea et al., 2011) (4) and south Greenland (Lasher and Axford, 2019; Massa et al., 2012) (1, 2) do not show strong long term cooling during the last 2000 years relative to the ice core records.

Gradual Neoglacial cooling over the last 2000 years culminated by 1900, when temperatures increased abruptly around the study region during the century spanning 1990 to 2000 (Fig. 6.2). Temperatures were cooler than this final century between 1100 and 1900 CE, a period that overlaps with various regional definitions of the Little Ice Age. Most studies in our 3000-year composite temperature record, also evident in the PCA analysis, indicate the coldest conditions between 1500 and 1900 CE. Around Greenland, several additional proxy records (both marine and terrestrial) indicate that the LIA was the coldest time within not only the last 3000 years, but much

of the Holocene (Axford et al., 2013; Briner et al., 2011; Perner et al., 2011; Seidenkrantz et al., 2008). Cold temperatures during this time are also associated with maximum advance of ice caps and the ice sheet, particularly around west Greenland (Briner et al., 2013; Kelley et al., 2012; Young and Briner, 2015; Young et al., 2015). LIA glacier and ice sheet advance is also recorded in the sediments of several south Greenland threshold lakes (Kaplan et al., 2002; Larsen et al., 2016). Proxy records and glacier histories from Iceland largely support maximum cooling and enhanced glacier advance during the LIA (Geirsdóttir et al., 2019; Geirsdóttir et al., 2013; Harning et al., 2016; Larsen et al., 2011). Continuing eastward towards Europe, glaciers in Scandinavia and the Alps also reached their maximum extents during the LIA (Solomina et al., 2016).

Although the majority of records within the study area show evidence for widespread glacier advance during the temperature minimum of the LIA, other investigations have found pre-LIA glacier advances that suggest additional sub-millennial temperature fluctuations within the middle to late Holocene. As early as 5 ka, snow-line lowering events were documented on the west Greenland coast and Baffin Island, and increased in frequency particularly in the last two to three millennia (Larsen et al., 2017; McKay et al., 2018; Miller et al., 2012; Miller et al., 2013; Pendleton et al., 2017; Schweinsberg et al., 2017; Schweinsberg et al., 2018). Ice caps and glaciers also advanced and re-entered lake catchments in southeast and eastern Greenland and Iceland within the last 3000 years and prior to the LIA (Balascio et al., 2015; Levy et al., 2013; Lowell et al., 2013). (Geirsdóttir et al., 2019). Notably, some studies have documented pre-LIA late Holocene moraines outboard of the LIA extent, suggesting equal or greater pre-LIA advance (Jomelli et al., 2016; Winsor et al., 2014; Young et al., 2015). In summary, over the last 3000 years until the 20th century, climate in our study region has cooled overall, forced by declining northern hemisphere

summer insolation, with the coldest temperatures occurring between 1500 and 1900 CE. Many glaciers around the region responded to this temperature trend by progressively advancing over the last three millennia, and in most cases reaching their maximum Holocene extents during the LIA. However, several studies argue that small glaciers and some ice caps responded to forcing and associated climatic feedbacks on shorter timescales (e.g. decadal to centennial) prior to the LIA, and/or that cold events prior to the LIA may have been comparable in magnitude. For example, evidence exists for cold conditions equal to or exceeding the minimum temperatures of the LIA between 500 and 800 CE (Lasher and Axford, 2019) which may have caused or aided glacier advance before the LIA.

6.4.3. Centennial scale climate anomalies and role of the subpolar gyre

Two notable climate events are superimposed on the long-term cooling. A potential warm event is evident in the centuries centered around 0 CE (2000 years ago) which coincides with the so called Roman Warm Period (Fig. 6.2). In the eastern sub-polar North Atlantic, sub-millennial warming at this time is inferred from increasing principal component scores in terrestrial and sea surface marine proxy records (Sejrup et al., 2016). This apparent warm event is also evident in a number of sub-surface sea surface temperature proxy records between southeast Greenland and Iceland (Ólafsdóttir et al., 2010; Sejrup et al., 2016) as well as in some indirect indicators of warm temperatures (e.g. foraminifera assemblages) (Andrews and Giraudeau, 2003; Moros et al., 2012). Decreases in sea ice concentrations off North Iceland inferred from the IP_{25} proxy are documented between -400 and 700 CE, simultaneous with the inferred warmth (Cabedo-Sanz et al., 2016). Off the east and west coast of Greenland, multiple sites show similar indirect evidence for warmer

ocean conditions between –400 and 900 CE (Krawczyk et al., 2017; Perner et al., 2016; Perner et al., 2012; Perner et al., 2015; Perner et al., 2011; Seidenkrantz et al., 2008) (5), though some south and southwest Greenland fjord records show coeval contrasting cool conditions, including enhanced sea ice cover near Nuuk (Lassen et al., 2004; Seidenkrantz et al., 2007). Warming at most of these sites has been attributed to enhanced warm Irminger Current (IC) influences, particularly around Iceland and the Denmark Strait. Strong IC influences on the West Greenland Current (WGC) have likewise been linked to RWP warming off west Greenland (Perner et al., 2011). Periods of enhanced IC influence in all of these areas are often associated with evidence for a strong SPG (Moffa-Sanchez and Hall, 2017), though warming south of Iceland has also been associated with a weakened or more contracted SPG (Quillmann, 2014).

A recent review of North Atlantic ocean current variability also suggested linkages between the strength of the SPG, and that of climate over Europe over the last 3000 years (Moffa-Sanchez and Hall, 2017). The evidence for relative warmth during the Roman Warm Period over Europe comes largely from records of glacier fluctuations in Scandinavia and central Europe, which show retreat or lack of advance around 0 CE (Solomina et al., 2016). Evidence elsewhere around Europe is less coherent. Milder climates in Britain, conducive to viticulture have been historically documented (McCormick et al., 2012); however paleoclimate records in Scotland suggest evidence for cooler, but potentially wetter conditions (Wang et al., 2012). External solar and volcanic forcing driving complex internal feedbacks over the European continent have been invoked to explain all of the above manifestations of climate during this and later climate anomalies (Luterbacher et al., 2016), though multiple lines of evidence discussed above support the idea that North Atlantic ocean circulation, including SPG dynamics plays a critical role. A

comparison of the SPG indicator proxies (PC1i) discussed by Moffa-Sanchez and Hall (2017) with our composite temperature record at a common time interval shows a strong linear relationship, and a strong correlation ($\rho = 0.64$) (Fig 6.6), which supports the qualitative conclusions of the authors.

Noticeably absent in the composite reconstruction is a strong Medieval Climate Anomaly expression. The cooling trend in the PC1 scores is briefly interrupted between 900 and 1000 CE, indicating short term warming. A longer, more distinct Medieval climatic event is, however, a dominant feature of the PC2 scores of the temperature-sensitive proxies (Fig. 6.3). Based on interpretation of the proxies, negative PC2 scores between 1000 and 1400 CE indicate a spatially localized warm MCA expressed most strongly in south Greenland and in the marine environment around Iceland (Lasher and Axford, 2019; Massa et al., 2012; Miettinen et al., 2015; Sicre et al., 2011; Thornalley et al., 2009) (1, 2, 7, 25, 23). The onset of the MCA may have started as early as 700 CE according to PC2, coincident with the tail end of the Dark Ages Cold Period (DACP) (Helama et al., 2017). This pattern is similar to overlapping regional studies, where warming is registered in many marine and terrestrial temperature records from the eastern North Atlantic and Fennoscandia around 1000 CE (Sejrup et al., 2016). Generally warmer spring and summer temperatures are inferred from biogenic silica values in an Icelandic lake record between 850 and 1400 CE (Geirsdóttir et al., 2009). More recent compilations of proxy records from several lakes around the island both support these conclusions, but also suggest that warming during the MCA is relatively minor in the context of the Holocene (Axford et al., 2011; Geirsdóttir et al., 2019; Geirsdóttir et al., 2013). Evidence for warming in our study region between 700 and 900 CE also aligns with initial retreat of glaciers across much of Europe and Svalbard (Solomina et al., 2016).

Overall, the spatial pattern of MCA temperature anomalies in the regional looks remarkably similar to previous reconstructions (Mann et al., 2009), notably the area of relatively warm conditions centered around south Greenland. The higher spatial resolution of the overall dataset used in this study reveals interesting heterogeneity of Medieval climate in the northwest North Atlantic region, notably localized surface cooling during the MCA around Baffin Bay and the western Labrador Sea (Krawczyk et al., 2017; Sicre et al., 2014) (5, 7).

Contrasting cool MCA conditions at some study sites warrants additional examination. Apparent cold conditions around Disko Bay near the Jakobshavn Isbrae outlet glacier come from diatom transfer function results showing both cooler July SSTs and increased April sea ice concentration (Krawczyk et al., 2010; Krawczyk et al., 2017; Moros et al., 1996) (5). The cold surface conditions during the MCA at this site may actually offer evidence for atmospheric warmth over southern Greenland: Enhanced spring melting of the GrIS and/or more abundant sea ice would result in cool, fresh water occupying Disko Bay in the subsequent months (Krawczyk et al., 2010). Estimated annual percent melt at the Dye-3 ice core site (3) (Fig. 6.1) was elevated between 950 and 1500 CE, with a pronounced increase centered at 1250 CE (Herron et al., 1981), overlapping temporally with the July SST minimum documented in Disko Bay. MCA cooling in surface waters near the major Helheim outlet glacier on the southeast coast of Greenland could reflect a similar response from enhanced surface melt in over the southern GrIS (Andresen et al., 2017). Cool surface water conditions in that region may have been limited to the fjords, as high SSTs are documented at the same time slightly north on the southeast coast (Miettinen et al., 2015) (13). Importantly though, ^{10}Be ages on moraines in west Greenland and on Baffin Island have been interpreted to record MCA glacier advances, suggesting cool MCA summers in these locales

(Jomelli et al., 2016; Young et al., 2015). Meanwhile, other marine records in Disko Bay show MCA warming or ambiguous sea ice and sea surface temperature histories (Perner et al., 2011; Ribeiro et al., 2012; Sha et al., 2014), so additional high resolution terrestrial and marine surface temperatures are needed to clarify late Holocene climate in the area.

Similar to the RWP, North Atlantic Ocean currents and the SPG have been linked to MCA climate patterns around our study region (Moffa-Sanchez and Hall, 2017; Moffa-Sánchez et al., 2014b). Our PCA results show a spatial pattern consistent with effects of a stronger SPG during the MCA. Warm SSTs and reduced sea ice conditions around Iceland (Cabedo-Sanz et al., 2016; Massé et al., 2008; Sicre et al., 2011), evidence for warm water in south Greenland fjords (Lassen et al., 2004), and cold temperatures off the coast of Labrador (Sicre et al., 2014) (7) during this time suggest that a strong SPG characterized the MCA, though the warming effects were spatially limited (Fig. 6.3B, Fig. 6.7A). Warm WGC waters (implying a strong, warm IC influence) infiltrated the benthic environment in Disko Bay (Lloyd, 2006), but this effect was masked in some proxy records by the cold surface waters previously discussed (Krawczyk et al., 2010). Warmer waters around south Greenland due to enhanced SPG strength could be responsible for warmer atmospheric temperatures, causing the enhanced melt over the ice sheet, and complex and contrasting temperature expressions documented in the marine environment and terrestrial records. Local land and ice feedbacks may have also played a role. The large ice-free landscape of south Greenland may have amplified the SPG warming there during Medieval times. Furthermore, unlike Disko Bay or Sermilik Fjord, south Greenland lacks an equivalent large outlet glacier, minimizing the possible effects of cold fjord waters muting surface air temperatures in the area.

A strong SPG generally requires increased Labrador Sea Water formation, associated with higher latent heat loss in the western Labrador sea during the winter months (Kuhlbrodt et al., 2007; Langehaug et al., 2012). Cold winter air temperature coupled with greater wind stress across the Labrador Sea can increase this heat loss, driving deep water formation and accelerated counter-clockwise rotation of the gyre (Yashayaev, 2007). Such conditions are often linked with a strong positive Arctic Oscillation (AO), or North Atlantic Oscillation (NAO) (Reverdin, 2010). A strong positive NAO during the MCA has been proposed and could be responsible for the enhanced SPG effects documented around the region (Olsen et al., 2012; Trouet et al., 2009; Trouet et al., 2012). If a strong positive NAO anomaly was responsible for SPG effects, it must have been a strongly seasonal phenomenon, limited to the winter. Anomalously cool NAO-linked conditions during the winter season could explain both the high sea ice concentrations in Baffin Bay (Krawczyk et al., 2017) (5) and provide a mechanism for a vigorous SPG warming south Greenland in the spring and summer. Interannual variability in the strength of the SPG due to seasonal atmospheric temperature fluctuations has been previously documented (Foukal and Lozier, 2017), but whether or not such strong seasonal effects can persist over multiple centuries remains unknown. Additionally, the notion of a strong positive NAO anomaly in the past remains an open question. While some studies argue that a positive NAO dominated much of the MCA (Trouet et al., 2009), other studies argue for a more stable NAO over much of the last two millennia (Lehner et al., 2012; Ortega et al., 2015) Oxygen isotope values from Scoop Lake in south Greenland (Lasher and Axford, 2019) (1) which are sensitive to changes in NAO conditions (Bonne et al., 2014; Rimbu et al., 2016; Sodemann et al., 2008) do not support the dominant positive MCA NAO anomaly, implying possible alternative drivers of the SPG during the MCA.

There is broad consensus that the onset of the LIA was associated with a slowdown in the SPG (Moffa-Sánchez et al., 2014b; Moreno-Chamarro et al., 2016). Whether this slowdown is a cessation of anomalously strong SPG conditions that only lasted during the MCA, or the culmination of a long term late Holocene trend remains unresolved. Multiple lines of evidence support the latter hypothesis (Perner et al., 2012; Perner et al., 2011; Rashid et al., 2017), however, additional studies provide some evidence for anomalous SPG activity superimposed on a long term slowing trend (Moffa-Sanchez and Hall, 2017; Thornalley et al., 2009). Both scenarios are reflected in the PC1i and PC2i scores which show sub millennial variability in the midst of generally decreasing scores PC (Fig. 6.5). As is true with the possible MCA SPG anomaly, multiple hypotheses exist to explain the weak LIA SPG and associated regional cooling including: changes in the NAO from a positive to negative mode (e.g. Copard et al., 2012), external volcanic or solar forcing (Miller et al., 2012; Moffa-Sánchez et al., 2014a), and internal variability / feedbacks (Lehner et al., 2013; Moffa-Sanchez and Hall, 2017; Moreno-Chamarro et al., 2016). Although the cause of the SPG weakening at the end of the MCA remains an open question, the climatic implications are clear. As discussed above in section 6.4.2, widespread cooling during the LIA is evident in a high percentage of the temperature-sensitive proxies used in this study, coincident with independent evidence for LIA glacier and GrIS advance. Figure 6.7 also demonstrates how the reduction in the SPG results in a more coherent climate pattern across the whole region during the last 1000 years. Temperatures in south Greenland at Scoop Lake (thought to be linked to the strength of the SPG) are only positively correlated with nearby sites also linked to strong SPG effects over the last 2000 years implying a limited spatial influence of the SPG (Lasher and Axford, 2019) (1). This changes after 900 CE when positive correlations between

Scoop Lake and other proxy records are widespread. Additional investigations spanning the last 3000 years are needed around the boundaries of the SPG to fully assess the spatial extent of it influence on the regions' climate.

6.5. Conclusions

A composite temperature reconstruction from twenty-nine proxy records covering the region 50° to 80° N latitude and 80° W to 20° E longitude shows broad cooling over the last 3000 years. The coldest temperatures are present during the last 1000 years except for the 20th century CE which appears to show early rapid anthropogenically linked warming around much of the study region. This trend is largely consistent with other late Holocene and Common Era reconstructions of temperature in the Northern Hemisphere and the Arctic, and based upon estimates from past synthesis studies could correspond to as little as 0.16°C of cooling or as high as 2°C of cooling (Briner et al., 2016; Christiansen and Ljungqvist, 2012; Kaufman et al., 2009; Sejrup et al., 2016). Multiple proxies sensitive to the strength of the subpolar gyre correlate well ($\rho = 0.64$) with our temperature reconstruction (Moffa-Sanchez and Hall, 2017), supporting that North Atlantic ocean currents play an important role in modulating late Holocene climate in our study region. Principal component analysis of centennially resolved records over the last 2000 years highlights first-order trends and regional heterogeneity superimposed on the overall late Holocene cooling. The first principal component reflects insolation-driven cooling from 0 CE to 2000 CE. Principal component two reflects warming between 1000 and 1400 CE around south Greenland and Iceland. Multi decadal to centennial scale anomalies in the strength of the subpolar gyre likely drove this Medieval-era warming, as well as seemingly contradictory trends elsewhere in the study area.

Additional temporally expanded high resolution studies are needed to better document SPG behavior over the Holocene. Since recent studies suggest that AMOC and the SPG is slowing in response to current atmospheric warming (Thornalley et al., 2018), it is critical that we understand what impacts changing SPG strength may have on future climate change around Baffin Bay, Labrador, Greenland and the wider subpolar North Atlantic.

CHAPTER 7:

Conclusions

Numerous investigations of Holocene glacial landforms and sedimentary deposits around Greenland and the Arctic clearly show that the ice sheet, local ice caps and small mountain glaciers responded to past changes in climate (Carlson et al., 2014; Corbett et al., 2015; Funder et al., 2011; Kelley et al., 2012; Kelly et al., 1999; Levy et al., 2013; Levy et al., 2017; Lowell et al., 2013; Sinclair et al., 2016; Young and Briner, 2015). Oxygen isotopes measured in the early ice core record from Camp Century showed increasing temperatures over the ice sheet from the start of the Holocene to ~ 7 ka before leveling out and decreasing over the next 4000 years. (Dansgaard et al., 1969). Later ice core records at Dye3 in southern Greenland, GRIP and GISP2 over the central ice sheet as well as a handful of other cores from peripheral ice caps all showed a relatively similar pattern (Johnsen et al., 2001). Early Holocene warming peaked between 9 and 5 ka followed by gradual cooling into the neoglacial, driven by summer insolation trends in the Northern Hemipshere (Kaufman et al., 2004). Continued glacial investigations, paired with paleoclimate reconstructions beyond the ice sheet now show that response of the cryosphere was not uniform around Greenland (Sinclair et al., 2016; Young and Briner, 2015), nor was climate (Briner et al., 2016). A growing collection of paleoclimate records across the Arctic is highlighting significant regional heterogeneity superimposed on the long-term insolation driven trend that dominated the ice core records (e.g. Axford et al., 2009; Axford et al., 2013; Briner et al., 2016; Frechette and de Vernal, 2009; Gajewski, 2015; Wooller et al., 2004). The main objective of my research and this dissertation was to reconstruct new millennial and centennial scale temperature histories in the ice-free margins of Greenland using oxygen isotopes in chironomid head capsules.

Subfossil chironomid head capsules in lake sediments have long been used to reconstruct paleoclimate in the Arctic by identifying shifts in species assemblages (Brooks and Birks, 2001). Since 2004, a growing collection of data suggests that oxygen isotopes preserved in the head capsules are also a strong proxy for the lake water in which the aquatic insects grew (van Hardenbroek et al., 2018). Paired modern lake water and chironomid $\delta^{18}O$ data collected and presented in Chapter two suggests that chironomids are enriched relative to lake water by a consistent amount (22.5 ± 2.3 ‰). This enrichment factor has been used to reconstruct paleo lake water values from lakes around Greenland, three of which are presented in this dissertation. While this is a good first step, as more modern paired samples are added to this compendium, the relationship between chironomid head capsules $\delta^{18}O$ values and lake water $\delta^{18}O$ values will evolve. There is a growing effort within the paleoclimate community to better quantify errors around our reconstructions, be it errors on $\delta^{18}O$ values inferred from proxies, or temperatures inferred from proxies. In the future, applying advanced error propagation methods (e.g. Pryor et al., 2014) will be useful in quantifying uncertainties around paleoclimate reconstructions. In addition to showing a strong relationship between head capsules and lake water $\delta^{18}O$ values, Chapter 2 also highlights the need to carefully assess lake hydrology before interpreting down core $\delta^{18}O$ values from any proxy. Inferring a climate variable such as temperature requires that the relationship between chironomid $\delta^{18}O$ values and temperature can be linked or explained. Finally, the use of FT-IR has advanced our understanding about how well chironomid subfossils preserve through time. Previous work has suggested that these insect remains preserve well through geologic time (Gupta, 2010; Verbruggen et al., 2009), and these results are now supported by new data presented in Chapter 2. Many questions regarding chironomids $\delta^{18}O$ remain, however. How

does changing molecular composition alter $\delta^{18}O$ values? Are there species dependent fractionation effects for $\delta^{18}O$? Are there variations in $\delta^{18}O$ values attributable to different instars, or seasonality of hatching? Despite these outstanding questions, the evidence to date shows that chironomid $\delta^{18}O$ values are a potentially powerful tool for reconstruction paleo lake water values through time and can, at appropriate sites, be used to infer paleo precipitation and climatic factors that influence precipitation $\delta^{18}O$ values. Three new lake sediment records are now available from the ice-free margins of Greenland using this tool, adding much needed information about how climate changed over the Holocene in previously unstudied areas.

It is surprisingly fitting that my first field seasons in 2013 and 2014 took me to Thule, not far from where the first deep Greenland ice core was collected nearly half a century earlier at Camp Century. The $\delta^{18}O$ inferred temperature record from Secret Lake (Chapter 3) suggests that temperatures were between 2.5 and 4 °C warmer than present between 7.7 and 6 ka, and then cooled by ~6 °C over 5000 years, forced by declining northern Hemisphere insolation. The $\delta^{18}O$ values inferred from chironomids are supported by aquatic moss $\delta^{18}O$ values that show greater variability during the record, but similar inferred lake water $\delta^{18}O$ values. While this record does not capture the early Holocene (a common issue with lake sediment records around Greenland due to later deglaciation in many ice-free areas), temperature changes of this magnitude resulted in advance of the northwestern GrIS margin (Reusche et al., 2018) as well as local ice caps near Thule in the last few millennia (Farnsworth et al., 2018). This temperature record agrees well with other high latitude Greenland climate studies, many of which extend earlier into the Holocene (Axford et al., 2017; Lecavalier et al., 2017; McFarlin et al., 2018), but support the range of temperatures proposed at Secret Lake.

Temperature estimates from Secret Lake were conservatively described as maximum likely temperature anomalies. Reduced sea ice conditions in Baffin Bay in the early Holocene (Levac et al., 2001) may have provided a more proximal moisture source (resulting in more positive $\delta^{18}O$ values) for precipitation falling over the lake. That other new regional (isotope independent) temperature records now suggest temperature anomalies in excess of the Secret Lake could be due to a number of possible factors. First, changes in sea ice may have had little effect on regional $\delta^{18}O$ values of precipitation. Second, seasonality of precipitation was different in the early to middle Holocene (e.g. increased winter precipitation decreased $\delta^{18}O$ isotope values archived in chironomids (Thomas et al., 2016)), effectively muting inferred temperatures. Third, the $\delta^{18}O$ - temperature relationship relationships used to infer temperatures at Secret Lake were different in the past. It is also possible that some combination of these factors played a role during the Holocene.

The magnitude of temperature change inferred from chironomid $\delta^{18}O$ at Secret Lake (~ 6 °C) near Thule contrasts with $\delta^{18}O$ values measured in chironomids at lakes T1 and T2 near Nuuk, Greenland (Chapter 4). The overall trend is similar, i.e. gradual cooling during the Holocene in response to declining insolation forcing, but the magnitude is much less (< 4°C). The insolation forcing at this lower latitude site was less that farther north near Thule, likely contributing to the difference in temperature magnitude between the two sites. Also, the sub-Arctic climate near Nuuk and lakes T1 and T2, as well as proximity to southern Baffin Bay likely modulated climate at this study site. Interestingly, using a modern local $\delta^{18}O$ – temperature relationship of 0.27 ‰ $°C^{-1}$ (Bowen, 2018) results in unrealistic magnitudes of temperature change over the Holocene, especially at a lower latitude site (> 6 °C). Instead, the 2 to 4 °C temperature change at T1 and T2

is indirectly inferred from other regional paleotemperature proxy records (Axford et al., 2013; Frechette and de Vernal, 2009; Wooller et al., 2004). A (constant) $\delta^{18}O$ – temperature relationship of ~0.67 ‰ $°C^{-1}$ is required to achieve 2 to 4 °C of temperature change at our site. One obvious implication of Chapters 3 and 4 is that better constraints on spatio-temporal $\delta^{18}O$ – temperature relationships are needed around the ice sheet margin to confidently reconstruct temperature change from isotopes in the future. Additionally, temperature changes of this magnitude over the Holocene were large enough to cause significant changes in local ice caps around Nuuk (Larsen et al., 2017). While it will likely take global temperatures until the end of the century to warm by 4 °C, warming in the Arctic of this magnitude is likely to occur before 2050 (Overland et al., 2018), implying that many local ice masses around west Greenland may be gone (or committed to future disappearance) in the next few decades.

Climate around Greenland is clearly heterogeneous on millennial timescales, with greater magnitude temperature change generally occurring at higher latitudes, and lesser magnitude change occurring in the south and southwest (Briner et al., 2016). The temporal resolution of Chapters 3 and 4 largely precluded making any observation about climate change around Greenland that happened on sub-millennial and centennial time scales. Chapters 5 and 6 explore climate changes around south Greenland on such time scales, and explore mechanisms that can affect the environment, cryosphere and civilizations in a matter of decades. Much of these final chapters focuses on the role of the subpolar gyre in modulating marine and terrestrial environments from Iceland to Labrador. Chironomid $\delta^{18}O$ measured in a south Greenland lake indicates that a generally warm climate characterized Medieval times (900 to 1400 CE), coincident with the arrival and departure of the Norse from Greenland (Jones, 1986). This unique record also indicates that a

hypothesized positive NAO anomaly during the Medieval Climate Anomaly (Trouet et al., 2009) did not cause widespread cooling during the time of Norse settlement. Chapter 6 confirms many of these conclusions by investing 28 addition centennially resolved climate records around the high latitude North Atlantic region. This area of the world has garnered much scientific attention recently (Thornalley et al., 2018). South Greenland hosts many small mountain glaciers, thought to be highly sensitive to changes in atmospheric temperature. Changes in the strength of the SPG, and AMOC will likely determine the fate of these ice masses. Additional studies, such as the high-resolution temperature record from Scoop Lake (Chapter 5) will aid in clarifying the impacts of changing subpolar gyre behavior on the south Greenland's mountain glaciers and marine terminating outlet glaciers from the main ice sheet. Increased (or decreased) warm water delivery to the south Greenland coast will affect Greenland's glaciers and thus have global implications for sea level rise.

References Cited

Alley, R.B., 2004. GISP2 Ice Core Temperature and Accumulation Data, in: Paleoclimatology, I.P.W.D.C.f. (Ed.), Data Contribution Series #2004-013, NOAA/NGDC Paleoclimatology Program, Boulder CO, USA.

Allison, P.A., Bottjer, D.J., 2011. Taphonomy: bias and process through time, Taphonomy. Springer, pp. 1-17.

Anderson, N.J., Leng, M.J., 2004. Increased aridity during the early Holocene in West Greenland inferred from stable isotopes in laminated-lake sediments. Quaternary Science Reviews 23, 841-849.

Anderson, N.J., Leng, M.J., Osburn, C.L., Fritz, S.C., Law, A.C., McGowan, S., 2018. A landscape perspective of Holocene organic carbon cycling in coastal SW Greenland lake-catchments. Quaternary Science Reviews 202, 98-108.

Andersson, C., Pausata, F.S.R., Jansen, E., Risebrobakken, B., Telford, R.J., 2010. Holocene trends in the foraminifer record from the Norwegian Sea and the North Atlantic Ocean. Climate of the Past 6, 179-193.

Andresen, C.S., Kokfelt, U., Sicre, M.A., Knudsen, M.F., Dyke, L.M., Klein, V., Kaczmar, F., Miles, M.W., Wangner, D., 2017. Exceptional 20th century glaciological regime of a major SE Greenland outlet glacier. Sci Rep 7, 13626.

Andrews, J.T., Giraudeau, J., 2003. Multi-proxy records showing significant Holocene environmental variability: the inner N. Icelandshelf (Hunafloi). Quaternary Science Reviews 22, 175-193.

Antonio, T., Robert, Z., 2019. Global Aridity Index and Potential Evapotranspiration (ET0) Climate Database v2.

Arppe, L., Kurki, E., Wooller, M.J., Luoto, T.P., Zajaczkowski, M., Ojala, A.E.K., 2017. A 5500-year oxygen isotope record of high arctic environmental change from southern Spitsbergen. The Holocene 27, 1948-1962.

Axford, Y., Andresen, C.S., Andrews, J.T., Belt, S.T., Geirsdóttir, Á., Massé, G., Miller, G.H., Ólafsdóttir, S., Vare, L.L., 2011. Do paleoclimate proxies agree? A test comparing 19 late Holocene climate and sea-ice reconstructions from Icelandic marine and lake sediments. J Quaternary Sci 26, 645-656.

Axford, Y., Briner, J.P., Cooke, C.A., Francis, D.R., Michelutti, N., Miller, G.H., Smol, J.P., Thomas, E.K., Wilson, C.R., Wolfe, A.P., 2009a. Recent changes in a remote Arctic lake are unique within the past 200,000 years. Proceedings of the National Academy of Sciences of the United States of America 106, 18443-18446.

Axford, Y., Briner, J.P., Miller, G.H., Francis, D.R., 2009b. Paleoecological evidence for abrupt cold reversals during peak Holocene warmth on Baffin Island, Arctic Canada. Quaternary Research 71, 142-149.

Axford, Y., Levy, L.B., Kelly, M.A., Francis, D.R., Hall, B.L., Langdon, P.G., Lowell, T.V., 2017. Timing and magnitude of early to middle Holocene warming in East Greenland inferred from chironomids. Boreas.

Axford, Y., Losee, S., Briner, J.P., Francis, D.R., Langdon, P.G., Walker, I.R., 2013. Holocene temperature history at the western Greenland Ice Sheet margin reconstructed from lake sediments. Quaternary Science Reviews 59, 87-100.

Baas, M., Briggs, D.E.G., Vanheemst, J.D.H., Kear, A.J., Deleeuw, J.W., 1995. Selective Preservation of Chitin during the Decay of Shrimp. Geochimica Et Cosmochimica Acta 59, 945-951.

Balascio, N.L., D'Andrea, W.J., Bradley, R.S., 2015. Glacier response to North Atlantic climate variability during the Holocene. Climate of the Past 11, 1587-1598.

Balascio, N.L., D'Andrea, W.J., Bradley, R.S., Perren, B.B., 2013. Biogeochemical evidence for hydrologic changes during the Holocene in a lake sediment record from southeast Greenland. Holocene 23, 1428-1439.

Barlow, L.K., Sadler, J.P., Ogilvie, A.E.J., Buckland, P.C., Amorosi, T., Ingimundarson, J.H., Skidmore, P., Dugmore, A.J., McGovern, T.H., 1997. Interdisciplinary investigations of the end of the Norse western settlement in Greenland. Holocene 7, 489-499.

Barth, A., 2007. Infrared spectroscopy of proteins. Biochim Biophys Acta 1767, 1073-1101.

Bennike, O., Anderson, N.J., McGowan, S., 2010. Holocene palaeoecology of southwest Greenland inferred from macrofossils in sediments of an oligosaline lake. Journal of Paleolimnology 43, 787-798.

Bergthórsson, P., 1969. An estimate of drift ice and temperature in Iceland in 1000 years. Jokull 19, 94-101.

Berner, K.S., Koç, N., Godtliebsen, F., Divine, D., 2011. Holocene climate variability of the Norwegian Atlantic Current during high and low solar insolation forcing. Paleoceanography 26, n/a-n/a.

Bjella, K., 2013. An investigation into a white painted airfield on permafrost: Thule Air Base, Greenland, ISCORD 2013: Planning for Sustainable Cold Regions. ASCE, pp. 565-575.

Blaauw, M., Christen, A.J., 2011. Bacon.R, 2.2 ed.

Blaauw, M., Christen, A.J., 2018. rbacon: Age-Depth Modelling using Bayesian Statistics. R package version 2.3.4. https://CRAN.R-project.org/package=rbacon.

Blake, W., Boucherle, M., Fredskild, B., Janssens, J., Smol, J.P., 1992. The Geomorphological Setting, Glacial History and Holocene Development of "Kap Inglefield Sø", Inglefield Land, North-West Greenland. Meddeleser om Gronland 27.

Bonne, J.L., Masson-Delmotte, V., Cattani, O., Delmotte, M., Risi, C., Sodemann, H., Steen-Larsen, H.C., 2014. The isotopic composition of water vapour and precipitation in Ivittuut, southern Greenland. Atmospheric Chemistry and Physics 14, 4419-4439.

Bowen, G.J., 2018. The Online Isotopes in Precipitation Calculator, version 3.1 http://www.waterisotopes.org.

Bowen, G.J., Cai, Z., Fiorella, R.P., Putman, A.L., 2019. Isotopes in the Water Cycle: Regional- to Global-Scale Patterns and Applications. Annual Review of Earth and Planetary Sciences 47.

Briner, J.P., Håkansson, L., Bennike, O., 2013. The deglaciation and neoglaciation of Upernavik Isstrøm, Greenland. Quaternary Research 80, 459-467.

Briner, J.P., McKay, N.P., Axford, Y., Bennike, O., Bradley, R.S., de Vernal, A., Fisher, D., Francus, P., Fréchette, B., Gajewski, K., Jennings, A., Kaufman, D.S., Miller, G., Rouston, C., Wagner, B., 2016. Holocene climate change in Arctic Canada and Greenland. Quaternary Science Reviews 147, 340-364.

Briner, J.P., Stewart, H.A.M., Young, N.E., Philipps, W., Losee, S., 2010. Using proglacial-threshold lakes to constrain fluctuations of the Jakobshavn Isbræ ice margin, western Greenland, during the Holocene. Quaternary Science Reviews 29, 3861-3874.

Briner, J.P., Young, N.E., Thomas, E.K., Stewart, H.A.M., Losee, S., Truex, S., 2011. Varve and radiocarbon dating support the rapid advance of Jakobshavn Isbræ during the Little Ice Age. Quaternary Science Reviews 30, 2476-2486.

Brooks, S.J., Birks, H.J.B., 2001. Chironomid-inferred air temperatures from Lateglacial and Holocene sites in north-west Europe: progress and problems. Quaternary Science Reviews 20, 1723-1741.

Buizert, C., Gkinis, V., Severinghaus, J.P., He, F., Lecavalier, B.S., Kindler, P., Leuenberger, M., Carlson, A.E., Vinther, B., Masson-Delmotte, V., White, J.W., Liu, Z., Otto-Bliesner, B., Brook, E.J., 2014. Greenland temperature response to climate forcing during the last deglaciation. Science 345, 1177-1180.

Buizert, C., Keisling, B.A., Box, J.E., He, F., Carlson, A.E., Sinclair, G., DeConto, R.M., 2018. Greenland-Wide Seasonal Temperatures During the Last Deglaciation. Geophysical Research Letters.

Cabedo-Sanz, P., Belt, S.T., Jennings, A.E., Andrews, J.T., Geirsdóttir, Á., 2016. Variability in drift ice export from the Arctic Ocean to the North Icelandic Shelf over the last 8000 years: A multi-proxy evaluation. Quaternary Science Reviews 146, 99-115.

Cappelen, J., 2017. DMI Report 17-08: Weather observations from Greenland 1958-2016, in: Institute, D.M. (Ed.), Copenhagen.

Carlson, A.E., Winsor, K., Ullman, D.J., Brook, E.J., Rood, D.H., Axford, Y., LeGrande, A.N., Anslow, F.S., Sinclair, G., 2014. Earliest Holocene south Greenland ice sheet retreat within its late Holocene extent. Geophysical Research Letters 41, 5514-5521.

Chang, J.C., Shulmeister, J., Gröcke, D.R., Woodward, C.A., 2017. Toward more accurate temperature reconstructions based on oxygen isotopes of subfossil chironomid head-capsules in Australia. Limnology and Oceanography.

Chang, J.C., Shulmeister, J., Woodward, C., Michalski, G., 2016. Can stable oxygen and hydrogen isotopes from Australian subfossil Chironomus head capsules be used as proxies for past temperature change? Journal of Paleolimnology 56, 331-348.

Christiansen, B., Ljungqvist, F.C., 2012. The extra-tropical Northern Hemisphere temperature in the last two millennia: reconstructions of low-frequency variability. Climate of the Past 8, 765-786.

Coelho, R.R., Hovell, I., de Mello Monte, M.B., Middea, A., Lopes de Souza, A., 2006. Characterisation of aliphatic chains in vacuum residues (VRs) of asphaltenes and resins using molecular modelling and FTIR techniques. Fuel Processing Technology 87, 325-333.

Consortium, P.k., 2013. Continental-scale temperature variability during the past two millennia. Nature Geoscience 6, 339-346.

Consortium, P.k., 2017. A global multiproxy database for temperature reconstructions of the Common Era. Sci Data 4, 170088.

Copard, K., Colin, C., Henderson, G.M., Scholten, J., Douville, E., Sicre, M.A., Frank, N., 2012. Late Holocene intermediate water variability in the northeastern Atlantic as recorded by deep-sea corals. Earth Planet Sc Lett 313-314, 34-44.

Corbett, L.B., Bierman, P.R., Lasher, G.E., Rood, D.H., 2015. Landscape chronology and glacial history in Thule, northwest Greenland. Quaternary Science Reviews 109, 57-67.

Corbett, L.B., Bierman, P.R., Rood, D.H., 2016. Constraining multi-stage exposure-burial scenarios for boulders preserved beneath cold-based glacial ice in Thule, northwest Greenland. Earth Planet Sc Lett 440, 147-157.

Craig, H., 1961. Isotopic variations in meteoric waters. Science 133, 1702-1703.

Criss, R.E., 1999. Principles of stable isotope distribution. Oxford University Press on Demand.

Curtis, C.J., Kaiser, J., Marca, A., Anderson, N.J., Simpson, G., Jones, V., Whiteford, E., 2018. Spatial variations in snowpack chemistry, isotopic composition of NO3- and nitrogen deposition from the ice sheet margin to the coast of western Greenland. Biogeosciences 15, 529-550.

D'Andrea, W.J., Huang, Y., Fritz, S.C., Anderson, N.J., 2011. Abrupt Holocene climate change as an important factor for human migration in West Greenland. Proc Natl Acad Sci U S A 108, 9765-9769.

Dahl-Jensen, D., Mosegaard, K., Gundestrup, N., Clow, G.D., Johnsen, S.J., Hansen, A.W., Balling, N., 1998. Past temperatures directly from the greenland ice sheet. Science 282, 268-271.

Dansgaard, W., 1964. Stable isotopes in precipitation. Tellus 16, 436-468.

Dansgaard, W., Johnsen, S.J., Moller, J., Langway, C.C., Jr., 1969. One thousand centuries of climatic record from Camp Century on the greenland ice sheet. Science 166, 377-380.

Dawes, P., 2006. Geological Map of Greenland, 1: 500,000, Thule, Sheet 5, Geological Survey of Denmark and Greenland Map Series 2. Geological Survey of Denmark and Greenland, Danish Ministry of the Environment.

de Vernal, A., Hillaire-Marcel, C., Rochon, A., Fréchette, B., Henry, M., Solignac, S., Bonnet, S., 2013. Dinocyst-based reconstructions of sea ice cover concentration during the Holocene in the Arctic Ocean, the northern North Atlantic Ocean and its adjacent seas. Quaternary Science Reviews 79, 111-121.

DeNiro, M.J., Epstein, S., 1981. Isotopic Composition of Cellulose from Aquatic Organisms. Geochimica Et Cosmochimica Acta 45, 1885-1894.

DeNiro, M.J., Epstein, S.J.G.e.c.a., 1978. Influence of diet on the distribution of carbon isotopes in animals. 42, 495-506.

Dugmore, A.J., McGovern, T.H., Vesteinsson, O., Arneborg, J., Streeter, R., Keller, C., 2012. Cultural adaptation, compounding vulnerabilities and conjunctures in Norse Greenland. Proc Natl Acad Sci U S A 109, 3658-3663.

Ehrlich, H., Rigby, J.K., Botting, J.P., Tsurkan, M.V., Werner, C., Schwille, P., Petrasek, Z., Pisera, A., Simon, P., Sivkov, V.N., Vyalikh, D.V., Molodtsov, S.L., Kurek, D., Kammer, M., Hunoldt, S., Born, R., Stawski, D., Steinhof, A., Bazhenov, V.V., Geisler, T., 2013. Discovery of 505-million-year old chitin in the basal demosponge Vauxia gracilenta. Sci Rep 3, 3497.

Erbs-Hansen, D.R., Knudsen, K.L., Olsen, J., Lykke-Andersen, H., Underbjerg, J.A., Sha, L., 2013. Paleoceanographical development off Sisimiut, West Greenland, during the mid- and late Holocene: A multiproxy study. Marine Micropaleontology 102, 79-97.

Faber, A.-K., Vinther, B.M., Sjolte, J., Pedersen, R.A., 2016. How does sea ice influence δ18O of Arctic precipitation? Atmospheric Chemistry and Physics Discussions, 1-22.

Fallu, M.-A., Pienitz, R., Walker, I.R., Lavoie, M., 2005. Paleolimnology of a shrub-tundra lake and response of aquatic and terrestrial indicators to climatic change in arctic Québec, Canada. Palaeogeography, Palaeoclimatology, Palaeoecology 215, 183-203.

Farnsworth, L.B., Kelly, M.A., Bromley, G.R.M., Axford, Y., Osterberg, E.C., Howley, J.A., Jackson, M.S., Zimmerman, S.R., 2018. Holocene history of the Greenland Ice-Sheet margin in Northern Nunatarssuaq, Northwest Greenland. arktos 4.

Fetterer, F., Knowles, K., Meier, W.N., Savoire, M., Windnagel, A.K., 2019. Sea Ice Index, Version 3. 1978 to present. NSIDC: National Snow and Ice Data Center, Boulder, Colorado USA.

Fisher, D., Koerner, R., Paterson, W., Dansgaard, W., Gundestrup, N., Reeh, N.J.N., 1983. Effect of wind scouring on climatic records from ice-core oxygen-isotope profiles. 301, 205.

Fisher, D.A., Koerner, R.M., Bourgeois, J.C., Zielinski, G., Wake, C., Hammer, C.U., Clausen, H.B., Gundestrup, N., Johnsen, S., Goto-Azuma, K., Hondoh, T., Blake, E., Gerasimoff, M., 1998. Penny Ice Cap Cores, Baffin Island, Canada, and the Wisconsinan Foxe Dome Connection: Two States of Hudson Bay Ice Cover. Science 279, 692-695.

Fisher, D.A., Koerner, R.M., Reeh, N., 1995. Holocene Climatic Records from Agassiz Ice Cap, Ellesmere Island, Nwt, Canada. Holocene 5, 19-24.

Flannery, M.B., Stott, A.W., Briggs, D.E.G., Evershed, R.P., 2001. Chitin in the fossil record: identification and quantification of D-glucosamine. Organic Geochemistry 32, 745-754.

Foukal, N.P., Lozier, M.S., 2017. Assessing variability in the size and strength of the North Atlantic subpolar gyre. Journal of Geophysical Research: Oceans 122, 6295-6308.

Frechette, B., de Vernal, A., 2009. Relationship between Holocene climate variations over southern Greenland and eastern Baffin Island and synoptic circulation pattern. Climate of the Past 5, 347-359.

Fredskild, B., 1983. The Holocene vegetational development of the Godthåbsfjord area, West Greenland. Commission for Scientific Research in Greenland.

Fredskild, B., 1985. The Holocene vegetational development of the Tugtuligssuaq and Qeqertat, Northwest Greenland. Meddeleser om Gronland Geoscience 14.

Funder, S., Kjeldsen, K.K., Kjær, K.H., Ó Cofaigh, C., 2011. The Greenland Ice Sheet During the Past 300,000 Years: A Review. 15, 699-713.

Gajewski, K., 2015. Quantitative reconstruction of Holocene temperatures across the Canadian Arctic and Greenland. Global and Planetary Change 128, 14-23.

Geirsdóttir, Á., Miller, G.H., Andrews, J.T., Harning, D.J., Anderson, L.S., Florian, C., Larsen, D.J., Thordarson, T., 2019. The onset of neoglaciation in Iceland and the 4.2 ka event. Climate of the Past 15, 25-40.

Geirsdóttir, Á., Miller, G.H., Larsen, D.J., Ólafsdóttir, S., 2013. Abrupt Holocene climate transitions in the northern North Atlantic region recorded by synchronized lacustrine records in Iceland. Quaternary Science Reviews 70, 48-62.

Geirsdóttir, Á., Miller, G.H., Thordarson, T., Ólafsdóttir, K.B., 2009. A 2000 year record of climate variations reconstructed from Haukadalsvatn, West Iceland. Journal of Paleolimnology 41, 95-115.

GEUS, 2018. Geological map of South, South-West and southern West Greenland 1:100,000. Geological Survey of Denmark and Greenland (GEUS), maps.greenmin.gl/geusmap/.

Gibb, O.T., Steinhauer, S., Fréchette, B., de Vernal, A., Hillaire-Marcel, C., 2015. Diachronous evolution of sea surface conditions in the Labrador Sea and Baffin Bay since the last deglaciation. The Holocene 25, 1882-1897.

Goldthwait, R., 1960. Study of ice cliff in Nunatarssuaq, Greenland, U.S. Army Snow, Ice and Permafrost Reseach Establishment Technical Report 39, p. 106.

Graham, R.W., Belmecheri, S., Choy, K., Culleton, B.J., Davies, L.J., Froese, D., Heintzman, P.D., Hritz, C., Kapp, J.D., Newsom, L.A., Rawcliffe, R., Saulnier-Talbot, E., Shapiro, B., Wang, Y., Williams, J.W., Wooller, M.J., 2016. Timing and causes of mid-Holocene mammoth extinction on St. Paul Island, Alaska. Proc Natl Acad Sci U S A 113, 9310-9314.

Grønnow, B., Sørensen, M.J.D.o.n.s., 2004. Palaeo-eskimo migrations into Greenland: the Canadian connection. 59-74.

Guo, C.-Q., Ochyra, R., Wu, P.-C., Seppelt, R.D., Yao, Y.-F., Bian, L.-G., Li, S.-P., Li, C.-S., 2013. Warnstorfia exannulata, an aquatic moss in the Arctic: seasonal growth responses. Climatic Change 119, 407-419.

Gupta, N., 2010. Chitin: Formation and Diagensis. 173.

Gupta, N.S., Briggs, D.E.G., 2011. Taphonomy of Animal Organic Skeletons Through Time, in: Allison, P.A., Bottjer, D.J. (Eds.), Taphonomy: Process and Bias Through Time. Springer Netherlands, Dordrecht, pp. 199-221.

Gupta, N.S., Briggs, D.E.G., Collinson, M.E., Evershed, R.P., Michels, R., Pancost, R.D., 2007. Molecular preservation of plant and insect cuticles from the Oligocene Enspel Formation,

Germany: Evidence against derivation of aliphatic polymer from sediment. Organic Geochemistry 38, 404-418.

Gupta, P., Noone, D., Galewsky, J., Sweeney, C., Vaughn, B.H., 2009. Demonstration of high-precision continuous measurements of water vapor isotopologues in laboratory and remote field deployments using wavelength-scanned cavity ring-down spectroscopy (WS-CRDS) technology. Rapid communications in mass spectrometry : RCM 23, 2534-2542.

Harning, D.J., Geirsdóttir, Á., Miller, G.H., Anderson, L., 2016. Episodic expansion of Drangajökull, Vestfirðir, Iceland, over the last 3 ka culminating in its maximum dimension during the Little Ice Age. Quaternary Science Reviews 152, 118-131.

Hartman, S., Ogilvie, A.E.J., Ingimundarson, J.H., Dugmore, A.J., Hambrecht, G., McGovern, T.H., 2017. Medieval Iceland, Greenland, and the New Human Condition: A case study in integrated environmental humanities. Global and Planetary Change 156, 123-139.

Heiri, O., Schilder, J., Van Hardenbroek, M., 2012. Stable isotopic analysis of fossil chironomids as an approach to environmental reconstruction: state of development and future challenges. Fauna norvegica 31.

Heiri, O., Wooller, M., van Hardenbroek, M., Wang, Y., 2009. Stable isotopes in chitinous fossils of aquatic invertebrates. Pages news 17, 100-102.

Helama, S., Jones, P.D., Briffa, K.R., 2017. Dark Ages Cold Period: A literature review and directions for future research. The Holocene 27, 1600-1606.

Herron, M.M., Herron, S.L., Langway, C.C., 1981. Climatic signal of ice melt features in southern Greenland. Nature 293, 389-391.

Hofer, D., Raible, C.C., Stocker, T.F., 2011. Variations of the Atlantic meridional overturning circulation in control and transient simulations of the last millennium. Climate of the Past 7, 133-150.

Hurrell, J.W., Kushnir, Y., Ottersen, G., Visbeck, M., 2003. An overview of the North Atlantic oscillation. The North Atlantic Oscillation: climatic significance and environmental impact, 1-35.

IAEA/WMO, 2017. Global Network of Isotopes in Precipitation. The GNIP Database. Accessible at: http://www.iaea.org/water.

IPCC, 2014. Summary for Policymakers, in: Field, C.B., Barros, V.R., Dokken, D.J., Mach, K.J., Mastrandrea, M.D., Bilir, T.E., Chatterjee, M., Ebi, K.L., Estrada, Y.O., Genova, R.C., Girma, B., Kissel, E.S., Levy, A.N., MacCracken, S., Mastrandrea, P.R., White, L.L. (Eds.), Climate Change 2014: Impacts, Adaptation, and Vulnerability. Part A: Global and Sectoral Aspects. Contribution of Working Group II to the Fifth Assessment Report of the Intergovernmental

Panel on Climate Change. Cambridge University Press, Cambridge, United Kingdom, and New York, NY, USA, pp. 1-32.

Jansen, E., Andersson, C., Moros, M., Nisancioglu, K., Nyland, B.F., Telford, R.J., 2008. The early to mid-Holocene thermal optimum in the North Atlantic, in: Batterbee, R., Binney, H. (Eds.), Natural Climate Variability and Global Warming: A Holocene Perspective. Wiley-Blackwell, Chichester, pp. 123-137.

Jiang, H., Eiriksson, J., Schulz, M., Knudsen, K.L., Seidenkrantz, M.S., 2005. Evidence for solar forcing of sea-surface temperature on the North Icelandic Shelf during the late Holocene. Geology 33, 73-76.

Johnsen, S.J., Dahl-Jensen, D., Gundestrup, N., Steffensen, J.P., Clausen, H.B., Miller, H., Masson-Delmotte, V., Sveinbjörnsdottir, A.E., White, J., 2001. Oxygen isotope and palaeotemperature records from six Greenland ice-core stations: Camp Century, Dye-3, GRIP, GISP2, Renland and NorthGRIP. J Quaternary Sci 16, 299-307.

Jomelli, V., Lane, T., Favier, V., Masson-Delmotte, V., Swingedouw, D., Rinterknecht, V., Schimmelpfennig, I., Brunstein, D., Verfaillie, D., Adamson, K., Leanni, L., Mokadem, F., Team, A., 2016. Paradoxical cold conditions during the medieval climate anomaly in the Western Arctic. Sci Rep 6, 32984.

Jones, G., 1986. The Norse Atlantic saga: being the Norse voyages of discovery and settlement to Iceland, Greenland, and North America. Oxford University Press, USA.

Jones, M.C., Wooller, M., Peteet, D.M., 2014. A deglacial and Holocene record of climate variability in south-central Alaska from stable oxygen isotopes and plant macrofossils in peat. Quaternary Science Reviews 87, 1-11.

Justwan, A., Koç, N., 2016. Evolution of the East Greenland Current between 1150 and 1740 AD, revealed by diatom-based sea surface temperature and sea-ice concentration reconstructions. Polar Research 28, 165-176.

Kaplan, M.R., Wolfe, A.P., Miller, G.H., 2002. Holocene Environmental Variability in Southern Greenland Inferred from Lake Sediments. Quaternary Research 58, 149-159.

Kaufman, D., 2004. Holocene thermal maximum in the western Arctic (0–180°W). Quaternary Science Reviews 23, 529-560.

Kaufman, D.S., Axford, Y.L., Henderson, A.C.G., McKay, N.P., Oswald, W.W., Saenger, C., Anderson, R.S., Bailey, H.L., Clegg, B., Gajewski, K., Hu, F.S., Jones, M.C., Massa, C., Routson, C.C., Werner, A., Wooller, M.J., Yu, Z., 2016. Holocene climate changes in eastern Beringia (NW North America) – A systematic review of multi-proxy evidence. Quaternary Science Reviews.

Kaufman, D.S., Schneider, D.P., McKay, N.P., Ammann, C.M., Bradley, R.S., Briffa, K.R., Miller, G.H., Otto-Bliesner, B.L., Overpeck, J.T., Vinther, B.M., 2009. Recent warming reverses long-term arctic cooling. Science (New York, N.Y.) 325, 1236-1239.

Kaya, M., Baran, T., Mentes, A., Asaroglu, M., Sezen, G., Tozak, K.O., 2014. Extraction and Characterization of α-Chitin and Chitosan from Six Different Aquatic Invertebrates. Food Biophysics 9, 145-157.

Kaya, M., Baublys, V., Sargin, I., Šatkauskienė, I., Paulauskas, A., Akyuz, B., Bulut, E., Tubelytė, V., Baran, T., Seyyar, O., Kabalak, M., Yurtmen, H., 2015. How Taxonomic Relations Affect the Physicochemical Properties of Chitin. Food Biophysics 11, 10-19.

Kelley, S.E., Briner, J.P., Young, N.E., Babonis, G.S., Csatho, B., 2012. Maximum late Holocene extent of the western Greenland Ice Sheet during the late 20th century. Quaternary Science Reviews 56, 89-98.

Kelly, M., Funder, S., Houmark-Nielsen, M., Knudsen, K.L., Kronborg, C., Landvik, J., Sorby, L., 1999. Quaternary glacial and marine environmental history of northwest Greenland: a review and reappraisal. Quaternary Science Reviews 18, 373-392.

Kelly, M.A., Osterberg, E.C., Axford, Y., Farnsworth, L., Howley, J.A., Lasher, G.E., Zimmerman, S., 2015. Holocene fluctuations of North Ice Cap, a proxy for climate conditions along the northwestern margin of the Greenland Ice Sheet, AGU Fall Meeting, San Francisco, California.

Kobashi, T., Menviel, L., Jeltsch-Thommes, A., Vinther, B.M., Box, J.E., Muscheler, R., Nakaegawa, T., Pfister, P.L., Doring, M., Leuenberger, M., Wanner, H., Ohmura, A., 2017. Volcanic influence on centennial to millennial Holocene Greenland temperature change. Sci Rep 7, 1441.

Koerner, R.M., 1977. Devon Island ice cap: core stratigraphy and paleoclimate. Science 196, 15-18.

Krawczyk, D., Witkowski, A., Moros, M., Lloyd, J., Kuijpers, A., Kierzek, A., 2010. Late-Holocene diatom-inferred reconstruction of temperature variations of the West Greenland Current from Disko Bugt, central West Greenland. The Holocene 20, 659-666.

Krawczyk, D.W., Witkowski, A., Moros, M., Lloyd, J.M., Høyer, J.L., Miettinen, A., Kuijpers, A., 2017. Quantitative reconstruction of Holocene sea ice and sea surface temperature off West Greenland from the first regional diatom data set. Paleoceanography 32, 18-40.

Kuhlbrodt, T., Griesel, A., Montoya, M., Levermann, A., Hofmann, M., Rahmstorf, S., 2007. On the driving processes of the Atlantic meridional overturning circulation. Reviews of Geophysics 45.

Kumirska, J., Czerwicka, M., Kaczynski, Z., Bychowska, A., Brzozowski, K., Thoming, J., Stepnowski, P., 2010. Application of spectroscopic methods for structural analysis of chitin and chitosan. Mar Drugs 8, 1567-1636.

Laity, P.R., Gilks, S.E., Holland, C., 2015. Rheological behaviour of native silk feedstocks. Polymer 67, 28-39.

Lamb, H.H., 1965. The early medieval warm epoch and its sequel. Palaeogeography, Palaeoclimatology, Palaeoecology 1, 13-37.

Langehaug, H.R., Medhaug, I., Eldevik, T., Otterå, O.H., 2012. Arctic/Atlantic Exchanges via the Subpolar Gyre*. Journal of Climate 25, 2421-2439.

Larsen, D.J., Miller, G.H., Geirsdóttir, Á., Thordarson, T., 2011. A 3000-year varved record of glacier activity and climate change from the proglacial lake Hvítárvatn, Iceland. Quaternary Science Reviews 30, 2715-2731.

Larsen, N.K., Find, J., Kristensen, A., Bjork, A.A., Kjeldsen, K.K., Odgaard, B.V., Olsen, J., Kjaer, K.H., 2016. Holocene ice marginal fluctuations of the Qassimiut lobe in South Greenland. Sci Rep 6, 22362.

Larsen, N.K., Funder, S., Kjaer, K.H., Kjeldsen, K.K., Knudsen, M.F., Linge, H., 2014. Rapid early Holocene ice retreat in West Greenland. Quaternary Science Reviews 92, 310-323.

Larsen, N.K., Kjær, K.H., Lecavalier, B., Bjørk, A.A., Colding, S., Huybrechts, P., Jakobsen, K.E., Kjeldsen, K.K., Knudsen, K.-L., Odgaard, B.V., 2015a. The response of the southern Greenland ice sheet to the Holocene thermal maximum. Geology 43, 291-294.

Larsen, N.K., Kjaer, K.H., Lecavalier, B., Bjork, A.A., Colding, S., Huybrechts, P., Jakobsen, K.E., Kjeldsen, K.K., Knudsen, K.L., Odgaard, B.V., Olsen, J., 2015b. The response of the southern Greenland ice sheet to the Holocene thermal maximum. Geology.

Larsen, N.K., Strunk, A., Levy, L.B., Olsen, J., Bjørk, A., Lauridsen, T.L., Jeppesen, E., Davidson, T.A., 2017. Strong altitudinal control on the response of local glaciers to Holocene climate change in southwest Greenland. Quaternary Science Reviews 168, 69-78.

Lasher, G.E., Axford, Y., 2019. Medieval warmth confirmed at the Norse Eastern Settlement in Greenland. Geology.

Lasher, G.E., Axford, Y., McFarlin, J.M., Kelly, M.A., Osterberg, E.C., Berkelhammer, M.B., 2017. Holocene temperatures and isotopes of precipitation in Northwest Greenland recorded in lacustrine organic materials. Quaternary Science Reviews 170, 45-55.

Lassen, S.J., Kuijpers, A., Kunzendorf, H., Hoffmann-Wieck, G., Mikkelsen, N., Konradi, P., 2004. Late-Holocene Atlantic bottom-water variability in Igaliku Fjord, South Greenland, reconstructed from foraminifera faunas. The Holocene 14, 165-171.

Law, A.C., Anderson, N.J., McGowan, S., 2015. Spatial and temporal variability of lake ontogeny in south-western Greenland. Quaternary Science Reviews 126, 1-16.

Leavitt, S.W., Danzer, S.R., 1993. Method for batch processing small wood samples to holocellulose for stable-carbon isotope analysis. Analytical Chemistry 65, 87-89.

Lecavalier, B.S., Fisher, D.A., Milne, G.A., Vinther, B.M., Tarasov, L., Huybrechts, P., Lacelle, D., Main, B., Zheng, J., Bourgeois, J., Dyke, A.S., 2017. High Arctic Holocene temperature record from the Agassiz ice cap and Greenland ice sheet evolution. Proc Natl Acad Sci U S A 114, 5952-5957.

Lecavalier, B.S., Milne, G.A., Simpson, M.J.R., Wake, L., Huybrechts, P., Tarasov, L., Kjeldsen, K.K., Funder, S., Long, A.J., Woodroffe, S., Dyke, A.S., Larsen, N.K., 2014. A model of Greenland ice sheet deglaciation constrained by observations of relative sea level and ice extent. Quaternary Science Reviews 102, 54-84.

Lecavalier, B.S., Milne, G.A., Vinther, B.M., Fisher, D.A., Dyke, A.S., Simpson, M.J.R., 2013. Revised estimates of Greenland ice sheet thinning histories based on ice-core records. Quaternary Science Reviews 63, 73-82.

Ledu, D., Rochon, A., de Vernal, A., St-Onge, G., 2008. Palynological evidence of Holocene climate change in the eastern Arctic: a possible shift in the Arctic oscillation at the millennial time scaleThis article is one of a series of papers published in this Special Issue on the themePolar Climate Stability Network. Canadian Journal of Earth Sciences 45, 1363-1375.

Lehmann, M.F., Bernasconi, S.M., Barbieri, A., McKenzie, J.A., 2002. Preservation of organic matter and alteration of its carbon and nitrogen isotope composition during simulated and in situ early sedimentary diagenesis. Geochimica et Cosmochimica Acta 66, 3573-3584.

Lehner, F., Born, A., Raible, C.C., Stocker, T.F., 2013. Amplified Inception of European Little Ice Age by Sea Ice–Ocean–Atmosphere Feedbacks. Journal of Climate 26, 7586-7602.

Lehner, F., Raible, C.C., Stocker, T.F., 2012. Testing the robustness of a precipitation proxy-based North Atlantic Oscillation reconstruction. Quaternary Science Reviews 45, 85-94.

Leng, M., Lamb, A., Heaton, T., Marshall, J., Wolfe, B., Jones, M., Holmes, J., Arrowsmith, C., 2006. Isotopes in lake sediments, in: Leng, M. (Ed.), Isotopes in Paleoenvironmental Research.

Leng, M.J., Anderson, N.J., 2003. Isotopic variation in modern lake waters from western Greenland. The Holocene 13, 605-611.

Leng, M.J., Henderson, A.C.G., 2013. Recent advances in isotopes as palaeolimnological proxies. Journal of Paleolimnology 49, 481-496.

Leng, M.J., Lewis, J.P., 2017. C/N ratios and Carbon Isotope Composition of Organic Matter in Estuarine Environments, Applications of Paleoenvironmental Techniques in Estuarine Studies, pp. 213-237.

Leng, M.J., Marshall, J.D., 2004. Palaeoclimate interpretation of stable isotope data from lake sediment archives. Quaternary Science Reviews 23, 811-831.

Leng, M.J., Wagner, B., Anderson, N.J., Bennike, O., Woodley, E., Kemp, S.J., 2012. Deglaciation and catchment ontogeny in coastal south-west Greenland: implications for terrestrial and aquatic carbon cycling. J Quaternary Sci 27, 575-584.

Lesnek, A.J., Briner, J.P., 2018. Response of a land-terminating sector of the western Greenland Ice Sheet to early Holocene climate change: Evidence from 10Be dating in the Søndre Isortoq region. Quaternary Science Reviews 180, 145-156.

Levac, E., Vernal, A.D., Blake Jr, W., 2001. Sea-surface conditions in northernmost Baffin Bay during the Holocene: palynological evidence. J Quaternary Sci 16, 353-363.

Levy, L.B., Kelly, M.a., Lowell, T.V., Hall, B.L., Hempel, L.a., Honsaker, W.M., Lusas, A.R., Howley, J.a., Axford, Y.L., 2013. Holocene fluctuations of Bregne ice cap, Scoresby Sund, east Greenland: a proxy for climate along the Greenland Ice Sheet margin. Quaternary Science Reviews, 1-12.

Levy, L.B., Larsen, N.K., Davidson, T.A., Strunk, A., Olsen, J., Jeppesen, E., 2017. Contrasting evidence of Holocene ice margin retreat, south-western Greenland. J Quaternary Sci.

Liu, X., Colman, S.M., Brown, E.T., Minor, E.C., Li, H., 2013. Estimation of carbonate, total organic carbon, and biogenic silica content by FTIR and XRF techniques in lacustrine sediments. Journal of Paleolimnology 50, 387-398.

Lloyd, J., 2006. Late Holocene environmental change in Disko Bugt, west Greenland: interaction between climate, ocean circulation and Jakobshavn Isbrae. Boreas 35, 35-49.

Lochte, A.A., Repschläger, J., Seidenkrantz, M.-S., Kienast, M., Blanz, T., Schneider, R.R., 2019. Holocene water mass changes in the Labrador Current. The Holocene.

Lombino, A., 2014. The systematics of oxygen isotopes in chironomids (Insecta: Diptera): a tool for reconstructing past climate, Department of Geography. University College London.

Lombino, A., Jones, V., Holmes, J., Atkinson, T., Brooks, S.J., Grocke, D.R., 2014. Chironomids as a proxy for reconstructing past lake water δ18O: a late glacial down- core record from Hawes Water, Quaternary Research Association Annual Discussion Meeting, London.

Long, A.J., Woodroffe, S.A., Roberts, D.H., Dawson, S., 2011. Isolation basins, sea-level changes and the Holocene history of the Greenland Ice Sheet. Quaternary Science Reviews 30, 3748-3768.

Lowell, T.V., Hall, B.L., Kelly, M.A., Bennike, O., Lusas, A.R., Honsaker, W., Smith, C.A., Levy, L.B., Travis, S., Denton, G.H., 2013. Late Holocene expansion of Istorvet ice cap, Liverpool Land, east Greenland. Quaternary Science Reviews 63, 128-140.

Lu, R., Gan, W., Wu, B.-h., Zhang, Z., Guo, Y., Wang, H.-f.J.T.J.o.P.C.B., 2005. C− H stretching vibrations of methyl, methylene and methine groups at the vapor/alcohol (n= 1− 8) interfaces. 109, 14118-14129.

Luterbacher, J., Werner, J.P., Smerdon, J.E., Fernández-Donado, L., González-Rouco, F.J., Barriopedro, D., Ljungqvist, F.C., Büntgen, U., Zorita, E., Wagner, S., Esper, J., McCarroll, D., Toreti, A., Frank, D., Jungclaus, J.H., Barriendos, M., Bertolin, C., Bothe, O., Brázdil, R., Camuffo, D., Dobrovolný, P., Gagen, M., García-Bustamante, E., Ge, Q., Gómez-Navarro, J.J., Guiot, J., Hao, Z., Hegerl, G.C., Holmgren, K., Klimenko, V.V., Martín-Chivelet, J., Pfister, C., Roberts, N., Schindler, A., Schurer, A., Solomina, O., von Gunten, L., Wahl, E., Wanner, H., Wetter, O., Xoplaki, E., Yuan, N., Zanchettin, D., Zhang, H., Zerefos, C., 2016. European summer temperatures since Roman times. Environmental Research Letters 11.

Majtan, J., Bilikova, K., Markovic, O., Grof, J., Kogan, G., Simuth, J., 2007. Isolation and characterization of chitin from bumblebee (Bombus terrestris). Int J Biol Macromol 40, 237-241.

Malmierca-Vallet, I., Sime, L.C., Tindall, J.C., Capron, E., Valdes, P.J., Vinther, B.M., Holloway, M.D., 2018. Simulating the Last Interglacial Greenland stable water isotope peak: The role of Arctic sea ice changes. Quaternary Science Reviews 198, 1-14.

Mann, M.E., Zhang, Z., Hughes, M.K., Bradley, R.S., Miller, S.K., Rutherford, S., Ni, F., 2008. Proxy-based reconstructions of hemispheric and global surface temperature variations over the past two millennia. Proc Natl Acad Sci U S A 105, 13252-13257.

Mann, M.E., Zhang, Z., Rutherford, S., Bradley, R.S., Hughes, M.K., Shindell, D., Ammann, C., Faluvegi, G., Ni, F., 2009. Global signatures and dynamical origins of the Little Ice Age and Medieval Climate Anomaly. Science 326, 1256-1260.

Marcott, S.A., Shakun, J.D., Clark, P.U., Mix, A.C., 2013. A reconstruction of regional and global temperature for the past 11,300 years. Science 339, 1198-1201.

Massa, C., Perren, B.B., Gauthier, É., Bichet, V., Petit, C., Richard, H., 2012. A multiproxy evaluation of Holocene environmental change from Lake Igaliku, South Greenland. Journal of Paleolimnology 48, 241-258.

Massé, G., Rowland, S.J., Sicre, M.-A., Jacob, J., Jansen, E., Belt, S.T., 2008. Abrupt climate changes for Iceland during the last millennium: Evidence from high resolution sea ice reconstructions. Earth Planet Sc Lett 269, 565-569.

Mayr, C., Laprida, C., Lücke, A., Martín, R.S., Massaferro, J., Ramón-Mercau, J., Wissel, H., 2014. Oxygen isotope ratios of chironomids, aquatic macrophytes and ostracods for lake-water isotopic reconstructions – results of a calibration study in Patagonia. Journal of Hydrology.

McCormick, M., Büntgen, U., Cane, M.A., Cook, E.R., Harper, K., Huybers, P., Litt, T., Manning, S.W., Mayewski, P.A., More, A.F.M., Nicolussi, K., Tegel, W., 2012. Climate Change during and after the Roman Empire: Reconstructing the Past from Scientific and Historical Evidence. Journal of Interdisciplinary History 43, 169-220.

McFarlin, J.M., Axford, Y., Osburn, M.R., Kelly, M.A., Osterberg, E.C., Farnsworth, L.B., 2018. Pronounced summer warming in northwest Greenland during the Holocene and Last Interglacial. Proc Natl Acad Sci U S A 115, 6357-6362.

McGowan, S., Ryves, D.B., Anderson, N.J., 2003. Holocene records of effective precipitation in West Greenland. The Holocene 13, 239-249.

McKay, N.P., Heiser, C., Kinder, D., Emile-Geay, J., 2017. geoChronR: Tools to analyze and visualize time-uncertain geoscientific data. R package, 0.2 ed.

McKay, N.P., Kaufman, D.S., Routson, C.C., Erb, M.P., Zander, P.D., 2018. The Onset and Rate of Holocene Neoglacial Cooling in the Arctic. Geophysical Research Letters 45, 12,487-412,496.

Menne, M.J., Durre, I., Korzeniewski, B., McNeal, S., K., T., Yin, X., Anthony, S., Ray, R., Vose, R.S., Gleason, B.E., Houston, T.G., 2012. Global Historical Climatology Network - Daily (GHCN-Daily), Version 3., NOAA National Climatic Data Center.

Miettinen, A., Divine, D., Koç, N., Godtliebsen, F., Hall, I.R., 2012. Multicentennial Variability of the Sea Surface Temperature Gradient across the Subpolar North Atlantic over the Last 2.8 kyr*,+. Journal of Climate 25, 4205-4219.

Miettinen, A., Divine, D.V., Husum, K., Koç, N., Jennings, A., 2015. Exceptional ocean surface conditions on the SE Greenland shelf during the Medieval Climate Anomaly. Paleoceanography 30, 1657-1674.

Miller, G.H., Brigham-Grette, J., Alley, R.B., Anderson, L., Bauch, H.a., Douglas, M.S.V., Edwards, M.E., Elias, S.a., Finney, B.P., Fitzpatrick, J.J., Funder, S.V., Herbert, T.D., Hinzman, L.D., Kaufman, D.S., MacDonald, G.M., Polyak, L., Robock, a., Serreze, M.C., Smol, J.P., Spielhagen, R., White, J.W.C., Wolfe, a.P., Wolff, E.W., 2010. Temperature and precipitation history of the Arctic. Quaternary Science Reviews 29, 1679-1715.

Miller, G.H., Geirsdottir, A., Zhong, Y.F., Larsen, D.J., Otto-Bliesner, B.L., Holland, M.M., Bailey, D.A., Refsnider, K.A., Lehman, S.J., Southon, J.R., Anderson, C., Bjornsson, H., Thordarson, T., 2012. Abrupt onset of the Little Ice Age triggered by volcanism and sustained by sea-ice/ocean feedbacks. Geophysical Research Letters 39.

Miller, G.H., Lehman, S.J., Refsnider, K.A., Southon, J.R., Zhong, Y.F., 2013. Unprecedented recent summer warmth in Arctic Canada. Geophysical Research Letters 40, 5745-5751.

Millet, L., Massa, C., Bichet, V., Frossard, V., Belle, S., Gauthier, E., 2014. Anthropogenic versus climatic control in a high-resolution 1500-year chironomid stratigraphy from a southwestern Greenland lake. Quaternary Research 81, 193-202.

Moffa-Sánchez, P., Born, A., Hall, I.R., Thornalley, D.J.R., Barker, S., 2014a. Solar forcing of North Atlantic surface temperature and salinity over the past millennium. Nature Geoscience 7, 275-278.

Moffa-Sanchez, P., Hall, I.R., 2017. North Atlantic variability and its links to European climate over the last 3000 years. Nature communications 8, 1726.

Moffa-Sánchez, P., Hall, I.R., Barker, S., Thornalley, D.J.R., Yashayaev, I., 2014b. Surface changes in the eastern Labrador Sea around the onset of the Little Ice Age. Paleoceanography 29, 160-175.

Moller, H.S., Jensen, K.G., Kuijpers, A., Aagaard-Sorensen, S., Seidenkrantz, M.S., Prins, M., Endler, R., Mikkelsen, N., 2006. Late-Holocene environment and climatic changes in Ameralik Fjord, southwest Greenland: evidence from the sedimentary record. Holocene 16, 685-695.

Moore, J.J., Hughen, K.A., Miller, G.H., Overpeck, J.T., 2001. Little Ice Age recorded in summer temperature reconstruction from varved sediments of Donard Lake, Baffin Island, Canada. Journal of Paleolimnology 25, 503–517.

Moreno-Chamarro, E., Zanchettin, D., Lohmann, K., Jungclaus, J.H., 2016. An abrupt weakening of the subpolar gyre as trigger of Little Ice Age-type episodes. Climate Dynamics 48, 727-744.

Moros, M., Jansen, E., Oppo, D.W., Giraudeau, J., Kuijpers, A., 2012. Reconstruction of the late-Holocene changes in the Sub-Arctic Front position at the Reykjanes Ridge, north Atlantic. The Holocene 22, 877-886.

Moros, M., Jensen, K., Kuijpers, A., 1996. Mid- to late-Holocene hydrological and climatic variability in Disko Bugt, central West Greenland. The Holocene 16, 357-367.

Moros, M., Lloyd, J.M., Perner, K., Krawczyk, D., Blanz, T., de Vernal, A., Ouellet-Bernier, M.-M., Kuijpers, A., Jennings, A.E., Witkowski, A., Schneider, R., Jansen, E., 2016. Surface and sub-surface multi-proxy reconstruction of middle to late Holocene palaeoceanographic changes in Disko Bugt, West Greenland. Quaternary Science Reviews 132, 146-160.

Nation, J.L., 2011. Insect physiology and biochemistry. CRC press.

Nielson, K.E., Bowen, G.J., 2010. Hydrogen and oxygen in brine shrimp chitin reflect environmental water and dietary isotopic composition. Geochimica et Cosmochimica Acta 74, 1812-1822.

Nørgaard-Pedersen, N., Mikkelsen, N., 2009. 8000 year marine record of climate variability and fjord dynamics from Southern Greenland. Marine Geology 264, 177-189.

Okasanen, J., Blanchet, F.G., Friendly, M., Kindt, R., Legrendre, P., McGlinn, D., Minchin, P.R., O'Hara, R.B., Simpson, G.L., Solymos, P., Stevens, M.H.M., Szoecs, E., Wagner, H., 2018. vegan: Community Ecology Package: R package version 2.4-6. https://CRAN.R-project.org/package=vegan, 2.4-6 ed.

Ólafsdóttir, S., Jennings, A.E., Geirsdóttir, Á., Andrews, J., Miller, G.H., 2010. Holocene variability of the North Atlantic Irminger current on the south- and northwest shelf of Iceland. Marine Micropaleontology 77, 101-118.

Olsen, J., Anderson, N.J., Knudsen, M.F., 2012. Variability of the North Atlantic Oscillation over the past 5,200 years. Nature Geoscience 5, 808-812.

Ortega, P., Lehner, F., Swingedouw, D., Masson-Delmotte, V., Raible, C.C., Casado, M., Yiou, P., 2015. A model-tested North Atlantic Oscillation reconstruction for the past millennium. Nature 523, 71-74.

Osburn, C.L., Anderson, N.J., Stedmon, C.A., Giles, M.E., Whiteford, E.J., McGenity, T.J., Dumbrell, A.J., Underwood, G.J.C., 2017. Shifts in the Source and Composition of Dissolved Organic Matter in Southwest Greenland Lakes Along a Regional Hydro-climatic Gradient. Journal of Geophysical Research: Biogeosciences 122, 3431-3445.

Osterberg, E.C., Hawley, R.L., Wong, G., Kopec, B., Ferris, D., Howley, J., 2015. Coastal ice-core record of recent northwest Greenland temperature and sea-ice concentration. Journal of Glaciology 61, 1137-1146.

Ouellet-Bernier, M.-M., de Vernal, A., Hillaire-Marcel, C., Moros, M., 2014. Paleoceanographic changes in the Disko Bugt area, West Greenland, during the Holocene. The Holocene 24, 1573-1583.

Overland, J., Dunlea, E., Box, J.E., Corell, R., Forsius, M., Kattsov, V., Olsen, M.S., Pawlak, J., Reiersen, L.-O., Wang, M., 2018. The urgency of Arctic change. Polar Science.

Pendleton, S.L., Miller, G.H., Anderson, R.A., Crump, S.E., Zhong, Y., Jahn, A., Geirsdottir, Á., 2017. Episodic Neoglacial expansion and rapid 20th century retreat of a small ice cap on Baffin Island, Arctic Canada, and modeled temperature change. Climate of the Past 13, 1527-1537.

Perga, M.-E., 2011. Taphonomic and early diagenetic effects on the C and N stable isotope composition of cladoceran remains: implications for paleoecological studies. Journal of Paleolimnology 46, 203-213.

Perner, K., Jennings, A.E., Moros, M., Andrews, J.T., Wacker, L., 2016. Interaction between warm Atlantic-sourced waters and the East Greenland Current in northern Denmark Strait (68°N) during the last 10 600 cal a BP. J Quaternary Sci 31, 472-483.

Perner, K., Moros, M., Jennings, A., Lloyd, J.M., Knudsen, K.L., 2012. Holocene palaeoceanographic evolution off West Greenland. The Holocene 23, 374-387.

Perner, K., Moros, M., Lloyd, J.M., Jansen, E., Stein, R., 2015. Mid to late Holocene strengthening of the East Greenland Current linked to warm subsurface Atlantic water. Quaternary Science Reviews 129, 296-307.

Perner, K., Moros, M., Lloyd, J.M., Kuijpers, A., Telford, R.J., Harff, J., 2011. Centennial scale benthic foraminiferal record of late Holocene oceanographic variability in Disko Bugt, West Greenland. Quaternary Science Reviews 30, 2815-2826.

Perren, B.B., Anderson, N.J., Douglas, M.S.V., Fritz, S.C., 2012a. The influence of temperature, moisture, and eolian activity on Holocene lake development in West Greenland. Journal of Paleolimnology 48, 223-239.

Perren, B.B., Wolfe, A.P., Cooke, C.A., Kjaer, K.H., Mazzucchi, D., Steig, E.J., 2012b. Twentieth-century warming revives the world's northernmost lake. Geology 40, 1003-1006.

Poulicek, M., Jeuniaux, C., 1991. Chitin biodegredation in marine environments: an experimental approach. Biochemical Systematics and Ecology 19, 385-394.

Pryor, A.J.E., Stevens, R.E., O'Connell, T.C., Lister, J.R., 2014. Quantification and propagation of errors when converting vertebrate biomineral oxygen isotope data to temperature for palaeoclimate reconstruction. Palaeogeography, Palaeoclimatology, Palaeoecology 412, 99-107.

Quillmann, U., 2014. The Influence of Subpolar Gyre Dynamics on Centennial to Millennial Scale Holocene Climate Variability in the High-Latitude North Atlantic, Geological Sciences. University of Colorado, Boulder, p. 209.

Ramsey, C.B., 2009. Bayesian analysis of radiocarbon dates. Radiocarbon 51, 337-360.

Rashid, H., Piper, D.J.W., Lazar, K.B., McDonald, K., Saint-Ange, F., 2017. The Holocene Labrador Current: Changing linkages to atmospheric and oceanographic forcing factors. Paleoceanography 32, 498-510.

Rastner, P., Bolch, T., Mölg, N., Machguth, H., Le Bris, R., Paul, F., 2012. The first complete inventory of the local glaciers and ice caps on Greenland. The Cryosphere 6, 1483-1495.

Reig, F.B., Adelantado, J.V.G., Moreno, M.C.M.M., 2002. FTIR quantitative analysis of calcium carbonate (calcite) and silica (quartz) mixtures using the constant ratio method. Application to geological samples. Talanta 58, 811-821.

Reimer, P.J., Bard, E., Bayliss, A., Beck, J.W., Blackwell, P.G., Ramsey, C.B., Buck, C.E., Cheng, H., Edwards, R.L., Friedrich, M., 2013. IntCal13 and Marine13 radiocarbon age calibration curves 0–50,000 years cal BP. Radiocarbon 55, 1869-1887.

Reimer, P.J., Reimer, R.W., 2001. A marine reservoir correction database and on-line interface. Radiocarbon 43, 461-463.

Reusche, M.M., Marcott, S.A., Ceperley, E.G., Barth, A.M., Brook, E.J., Mix, A.C., Caffee, M.W., 2018. Early to Late Holocene Surface Exposure Ages From Two Marine-Terminating Outlet Glaciers in Northwest Greenland. Geophysical Research Letters 45, 7028-7039.

Reverdin, G., 2010. North Atlantic Subpolar Gyre Surface Variability (1895–2009). Journal of Climate 23, 4571-4584.

Ribeiro, S., Moros, M., Ellegaard, M., Kuijpers, A., 2012. Climate variability in West Greenland during the past 1500 years: evidence from a high-resolution marine palynological record from Disko Bay. Boreas 41, 68-83.

Richter, T.O., Peeters, F.J.C., van Weering, T.C.E., 2009. Late Holocene (0–2.4kaBP) surface water temperature and salinity variability, Feni Drift, NE Atlantic Ocean. Quaternary Science Reviews 28, 1941-1955.

Rimbu, N., Lohmann, G., Werner, M., Ionita, M., 2016. Links between central Greenland stable isotopes, blocking and extreme climate variability over Europe at decadal to multidecadal time scales. Climate Dynamics 49, 649-663.

Rozanski, K., Araguás-Araguás, L., Gonfiantini, R., 1993. Isotopic patterns in modern global precipitation. 78, 1-36.

Samartin, S., Heiri, O., Joos, F., Renssen, H., Franke, J., Brönnimann, S., Tinner, W., 2017. Warm Mediterranean mid-Holocene summers inferred from fossil midge assemblages. Nature Geoscience 10, 207-212.

Sauer, P.E., Miller, G.H., Overpeck, J.T., 2001. Oxygen isotope ratios of organic matter in arctic lakes as a paleoclimate proxy: field and laboratory investigations. Journal of Paleolimnology 25, 43-64.

Schaefer, J., Kramer, K.J., Garbow, J.R., Jacob, G.S., Stejskal, E.O., Hopkins, T.L., Speirs, R.D., 1987. Aromatic cross-links in insect cuticle: detection by solid-state 13C and 15N NMR. Science 235, 1200-1204.

Schilder, J., Tellenbach, C., Möst, M., Spaak, P., van Hardenbroek, M., Wooller, M.J., Heiri, O., 2015. The stable isotopic composition of Daphnia ephippia reflects changes in δ13C and δ18O values of food and water. Biogeosciences 12, 3819-3830.

Schimmelmann, A., 2011. Carbon, nitrogen and oxygen stable isotope ratios in chitin. 34, 81-103.

Schimmelmann, A., DeNiro, M., Poulicek, M., Voss-Foucart, M.-F., Goffinet, G., Jeuniaux, C., 1986. Stable isotopic composition of chitin from arthropods recovered in archaeological contexts as palaeoenvironmental indicators. Journal of Archeaological Science 13, 553-566.

Schimmelmann, A., DeNiro, M.J., 1986. Stable isotopic studies on chitin. III. The D/H and 18O/16O ratios in arthropod chitin. Geochimica et Cosmochimica Acta 50, 1485-1496.

Schmidt, S., Send, U., 2007. Origin and Composition of Seasonal Labrador Sea Freshwater. Journal of Physical Oceanography 37, 1445-1454.

Schweinsberg, A.D., Briner, J.P., Miller, G.H., Bennike, O., Thomas, E.K., 2017. Local glaciation in West Greenland linked to North Atlantic Ocean circulation during the Holocene. Geology 45, 195-198.

Schweinsberg, A.D., Briner, J.P., Miller, G.H., Lifton, N.A., Bennike, O., Graham, B.L., 2018. Holocene mountain glacier history in the Sukkertoppen Iskappe area, southwest Greenland. Quaternary Science Reviews 197, 142-161.

Sculthorpe, C.D., 1967. The biology of aquatic vascular plants. Edward Arnold Publishers, London.

Seidenkrantz, M.-S., 2013. Benthic foraminifera as palaeo sea-ice indicators in the subarctic realm – examples from the Labrador Sea–Baffin Bay region. Quaternary Science Reviews 79, 135-144.

Seidenkrantz, M.-S., Roncaglia, L., Fischel, A., Heilmann-Clausen, C., Kuijpers, A., Moros, M., 2008. Variable North Atlantic climate seesaw patterns documented by a late Holocene marine record from Disko Bugt, West Greenland. Marine Micropaleontology 68, 66-83.

Seidenkrantz, M.S., Aagaard-Sorensen, S., Sulsbruck, H., Kuijpers, A., Jensen, K.G., Kunzendorf, H., 2007. Hydrography and climate of the last 4400 years in a SW Greenland fjord: implications for Labrador Sea palaeoceanography. The Holocene 17, 387-401.

Sejrup, H.P., Haflidason, H., Andrews, J.T., 2011. A Holocene North Atlantic SST record and regional climate variability. Quaternary Science Reviews 30, 3181-3195.

Sejrup, H.P., Seppä, H., McKay, N.P., Kaufman, D.S., Geirsdóttir, Á., de Vernal, A., Renssen, H., Husum, K., Jennings, A., Andrews, J.T., 2016. North Atlantic-Fennoscandian Holocene climate trends and mechanisms. Quaternary Science Reviews 147, 365-378.

Serreze, M.C., Francis, J.A., 2006. The arctic amplification debate. Climatic Change 76, 241-264.

Sha, L., Jiang, H., Seidenkrantz, M.-S., Knudsen, K.L., Olsen, J., Kuijpers, A., Liu, Y., 2014. A diatom-based sea-ice reconstruction for the Vaigat Strait (Disko Bugt, West Greenland) over the last 5000yr. Palaeogeography, Palaeoclimatology, Palaeoecology 403, 66-79.

Sha, L., Jiang, H., Seidenkrantz, M.-S., Li, D., Andresen, C.S., Knudsen, K.L., Liu, Y., Zhao, M., 2017. A record of Holocene sea-ice variability off West Greenland and its potential forcing factors. Palaeogeography, Palaeoclimatology, Palaeoecology 475, 115-124.

Sicre, M.A., Hall, I.R., Mignot, J., Khodri, M., Ezat, U., Truong, M.X., Eiríksson, J., Knudsen, K.L., 2011. Sea surface temperature variability in the subpolar Atlantic over the last two millennia. Paleoceanography 26.

Sicre, M.A., Weckström, K., Seidenkrantz, M.S., Kuijpers, A., Benetti, M., Masse, G., Ezat, U., Schmidt, S., Bouloubassi, I., Olsen, J., Khodri, M., Mignot, J., 2014. Labrador current variability over the last 2000 years. Earth Planet Sc Lett 400, 26-32.

Siddiqui, S.A., Pandey, A.K., Dwivedi, A., Jain, S., Misra, N., 2010. Comparative conformational, structural and vibrational study on the molecular structure of tyrosine and L-DOPA using density functional theory. Journal of Chemical and Pharmaceutical Research 2, 835-850.

Sime, L.C., Hopcroft, P.O., Rhodes, R.H., 2019. Impact of abrupt sea ice loss on Greenland water isotopes during the last glacial period. Proc Natl Acad Sci U S A.

Simpson, G.L., 2019. gratia: Graceful 'ggplot'-Based Graphics and Other Functions for GAMs Fitted Using 'mgcv'. R package version 0.2-8. https://CRAN.R-project.org/package=gratia.

Sinclair, G., Carlson, A.E., Mix, A.C., Lecavalier, B.S., Milne, G., Mathias, A., Buizert, C., DeConto, R., 2016. Diachronous retreat of the Greenland ice sheet during the last deglaciation. Quaternary Science Reviews 145, 243-258.

Sodemann, H., Masson-Delmotte, V., Schwierz, C., Vinther, B.M., Wernli, H., 2008. Interannual variability of Greenland winter precipitation sources: 2. Effects of North Atlantic Oscillation variability on stable isotopes in precipitation. Journal of Geophysical Research 113.

Solomina, O.N., Bradley, R.S., Jomelli, V., Geirsdottir, A., Kaufman, D.S., Koch, J., McKay, N.P., Masiokas, M., Miller, G., Nesje, A., Nicolussi, K., Owen, L.A., Putnam, A.E., Wanner, H., Wiles, G., Yang, B., 2016. Glacier fluctuations during the past 2000 years. Quaternary Science Reviews 149, 61-90.

Soto, D.X., Wassenaar, L.I., Hobson, K.A., Raubenheimer, D., 2013. Stable hydrogen and oxygen isotopes in aquatic food webs are tracers of diet and provenance. Functional Ecology 27, 535-543.

Stacklies, W., Redestig, H., Scholz, M., Walther, D., Selbig, J.J.B., 2007. pcaMethods—a bioconductor package providing PCA methods for incomplete data. 23, 1164-1167.

Stankiewicz, B.A., Briggs, D.E., Evershed, R.P., Miller, R.F., Bierstedt, A., 1998a. The fate of chitin in Quaternary and Tertiary strata, Nitrogen-Containing Macromolecules in the Bio- and Geosphere, pp. 211-224.

Stankiewicz, B.A., Briggs, D.E.G., Evershed, R.P., Flannery, M.B., Wuttke, M., 1997. Preservation of chitin in 25-million-year-old fossils. Science 276, 1541-1543.

Stankiewicz, B.A., Mastalerz, M., Hof, C.H.J., Bierstedt, A., Flannery, M.B., Briggs, D.E.G., Evershed, R.P., 1998b. Biodegradation of the chitin-protein complex in crustacean cuticle. Organic Geochemistry 28, 67-76.

Stuvier, M., Reimer, P.J., Reimer, R.W., 2005. CALIB 7.1. WWW program and documentation.

Sundqvist, H.S., Kaufman, D.S., McKay, N.P., Balascio, N.L., Briner, J.P., Cwynar, L.C., Sejrup, H.P., Seppä, H., Subetto, D.A., Andrews, J.T., Axford, Y., Bakke, J., Birks, H.J.B., Brooks, S.J., de Vernal, A., Jennings, A.E., Ljungqvist, F.C., Rühland, K.M., Saenger, C., Smol, J.P., Viau, A.E., 2014. Arctic Holocene proxy climate database – new approaches to assessing geochronological accuracy and encoding climate variables. Climate of the Past 10, 1605-1631.

Tegelaar, E.W., Deleeuw, J.W., Derenne, S., Largeau, C., 1989. A Reappraisal of Kerogen Formation. Geochimica Et Cosmochimica Acta 53, 3103-3106.

Thomas, E.K., Axford, Y., Briner, J.P., 2007. Rapid 20th century environmental change on northeastern Baffin Island, Arctic Canada inferred from a multi-proxy lacustrine record. Journal of Paleolimnology 40, 507-517.

Thomas, E.K., Briner, J.P., 2009. Climate of the past millennium inferred from varved proglacial lake sediments on northeast Baffin Island, Arctic Canada. Journal of Paleolimnology 41, 209-224.

Thomas, E.K., Briner, J.P., Ryan-Henry, J.J., Huang, Y., 2016. A major increase in winter snowfall during the middle Holocene on western Greenland caused by reduced sea ice in Baffin Bay and the Labrador Sea. Geophysical Research Letters.

Thornalley, D.J., Elderfield, H., McCave, I.N., 2009. Holocene oscillations in temperature and salinity of the surface subpolar North Atlantic. Nature 457, 711-714.

Thornalley, D.J.R., Oppo, D.W., Ortega, P., Robson, J.I., Brierley, C.M., Davis, R., Hall, I.R., Moffa-Sanchez, P., Rose, N.L., Spooner, P.T., Yashayaev, I., Keigwin, L.D., 2018. Anomalously weak Labrador Sea convection and Atlantic overturning during the past 150 years. Nature 556, 227-230.

Trouet, V., Esper, J., Graham, N.E., Baker, A., Scourse, J.D., Frank, D.C., 2009. Persistent positive North Atlantic oscillation mode dominated the Medieval Climate Anomaly. Science 324, 78-80.

Trouet, V., Scourse, J.D., Raible, C.C., 2012. North Atlantic storminess and Atlantic Meridional Overturning Circulation during the last Millennium: Reconciling contradictory proxy records of NAO variability. Global and Planetary Change 84-85, 48-55.

van Hardenbroek, M., Chakraborty, A., Davies, K.L., Harding, P., Heiri, O., Henderson, A.C.G., Holmes, J.A., Lasher, G.E., Leng, M.J., Panizzo, V.N., Roberts, L., Schilder, J., Trueman, C.N., Wooller, M.J., 2018. The stable isotope composition of organic and inorganic fossils in lake sediment records: Current understanding, challenges, and future directions. Quaternary Science Reviews 196, 154-176.

van Hardenbroek, M., Lotter, A.F., Bastviken, D., Andersen, T.J., Heiri, O., 2014. Taxon-specific δ13C analysis of chitinous invertebrate remains in sediments from Strandsjön, Sweden. Journal of Paleolimnology 52, 95-105.

Verbruggen, F., Heiri, O., Reichart, G.-J., Lotter, a.F., 2010. Chironomid δ18O as a proxy for past lake water δ18O: a Lateglacial record from Rotsee (Switzerland). Quaternary Science Reviews 29, 2271-2279.

Verbruggen, F., Heiri, O., Reichart, G.J., Blaga, C., Lotter, a.F., 2011. Stable oxygen isotopes in chironomid and cladoceran remains as indicators for lake water δ18O. Limnology and Oceanography 56, 2071-2079.

Verbruggen, F., Heiri, O., Reichart, G.J., Leeuw, J.W., Nierop, K.G.J., Lotter, A.F., 2009. Effects of chemical pretreatments on δ18O measurements, chemical composition, and morphology of chironomid head capsules. Journal of Paleolimnology 43, 857-872.

Vinther, B.M., Andersen, K.K., Jones, P.D., Briffa, K.R., Cappelen, J., 2006. Extending Greenland temperature records into the late eighteenth century. Journal of Geophysical Research 111.

Vinther, B.M., Buchardt, S.L., Clausen, H.B., Dahl-Jensen, D., Johnsen, S.J., Fisher, D.a., Koerner, R.M., Raynaud, D., Lipenkov, V., Andersen, K.K., Blunier, T., Rasmussen, S.O., Steffensen, J.P., Svensson, a.M., 2009. Holocene thinning of the Greenland ice sheet. Nature 461, 385-388.

Vinther, B.M., Clausen, H.B., Fisher, D.A., Koerner, R.M., Johnsen, S.J., Andersen, K.K., Dahl-Jensen, D., Rasmussen, S.O., Steffensen, J.P., Svensson, A.M., 2008. Synchronizing ice cores from the Renland and Agassiz ice caps to the Greenland Ice Core Chronology. Journal of Geophysical Research 113.

Vinther, B.M., Jones, P.D., Briffa, K.R., Clausen, H.B., Andersen, K.K., Dahl-Jensen, D., Johnsen, S.J., 2010. Climatic signals in multiple highly resolved stable isotope records from Greenland. Quaternary Science Reviews 29, 522-538.

Wagner, B., Bennike, O., 2012. Chronology of the last deglaciation and Holocene environmental changes in the Sisimiut area, SW Greenland based on lacustrine records. Boreas 41, 481-493.

Walker, I.R., 1987. Chironomidae (Diptera) in Paleoecology. Quaternary Science Reviews 6, 29-40.

Walker, I.R., 2001. Midges: Chironomidae and related diptera, Tracking environmental change using lake sediments. Springer, pp. 43-66.

Wang, T., Surge, D., Mithen, S., 2012. Seasonal temperature variability of the Neoglacial (3300–2500BP) and Roman Warm Period (2500–1600BP) reconstructed from oxygen isotope ratios of limpet shells (Patella vulgata), Northwest Scotland. Palaeogeography, Palaeoclimatology, Palaeoecology 317-318, 104-113.

Wang, Y., Francis, D.R., O'Brien, D.M., Wooller, M.J., 2008. A protocol for preparing subfossil chironomid head capsules (Diptera: Chironomidae) for stable isotope analysis in paleoclimate reconstruction and considerations of contamination sources. Journal of Paleolimnology 40, 771-781.

Wang, Y.V., O'Brien, D.M., Jenson, J., Francis, D., Wooller, M.J., 2009. The influence of diet and water on the stable oxygen and hydrogen isotope composition of Chironomidae (Diptera) with paleoecological implications. Oecologia 160, 225-233.

Weidick, A., Bennike, O., Citterio, M., Nørgaard-Pedersen, N., 2012. Neoglacial and historical glacier changes around Kangersuneq fjord in southern West Greenland. Geological Survey of Denmark and Greenland Bulletin 27, 68.

Winsor, K., Carlson, A.E., Rood, D.H., 2014. 10Be dating of the Narsarsuaq moraine in southernmost Greenland: evidence for a late-Holocene ice advance exceeding the Little Ice Age maximum. Quaternary Science Reviews 98, 135-143.

Winsor, K., Carlson, A.E., Welke, B.M., Reilly, B., 2015. Early deglacial onset of southwestern Greenland ice-sheet retreat on the continental shelf. Quaternary Science Reviews 128, 117-126.

Woo, M., 1980. Hydrology of a small lake in the Canadian High Arctic. Arctic and Alpine Research, 227-235.

Woodroffe, S.A., Long, A.J., Lecavalier, B.S., Milne, G.A., Bryant, C.L., 2014. Using relative sea-level data to constrain the deglacial and Holocene history of southern Greenland. Quaternary Science Reviews 92, 345-356.

Wooller, M., Wang, Y., Axford, Y., 2007. A multiple stable isotope record of Late Quaternary limnological changes and chironomid paleoecology from northeastern Iceland. Journal of Paleolimnology 40, 63-77.

Wooller, M.J., Francis, D., Fogel, M.L., Miller, G.H., Walker, I.R., Wolfe, A.P., 2004. Quantitative paleotemperature estimates from d18O of chironomid head capsules preserved in arctic lake sediments. Journal of Paleolimnology, 267-274.

Xia, M.S., Yao, Z.T., Ge, L.Q., Chen, T., Li, H.Y., 2015. A potential bio-filler: The substitution effect of furfural modified clam shell for carbonate calcium in polypropylene. Journal of Composite Materials 49, 807-816.

Yashayaev, I., 2007. Hydrographic changes in the Labrador Sea, 1960–2005. Progress in Oceanography 73, 242-276.

Young, N.E., Briner, J.P., 2015. Holocene evolution of the western Greenland Ice Sheet: Assessing geophysical ice-sheet models with geological reconstructions of ice-margin change. Quaternary Science Reviews 114, 1-17.

Young, N.E., Schweinsberg, A.D., Briner, J.P., Schaefer, J.M., 2015. Glacier maxima in Baffin Bay during the Medieval Warm Period coeval with Norse settlement. Sci Adv 1, e1500806.

Zhang, L., Roy, S., Chen, Y., Chua, E.K., See, K.Y., Hu, X., Liu, M., 2014. Mussel-inspired polydopamine coated hollow carbon microspheres, a novel versatile filler for fabrication of high performance syntactic foams. ACS Appl Mater Interfaces 6, 18644-18652.

Zhang, M., Haga, A., Sekiguchi, H., Hirano, S.J.I.J.o.B.M., 2000. Structure of insect chitin isolated from beetle larva cuticle and silkworm (Bombyx mori) pupa exuvia. 27, 99-105.

Zhu, J., Lücke, A., Wissel, H., Mayr, C., Ohlendorf, C., Zolitschka, B., 2014. Characterizing oxygen isotope variability and host water relation of modern and subfossil aquatic mosses. Geochimica et Cosmochimica Acta 130, 212-228.

Appendix 1: Supplemental material for South Greenland study (Chapter 5)

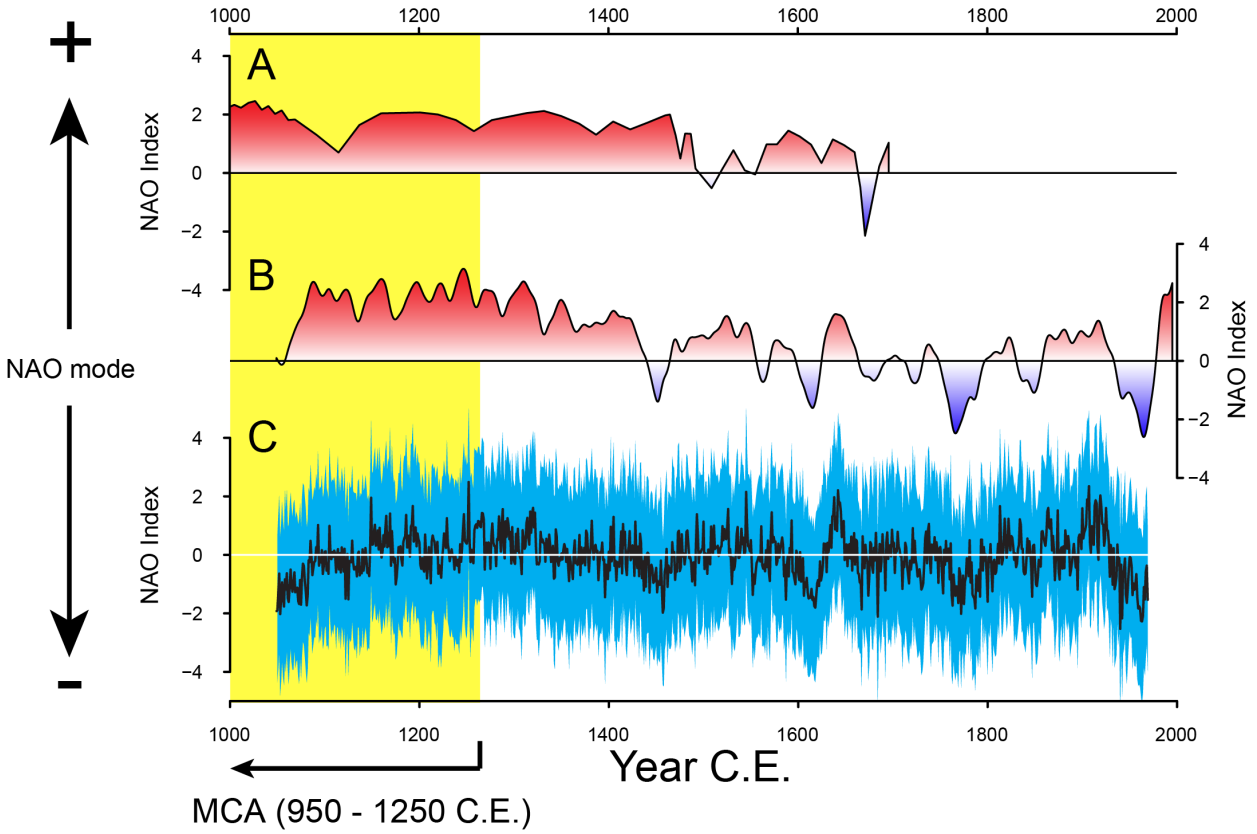

Figure A1: Examples of North Atlantic Oscillation (NAO) reconstructions. Some records support the dominant positive NAO anomaly during the Medieval Climate Anomaly, while some do not. A: West Greenland lake-record-inferred NAO index (Olsen et al., 2012). B: A bi-proxy analysis using NAO sensitive climate archives (Trouet et al., 2009). C: A multi-proxy informed annual NAO simulation (Ortega et al., 2015).

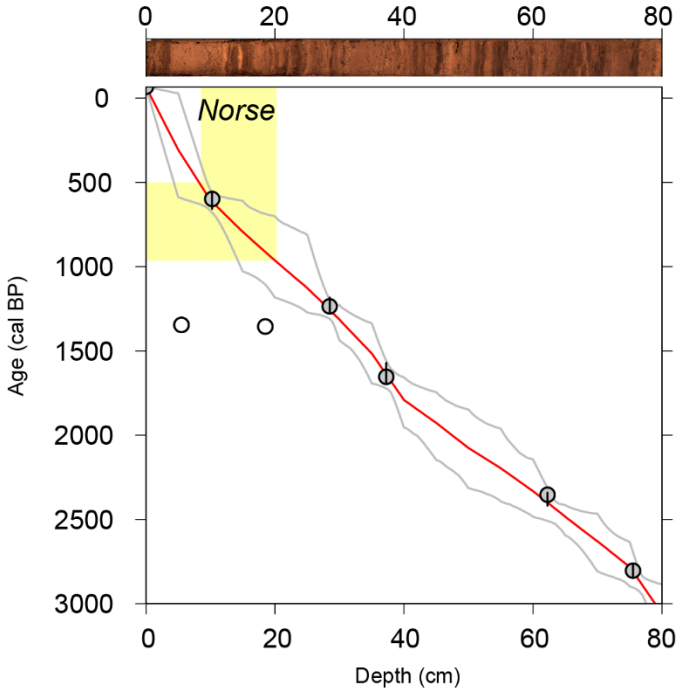

Figure A2: Age depth model and GEO-TEK scanned image of the top 80 cm of core 16-LOW-U2 from Scoop Lake, generated using the rbacon package in R (Blaauw and Christen, 2018). The top-most age is an inferred surface dating to August 2016. All other ages were calibrated using the IntCal13 curve, and plotted as the midpoint ± ½ of the 2σ range (Reimer et al., 2013). Ages in white were considered outliers after they fell outside the 95% confidence intervals of an initial model containing all ages. Thus, they were not included when running the final rbacon model. The red line is the mean of over 6 million iterations of the model and bounded in gray by 95% confidence intervals.

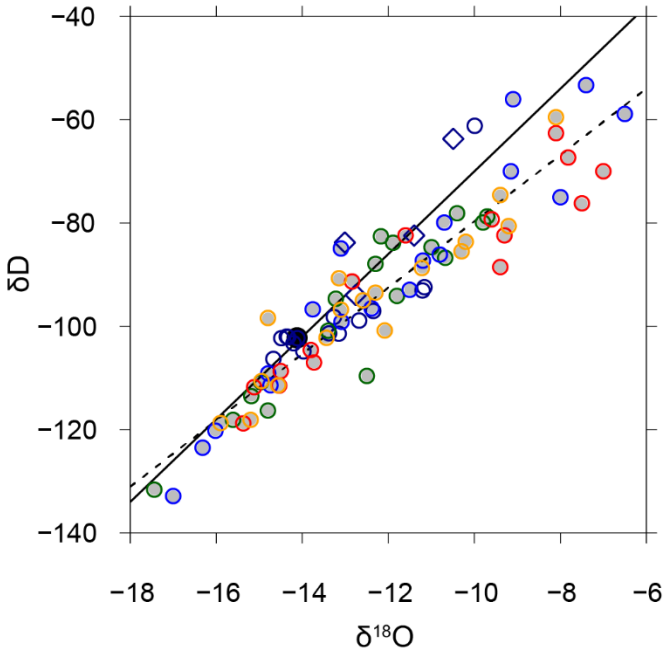

Figure A3: Isotopes of precipitation from South Greenland. Closed gray circles are historical precipitation values collected at Kangilinnguit, Greenland (150 km NW of Scoop Lake) between 1961 and 1974 (IAEA/WMO, 2017). Colors correspond to season: June, July August (JJA) – red. September, October, November (SOM) – orange. December, January, February (DJF) – green. March, April, May (MAM) – blue. Open diamonds represent precipitation collected in August, 2016 near Narsaq, Greenland. Open circles are lakes sampled during August, 2016. The black closed circle is lake water from Scoop Lake, collected in August, 2016. The solid black line is the Global Meteoric Water Line, and the dashed line is the "Local" Meteoric Water Line for the historic Kangilinnguit samples.

Table A1: Radiocarbon results from Scoop Lake

Core ID	Depth (top cm)	Depth (bottom cm)	^{14}C Age	^{14}C_error	Age (cal yr BP)	2σ lower	2σ upper	Material	Lab ID	Fraction Modern	δ^{13}C
Surface	0	1			-66						
16-LOW-U2	10	10.5	625	25	599	553	659	Aquatic Moss	OS-134547	0.9253	-28.7
16_LOW-U2	28	29	1280	15	1235	1182	1275	Leaf fragments	OS-139687	0.8528	-26
16-LOW-U2	37	37.5	1730	15	1654	1570	1699	Aquatic Moss	OS-134601	0.8066	-29
16-LOW-U2	62	62.5	2360	15	2354	2341	2420	Aquatic Moss	OS-134602	0.7458	-26
16_LOW-U2	75	76	2710	15	2805	2768	2848	and wood fragn	OS-139688	0.7136	-25.66
Ages not included in age-depth model											
*16_LOW-U2	5	6	1460	13	1345	1311	1376	: and terrestrial material			
16_LOW-U2	18	19	1470	15	1355	1314	1387	Plant/Wood	OS-139686	0.8325	-26
*Ages combined in OxCal											
16_LOW-U2	5	6	1380	15	1298	1284	1310	Aquatic Moss	OS-139684	0.8422	-29.13
16_LOW-U2	5	6	1670	25	1573	1528	1686	and wood fragn	OS-139685	0.8127	-25.68

*2 ages from the same depth combined using the R_combine function in OxCal v.4.3 (Ramsey, 2009).